LA-UR-16-26638
Approved for public release; distribution is unlimited.

Title: Colloid-Facilitated Radionuclide Transport: Current State of Knowledge from a Nuclear Waste Repository Risk Assessment Perspective

Author(s): Reimus, Paul William
Zavarin, Mavrik
Wang, Yifeng

Intended for: Report

Issued: 2017-01-25 (rev.1)

Colloid-Facilitated Radionuclide Transport: Current State of Knowledge from a Nuclear Waste Repository Risk Assessment Perspective

Fuel Cycle Research & Development

Prepared for
U.S. Department of Energy
Used Fuel Disposition
Paul W. Reimus,
Mavrik Zavarin,
Yifeng Wang
Los Alamos National Laboratory
Lawrence Livermore National Laboratory
Sandia National Laboratories

August 2016
FCRD-UFD-2016-000446
LA-UR-16-26638

FCT Quality Assurance Program Document

Appendix E
FCT Document Cover Sheet

Name/Title of Deliverable/Milestone	Colloid-Facilitated Radionuclide Transport: Current State of Knowledge from a Nuclear Waste Repository Risk Assessment Perspective; M3FT-16LA080504031
Work Package Title and Number	FEPS Analysis – LANL: FT-16LA08050403 (Rev. 1)
Work Package WBS Number	**1.02.08.05.04**
Responsible Work Package Manager	Paul W. Reimus, Paul W. Reimus (Name/Signature)
Date Submitted	August 2016

Quality Rigor Level for Deliverable/Milestone	☒ QRL-3	☐ QRL-2	☐ QRL-1 ☐ Nuclear Data	☐ N/A*

This deliverable was prepared in accordance with Los Alamos National Laboratory
(Participant/National Laboratory Name)

QA program which meets the requirements of
☒ DOE Order 414.1 ☐ NQA-1-2000

This Deliverable was subjected to:

☐ Technical Review

Technical Review (TR)

Review Documentation Provided

☐ Signed TR Report or,
☐ Signed TR Concurrence Sheet or,
☐ Signature of TR Reviewer(s) below

Name and Signature of Reviewers

David Sevougian

S. David Sevougian

☐ Peer Review

Peer Review (PR)

Review Documentation Provided

☐ Signed PR Report or,
☐ Signed PR Concurrence Sheet or,
☐ Signature of PR Reviewer(s) below

*Note: In some cases there may be a milestone where an item is being fabricated, maintenance is being performed on a facility, or a document is being issued through a formal document control process where it specifically calls out a formal review of the document. In these cases, documentation (e.g., inspection report, maintenance request, work planning package documentation or the documented review of the issued document through the document control process) of the completion of the activity along with the Document Cover Sheet is sufficient to demonstrate achieving the milestone. QRL for such milestones may be also be marked N/A in the work package provided the work package clearly specifies the requirement to use the Document Cover Sheet and provide supporting documentation.

This page left blank intentionally.

CONTENTS

FIGURES

TABLES

COLLOID-FACILITATED RADIONUCLIDE TRANSPORT: CURRENT STATE OF KNOWLEDGE FROM A NUCLEAR WASTE REPOSITORY RISK ASSESSMENT PERSPECTIVE

EXECUTIVE SUMMARY

This report provides an overview of the current state of knowledge of colloid-facilitated radionuclide transport from a nuclear waste repository risk assessment perspective. It draws on work that has been conducted over the past 3 decades, although there is considerable emphasis given to work that has been performed over the past 3-5 years as part of the DOE Used Fuel Disposition Campaign. The timing of this report coincides with the completion of a 3-year DOE membership in the Colloids Formation and Migration (CFM) partnership, an international collaboration of scientists studying colloid-facilitated transport of radionuclides at both the laboratory and field-scales in a fractured crystalline granodiorite at the Grimsel Test Site in Switzerland. This Underground Research Laboratory has hosted the most extensive and carefully-controlled set of colloid-facilitated solute transport experiments that have ever been conducted in an *in-situ* setting, and a summary of the results to date from these efforts, as they relate to transport over long time and distance scales, is provided in Chapter 3 of this report.

Chapter 2 of this report provides a perspective on colloid-facilitated radionuclide transport from a generalized modeling perspective, which is used to illustrate the processes and model parameterizations that can result in significant colloid-facilitated transport over the long time and distance scales that matter for nuclear waste repository risk assessments. The purpose here is not to introduce any new or advanced modeling concepts, but rather it is to evaluate process and parameter sensitivities and to gain insights into what sort of additional experimental work would most help in reducing uncertainties in the model parameters of greatest importance. Two primary colloid-facilitated radionuclide transport regimes of concern are discussed: (1) a kinetic regime in which a combination of slow radionuclide desorption kinetics from colloids and slow colloid filtration kinetics results in a small fraction of the radionuclide mass effectively transporting conservatively (at the rate of water flow) through the system in association with colloids that do not filter in the system, and (2) an equilibrium regime in which radionuclide interactions with colloids are strong enough and steady-state colloid concentrations are high enough that the transport velocity of the entire mass of radionuclide is significantly enhanced relative to its transport in the absence of colloids. Although these regimes are not necessarily mutually exclusive (nor all-inclusive), they are considered to be the two end-members of greatest concern for nuclear waste repository risk assessments, and presenting them helps to illustrate the inherent challenges of parameterizing the kinetic regime, which is believed to be the more likely regime to have an impact on repository risk assessments. Some suggested experimental approaches to interrogate the very slow radionuclide desorption kinetics (from colloids) and the very slow colloid filtration rates that typify the kinetic regime are discussed at the end of Chapter 2.

In the remainder of this report (Chapters 3-7 and Appendix A), we present summaries of recent case studies that the authors have been directly involved in where experimental attempts have been made to try to better parameterize colloid-facilitated radionuclide transport in specific systems, with emphasis on the kinetic transport regime that is believed to be of greater concern. These summaries include (1) results from Grimsel Test Site field experiments in a fractured granodiorite (Ch. 3), (2) results from a column methodology to interrogate both slow desorption kinetics (of radionuclides from colloids) and slow colloid filtration rates for colloid-facilitated transport of Cs, Am and Pu (Ch. 4), (3) results of a study in which the equilibrium transport regime was characterized, although it is shown that this particular system can transition to the kinetic regime under the right conditions (Ch. 5), (4) results from a study interrogating Pu desorption rates from clay colloids over long time scales that was used to parameterize a model accounting for surface redox

transformations that may be very important in the colloid-facilitated transport of redox-sensitive species such as Pu (Ch. 6), and (5) results from an evaluation of intrinsic Pu colloid stability that demonstrate a range in stabilities with respect to dissolution of intrinsic Pu colloids prepared in different ways (Ch. 7). Additionally, this report includes an appendix on how very small colloids (less than 100 nm in diameter, and typically in the 1-10 nm size range) can exhibit size-dependent surface chemistry and dissolution kinetics that differ significantly from that observed for larger particles or bulk surfaces, which may have an important influence on colloid-facilitated radionuclide transport in certain situations.

1. INTRODUCTION

1.1 Context for Colloid-Facilitated Radionuclide Transport

Colloid-facilitated transport is generally considered to be the most likely mechanism for transport of low-solubility and/or strongly adsorbing radionuclides over significant distances in groundwater in the geosphere. In the absence of colloids or very strong complexing agents (typically anions that form stable neutral or negatively-charged complexes with nuclides), such radionuclides will be predicted to migrate only very short distances in natural systems over time scales of concern because of their extremely strong interactions with geomedia surfaces (either as adsorbed species or surface precipitates). For instance, if we consider a radionuclide that has an effective equilibrium partition coefficient, or K_d value, of 1000 ml/g, then even for a relatively open flow system with an effective porosity of 0.5 (e.g., within a flowing fracture) the retardation factor will be about 2600, meaning that the radionuclide will take 2600 years to travel the same distance that a conservative solute travels in 1 year. Many strongly-adsorbing radionuclides have effective K_d values that exceed 10,000 ml/g, or even 100,000 ml/g, which means that for most scenarios they will be predicted to decay before they migrate significant distances as solutes.

Colloids or strong complexes change all this. If a strongly-adsorbing radionuclide becomes associated with a stable, mobile colloid instead of with immobile surfaces in the system, it will assume the transport characteristics of the colloid for as long it remains associated with the colloid. The radionuclide-colloid association may also take the form of a radionuclide forming a very fine colloid-sized precipitate or nanoparticle if the nuclide has a low solubility (either as a pure phase or a mixed phase with other elements) and supersaturated conditions exist (Soderholm et al., 2008; Walther et al., 2009). The first type of radionuclide-bearing colloid is generally called a pseudocolloid or an association colloid, whereas the latter type is often called an intrinsic colloid. In either case, if the transport of the colloid is conservative (nonsorbing), then the radionuclide will transport with the colloid with no retardation as long as the two remain associated.

Strong complexes can likewise transform a strongly-adsorbing radionuclide into a species that effectively transports with no retardation as long as it remains in the complexed form. The distinction between colloid-facilitated and complex-facilitated radionuclide transport can be rather arbitrary. Radionuclides often become associated with inorganic colloids by surface complexation reactions to form pseudocolloids, and if these are very small, they can behave much like large dissolved complexes. Similarly, high-molecular-weight organics such as humic or fulvic acids (or their bases, humates and fulvates) are among the more common naturally-occurring compounds that form strong complexes with radionuclides, and they are often large enough to behave as small colloids rather than solutes (Kim et al., 1992; Vilks and Bachinski, 1996; Reiller and Buckau, 2012; Zänker and Hennig, 2014). In this report, we distinguish both of these types of colloidal species from true solute-sized radionuclide complexes, such as complexes with EDTA or other strong chelating agents, which typically do not occur in nature and are certainly not expected to be present in nuclear waste repository environments unless they are anthropogenically introduced. One exception is siderophores, low-molecular-weight chelating agents that are produced by microbes to solubilize and complex iron (and can do likewise with some radionuclides; e.g., Gadd, 1996). However, siderophores are typically found at significant concentrations only in shallow biologically-active systems, which are almost universally precluded from consideration as nuclear waste disposal settings, and they also tend to be highly-specific to iron, with much lower affinities for other elements, except in the case of plutonium (Boukhalfa et al., 2007; Ruggiero et al., 2002; Xu et al., 2008).

From a predictive modeling perspective, there is fundamentally little difference in the way that any of the above situations are mathematically described other than by using different model parameters (often with different mechanistic underpinnings) to describe radionuclide interactions with colloids/complexes as well as the transport behavior of the colloids/complexes themselves. However, for solute-sized complexes, certain distinctions in transport behavior can be made; namely, solute complexes have much larger diffusion coefficients than colloids and can thus access pore spaces that colloids typically cannot, and reactions of

radionuclides with low molecular weight complexants are generally faster (equilibrium assumption is more valid) than reactions with larger molecules or colloids. Perhaps more importantly, solute complexes can generally be treated as being essentially homogeneous in their properties, with only as many species as there are molecular complexants present and with relatively simple interactions with surfaces. On the other hand, colloids in natural systems typically have wide variations in size, shape, and surface properties, and therefore they must be treated as heterogeneous populations, and they also experience much more complicated interactions with surfaces than solutes (see next section). All of these factors make colloid-facilitated radionuclide transport considerably more complicated to model or to parameterize in a model than solute-sized complexes. In this report, we do not consider the transport of radionuclide complexes that would typically be considered solutes, including siderophore complexes of plutonium, but rather we focus on radionuclide transport facilitated by inorganic colloids (including intrinsic colloids) or large organic molecules that take on the transport characteristics of colloids.

1.2 Definition and Properties of Colloids

Colloids are ubiquitous, naturally occurring, sub-micron particles found in groundwater. Colloids have high surface area per unit mass and a high capacity for sorption of low-solubility or strongly-adsorbing contaminants. They are generally defined as being between 1 and 1000 nm in diameter (Stumm, 1992). This definition is based on physical properties. Due to their small size, they have the ability to remain suspended by Brownian motion and ultimately transported in groundwater, particularly if they have surface properties that make them resistant to attachment to immobile surfaces. Particles greater than a few microns (2000 -3000 nm) in diameter will generally settle out of a fluid due to gravitational forces and those particles less than 1 nm are thought to behave as dissolved species (e.g., solute-sized complexes).

Recent work has shown that small colloids (less than 100 nm in diameter, and typically in the 1-10 nm size range) can exhibit size-dependent surface chemistry and dissolution kinetics that differ from that observed for larger particles or bulk surfaces (Wang, 2014). These characteristics may increase the importance of small colloids relative to larger colloids in colloid-facilitated radionuclide transport. An overview of the nanogeochemistry of small colloidal particles is provided in Appendix A. This appendix also applies to the general discussions in Sections 1.3 and 1.4. Chapter 7 of this report summarizes an investigation of the stability of very small intrinsic Pu colloids that are likely influenced by nanoscale geochemical properties. This investigation is of interest because intrinsic Pu colloids prepared in different ways exhibited significantly different dissolution/stability behavior.

Inorganic colloids are believed to be primarily generated by mechanical fragmentation (erosion or weathering) of the host rock in contact with groundwater caused by either chemical or physical perturbations. These changes can result from either a chemical process (pH, ionic strength, saturation index changes) and/or a change in the flow rate of a groundwater system. Chemical changes in ionic strength, pH and fluid composition have been found to greatly increase colloid generation. These changes can occur when groundwater is diluted by infiltration or precipitation. Inorganic colloids may also be formed when geochemical gradients along a flow pathway result in a mineral becoming supersaturated and forming small colloidal precipitates. Degueldre et al. (1989) showed that colloids were continuously produced from water flowing through fractured granite at the Grimsel Test Site, Switzerland. Ryan and Gschwend (1994) investigated colloid release rates in the laboratory with a hematite-quartz system and showed that release rates were correlated with increases in flow rates and decreases in ionic strength of solutions.

Organic colloids, typically humic and fulvic acids or their bases, are formed by the breakdown of organic matter, which is usually of recent biological origin. However, they can also be derived from organic material of much older origin, such as coal or lignite deposits.

In nuclear waste repositories, inorganic colloids would be expected to dominate colloid populations, as repository siting in most cases will exclude settings where significant organic source terms exist, although there could be exceptions in shale settings where organics tend to be more prevalent. Organic colloids would likely be present only if organic materials are anthropogenically introduced into a repository, and

even then they would likely be limited in quantity. However, some small background of organic colloids can probably never be ruled out. Inorganic colloids would be expected to include clays and other minerals (e.g., silicates, zeolites) that can form stable colloids when the host rock weathers and erodes, but they would also be expected to include colloids that are generated as a result of engineered barrier and waste package degradation. Bentonite backfill could be a long-term source of clay colloids, and corrosion of metallic waste package components could be a source of iron- or other metal-bearing corrosion-product colloids. Even waste forms could degrade to form colloid-sized fragments of unaltered waste form or colloidal minerals derived from waste form alteration (Bates et al., 1992; Zänker and Hennig, 2014). For instance, glass is known to alter to clays at elevated temperatures.

1.3 Colloid Interactions with Surfaces

Colloid interactions with immobile surfaces in hydrologic systems are generally considered to be governed by a two-step process: (1) colloid collisions with immobile surfaces, a necessary prerequisite for a surface interaction to occur, and (2) a specific interaction at the surface that results in a colloid either sticking to the surface or reflecting off the surface and continuing to transport. In fact, the same two-step process can be considered to apply to solutes, but whereas for solutes step (1) is governed entirely by diffusion, for colloids it is considered to be a balance between diffusion, gravity sedimentation, and direct advective collision, also called interception. Diffusion tends to dominate for smaller colloids, and gravity settling and interception play a bigger role for larger and denser colloids. The specific surface interactions for colloids are also more complex than the interactions that occur for solutes, which generally consist of either ion exchange or surface complexation processes. With colloids, the interactions are governed by both electrochemical processes and body forces that occur under the influence of dynamic relative motion of the surfaces. These processes result in very complex interactions that are a function of colloid size, shape and composition, local geometry and hydrodynamic conditions, and electrochemical properties of both the colloid and immobile surfaces (surface charge/ potential, electrical double-layer thickness), which are influenced by water chemistry (ionic strength, pH, major ion chemistry). Derjaguin, Landau, Verwey, and Overbeek theory, or DLVO theory (Hiemenz, 1986), has been in existence for decades to describe some of these interactions in idealized geometries (namely van der Waals body forces and static electrochemical forces as a function of water chemistry), but it has been recognized in recent years that additional dynamic forces (e.g., electroviscous forces, viscous drag; e.g., Chun and Ladd, 2004) and solvent structural forces (e.g., hydrophobic/hydrophilic interactions; e.g., Israelachvili, 1992) also play a role in colloid-surface interactions . For large organic molecules, charge distribution and steric factors can also play a role in surface interactions, and in some systems where large organic molecules are ubiquitous, surfaces can become effectively coated with these molecules to effectively block further surface interaction with suspended molecules.

A full review of the literature on colloid-surface interactions goes well beyond the scope of this report. For the purposes of this report, we summarize by saying that the combination of colloid filtration theory (e.g., Yao et al., 1971), which explicitly accounts for collision processes (generally assuming surface interactions to be governed by an "attachment efficiency"), and extended DLVO theory, which explicitly accounts for surface interactions (though limited to idealized conditions), yields what ultimately amounts to a prediction of a first-order reversible rate law describing colloid attachment to and detachment from immobile surfaces (e.g., Ruckenstein and Prieve, 1976). However, the attachment and detachment rate constants are expected to be influenced by all of the variables mentioned above, meaning that they can have spatial dependence in a steady-state system, space and time dependence in an evolving system, and dependence on individual colloid properties in both space and time. We can summarize by providing some generalizations that colloids tend to be more stable and more mobile at lower ionic strengths than at higher ionic strengths because the latter collapses the stabilizing electrical double layers surrounding the colloids. We can also state that in order to transport any significant distance, colloids must have the same surface charge as the immobile surfaces in the system under the prevailing geochemical conditions. A good recent review of colloid transport in porous media is provided by Molnar et al. (2015).

1.4 Colloid Interactions with Radionuclides

In general, radionuclides that interact very strongly with mineral surfaces tend to also interact strongly with colloids. A good review of radionuclide interactions with colloids is provided in Poinssot and Geckeis (2012), and in particular in Ch. 10 of that book by Kersting (2012). Schäfer et al. (2012) also review this subject. For inorganic pseudocolloids, these interactions are typically governed by cation exchange or surface complexation processes, depending on the radionuclide. However, surface precipitation processes (formation of mixed mineral phases on surfaces) and/or coprecipitation processes (incorporation of radionuclides into secondary mineral colloids) are also possible for low-solubility radionuclides. Alkali metal or alkaline earth fission products such as Cs and Sr are expected to interact primarily by cation exchange and to have high affinity for clay and zeolite colloids with high cation exchange capacities. Actinides, such as Am and Pu, are expected to have interactions with inorganic colloids that are governed more by surface complexation processes, and some actinides such as Np and Pu are known to have interactions that are highly influenced by redox reactions, with the lower oxidation states generally tending to be more strongly associated with colloids than higher ones. In some cases, surface-mediated reduction can occur on colloid surfaces, causing a radionuclide to effectively transform on the surface from a species that can readily desorb to a species that is much more likely to remain adsorbed or even to be incorporated into a surface precipitate (Begg et al., 2015; Begg et al., 2013; Zhao et al., 2016). Radionuclides with low solubilities, particularly under reducing conditions, can also form intrinsic colloids. Perhaps of greater practical concern in a nuclear waste repository scenario, low-solubility radionuclides can also be directly incorporated into the structure of waste form alteration product or corrosion product colloids, which can render them essentially irreversibly-associated with the colloids (Bates et al., 1992).

From the standpoint of nuclear waste repository risk assessments, the radionuclides generally considered to be of greatest concern for colloid-facilitated transport are the long-lived isotopes of Pu, Am, and Np (the latter under reducing conditions). The transport of radioisotopes of other actinides or lanthanides (e.g., Cm, Th, Pa, Ce, Eu - not intended to be all inclusive) would also be expected to be dominated by colloid-facilitated transport, but the inventories of these nuclides are typically much lower than those of Pu, Am and Np in high-level nuclear waste, so they generally contribute less to overall risk calculations. The transport of Cs fission-product isotopes are also expected to be strongly influenced by colloids, but the half-lives of these isotopes are short enough and/or their inventories small enough that they typically impact risk calculations only for a limited number of low-probability scenarios that involve early releases and rapid transport. Isotopes of uranium represent a special case of very high-inventory (at least for used fuel), long-lived radioisotopes that have the potential to contribute significantly to risk calculations, but their transport is generally considered to be dominated by solute processes, not colloid-facilitated transport processes. This is particularly true under oxidizing conditions because U(VI) is quite soluble and does not interact strongly with most surfaces. However, exceptions may occur in highly-reducing environments where the relatively insoluble and adsorptive U(IV) oxidation state is dominant, or in cases where U remains incorporated into waste form alteration colloids.

1.5 Examples of Colloid-Facilitated Radionuclide Transport in the Environment

Several examples of colloid-facilitated transport of radionuclides in the environment have been published. Kersting (2013) provides a summary specific to colloid-facilitated transport of Pu, including observations at the Nevada Test Site (now Nevada National Security Site), the Rocky Flats Environmental Technology Site, Colorado, the Mayak Production Association, Russia, and the Hanford Site, Washington. These observations include both Pu associations with inorganic colloids and macromolecular organic colloids. Pu has garnered much attention for its potential to be transported by colloids because it exists in significant quantities at many nuclear materials processing facilities and nuclear weapons manufacturing or testing sites, it is very insoluble and strongly-adsorbing, it has long-lived isotopes, and it can be detected at extremely low concentrations in the environment. McCarthy (1998) reported strong actinide associations

with natural organic matter, which effectively mobilized the actinides as small colloid-sized species from shallow disposal trenches at Oak Ridge, Tennessee. These observations and some of those at the Nevada Test Site, Rocky Flats, and Mayak serve as good examples of actinide transport facilitated by organic macromolecules. Uranium was detected in colloidal form at the Tomsk Site, Russia (Kalmykov et al., 2011), an apparent result of a situation where U(VI) was released at relatively high concentrations into an anaerobic environment where it reduced to U(IV) and formed intrinsic colloids. Actinides have also been associated with colloids in the aftermath of the Chernobyl nuclear accident (Zänker and Hennig, 2014). Nearly all of these observations have had multiple laboratory characterizations and investigations conducted in association with them to try to better understand the field observations. The reader is referred to the recent reviews by Kersting (2013) and Zänker and Hennig (2014), as well as the compendium of Kalmykov and Denecke (2011), for discussion of some of the more relevant laboratory findings and a plethora of citations.

For obvious reasons there have been no direct observations of colloid-facilitated radionuclide transport from deep geologic nuclear waste repositories, but there have been numerous laboratory studies conducted to better understand the risks associated with colloid-facilitated transport from such repositories. A majority of these have been conducted in Europe in association with national nuclear waste disposal programs (see Zänker and Hennig, 2014, and Kalmykov and Denecke, 2011), although work has also been conducted in the U.S. (Dittrich et al., 2015; Wang et al., 2015; Zavarin et al., 2012; Begg et al., 2013; Begg et al., 2015), Canada (Vilks and Baik, 2001), Japan (Yamaguchi et al., 2008), and more recently China (Xie et al., 2014; Lin et al., 2014; Xie et al., 2013a; Xie et al., 2013b). It goes beyond the scope of this report to summarize all the various laboratory studies on colloid-facilitated radionuclide transport that have been conducted.

Since 2002, a series of colloid-facilitated radionuclide and colloid-facilitated radionuclide analogue transport experiments have been conducted in a crystalline granodiorite at the Grimsel Underground Research Laboratory (Grimsel Test Site, or GTS) in the Swiss Alps (Möri, 2004; Kosakowski and Smith, 2004; Wang et al., 2013; Wang et al., 2014b; Viswanathan et al., 2016; Noseck et al., 2016). These experiments were part of two separate but sequential international partnership projects based at the GTS, namely the Colloids and Radionuclide Retention (CRR) project (1998-2003) and the Colloids Formation and Migration (CFM) project (2004-present). The U.S. Department of Energy was a participant in the CFM project from 2013 through 2015. The CRR and CFM experiments have been unique in that they evaluated colloid-facilitated radionuclide transport in a field setting intended to mimic a high-level nuclear waste repository scenario. The experiments were conducted by injecting "cocktails" of radionuclides and colloids into a conductive shear zone with well-controlled flow conditions. The colloids used in these experiments were generated by dispersing a Spanish bentonite in groundwater from the site, and as such, these colloids were intended to be representative of colloids generated by the swelling and erosion of a bentonite backfill material in a crystalline rock repository. Radionuclides have been used in other Underground Research Laboratories, for example at Aspö in Sweden (Andersson et al., 2002), but these experiments did not also involve colloids and hence were not colloid-facilitated radionuclide transport experiments.

1.6 Purpose, Scope and Organization of This Report

The purpose of this report is to provide an overview of the current state of knowledge of colloid-facilitated radionuclide transport from a nuclear waste disposal perspective. This report is not intended to provide an exhaustive literature review of the subject; several of these have been recently published (e.g., Zänker and Hennig, 2014; Kersting, 2012; compendium of Kalmykov and Denecke, 2011). It is also not intended to delve deeply into the subtle mechanistic details of colloid formation, stability and transport, radionuclide-colloid interactions, or colloid-facilitated radionuclide transport, which are highly site, system, and radionuclide specific.

Rather, this report first presents a perspective on colloid-facilitated radionuclide transport from a generalized modeling perspective, which is used to illustrate the processes and model parameterizations that can result in significant colloid-facilitated transport over the long time and distance scales that matter

for nuclear waste repository risk assessments. Many other works on modeling of colloid-facilitated radionuclide or contaminant transport have appeared in the literature (e.g., Smith and Degueldre, 1993; Ibaraki and Sudicky, 1995; Lührmann et al., 1998; Contardi et al., 2001; Meier et al., 2003), and the work here does not represent any major advances in the state-of-the-art of modeling over these efforts. Instead the emphasis here is on using a generalized model to illustrate parameter sensitivities and to gain insights into what sort of additional experimental work would most help in reducing uncertainties in the most important model parameters. Fig. 1-1 is an often-used schematic (taken from Zänker and Hennig, 2014) that has been in existence for nearly three decades to summarize the conditions that are necessary for significant colloid-facilitated radionuclide transport. These conditions are all still valid, but in this report we attempt to provide some more quantitative criteria and discuss some experimental approaches for answering the questions posed in the figure.

Two dominant colloid-facilitated transport regimes of concern are discussed: (1) a kinetic regime in which a combination of slow radionuclide desorption kinetics from colloids and slow colloid filtration kinetics results in a small fraction of the radionuclide mass effectively transporting conservatively (at the rate of water flow) through the system in association with colloids that do not filter in the system, and (2) an equilibrium regime in which radionuclide interactions with colloids are strong enough and steady-state colloid concentrations are high enough that the transport velocity of the entire mass of radionuclide is significantly enhanced relative to its transport in the absence of colloids. Although these regimes are not necessarily mutually exclusive (nor all-inclusive), they are considered to be the two end-members of greatest concern for nuclear waste repository risk assessments, and presenting them up front helps to illustrate the inherent challenges of parameterizing the kinetic regime, which is believed to be the more likely regime to have an impact on repository risk assessments.

In the remainder of the report, we present summaries of recent case studies that the authors have been directly involved in where experimental attempts have been made to try to better parameterize colloid-facilitated radionuclide transport in specific systems, with emphasis on the kinetic transport regime. These summaries include (1) results from Grimsel Test Site field experiments in a fractured granodiorite (Ch. 3), (2) results from a column methodology to interrogate both slow desorption kinetics (of radionuclides from colloids) and slow colloid filtration rates for colloid-facilitated transport of Cs, Am and Pu (Ch. 4), (3) results of a study in which the equilibrium transport regime was characterized, although it is shown that this particular system can transition to the kinetic regime under the right conditions (Ch. 5), (4) results from a study interrogating Pu desorption rates from clay colloids over long time scales that was used to parameterize a model accounting for surface redox transformations that may be very important in the colloid-facilitated transport of redox-sensitive species such as Pu (Ch. 6), and (5) results from an evaluation of intrinsic Pu colloid stability that demonstrate a range in stabilities with respect to dissolution of Pu colloids prepared in different ways (Ch. 7).

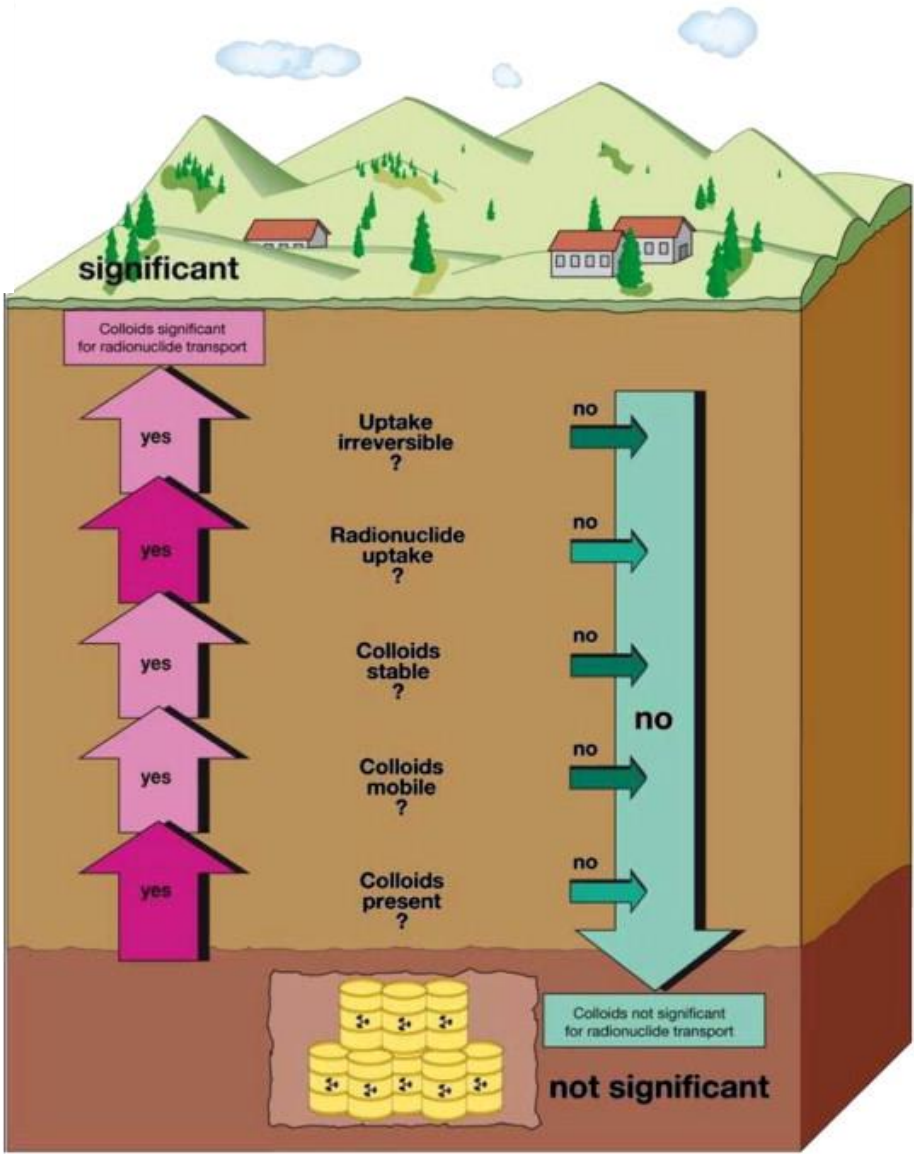

Figure 1-1. "Colloid-facilitated transport ladder" (from Zänker and Hennig, 2014) summarizing the conditions that must be met to have a significant amount of colloid-facilitated radionuclide transport. In this report, we attempt to provide more quantitative criteria for answering the questions.

2. COLLOID-FACILITATED RADIONUCLIDE TRANSPORT CONSIDERATIONS FROM GENERALIZED MODELING

A generalized mathematical model for colloid facilitated radionuclide transport, written for flow in parallel-plate fractures with diffusion into a surrounding matrix (y-direction), which represents non-flowing or secondary porosity, is provided below. The model equations also apply equally well to a porous medium if the matrix or secondary porosity is set equal to zero and the fracture properties are taken to be the porous medium properties (in this case, all equations for transport in the matrix can be ignored). The model is based on work presented in two recent Used Fuel Disposition reports (Wang et al., 2013, Ch. 2; Wang et al., 2014b, Ch. 7) and, in particular, on work conducted as part of the Colloids Formation and Migration (CFM) international partnership project (Noseck et al., 2016).

The equations are written for only a single type of colloid and a single radionuclide solute species, but in general there could be an entire population of colloids having different properties and a number of solute species that may not only interact with surfaces and colloids but could also potentially interact with each other. A separate set of equations must be written for each separate colloid or solute. Spatially-varying properties/parameters can be assumed, but these are not considered here. Additional species and spatial variability are not needed to illustrate the main points associated with colloid-facilitated transport. However, we do allow for the possibility of multiple solute adsorption sites on both the colloids and immobile surfaces in the system because this feature turns out to be rather important for illustrating key points, and it is also useful for interpreting the GTS field experiments. We consider here only two types of colloid filtration sites on immobile surfaces in fractures, a reversible site and an irreversible site, although in principle there could be many types of filtration sites that are distinguished by their filtration and resuspension rate constants (analogous to multiple sites for solute adsorption).

Mobile Colloid Transport, Generation and Filtration in Fractures:

$$\frac{\partial C_c}{\partial t} + div(v_c C_c - D_c \nabla C_c) = -k_{cs}\frac{SA}{V}C_c\left(1 - \frac{S_c}{S_{c,max}}\right) + k_{sc}\frac{SA}{V}S_c - k_{cs,ir}\frac{SA}{V}C_c\left(1 - \frac{S_{c,ir}}{S_{c,ir,max}}\right) + \frac{SA}{V}P_c \quad (2\text{-}1)$$

Reversibly Filtered/Immobilized Colloids in Fractures:

$$\frac{\partial S_c}{\partial t} = k_{cs}C_c\left(1 - \frac{S_c}{S_{c,max}}\right) - k_{sc}S_c \quad (2\text{-}2)$$

Irreversibly Filtered/Immobilized Colloids in Fractures:

$$\frac{\partial S_{c,ir}}{\partial t} = k_{cs,ir}C_c\left(1 - \frac{S_{c,ir}}{S_{c,ir,max}}\right) \quad (2\text{-}3)$$

Mobile Solute in Fractures:

Advective and Dispersive Transport: $\frac{\partial C_a}{\partial t} + div(v_a C_a - D_a \nabla C_a) =$

Reactions with Immobile Surfaces: $\sum_{i=1}^{nsites}\left[-k_{as,i}\frac{\rho_B}{\emptyset}C_a\left(1 - \frac{S_{a,i}}{S_{a,max,i}}\right) + k_{sa,i}\frac{\rho_B}{\emptyset}S_{a,i}\right] +$

Reactions with Mobile Colloids: $\sum_{i=1}^{ncolsites}\left[-k_{ac,i}C_aC_c\left(1 - \frac{C_{ac,i}C_c}{C_{ac,max,i}C_c}\right) + k_{ca,i}C_{ac,i}C_c\right] +$

Reactions with Immobile Colloids:
$$\sum_{i=1}^{ncolsites} \frac{SA}{V}\left[-k_{ac,i}C_a S_c\left(1-\frac{C_{ac,i}S_c}{C_{ac,max,i}S_c}\right)+k_{ca,i}C_{ac,i}S_c - k_{ac,i}C_a S_{c,ir}\left(1-\frac{C_{ac,i}S_{c,ir}}{C_{ac,max,i}S_{c,ir}}\right)+k_{ca,i}C_{ac,i}S_{c,ir}\right]$$

Diffusion in and out of Matrix:
$$-\frac{\emptyset_m D_{ma}}{b\emptyset}\frac{\partial C_a}{\partial y}\Big|_{y=b} \quad (2\text{-}4)$$

Solute Adsorbed onto Immobile Surfaces in Fractures (nsites equations):
$$\frac{\partial S_{a,i}}{\partial t} = k_{as,i}C_a\left(1-\frac{S_{a,i}}{S_{a,max,i}}\right)-k_{sa,i}S_{a,i} \quad (2\text{-}5)$$

Solute Adsorbed onto Mobile Colloids in Fractures (ncolsites equations):
$$\frac{\partial C_{ac,i}C_c}{\partial t}+div\left(v_a C_{ac,i}C_c - D_c\nabla C_{ac,i}C_c\right)=k_{ac,i}C_{ac,i}C_c\left(1-\frac{C_{ac,i}C_c}{C_{ac,max,i}C_c}\right)-k_{ca,i}C_{ac,i}C_c$$
$$-k_{cs}\frac{SA}{V}C_{ac,i}C_c\left(1-\frac{S_c}{S_{c,max}}\right)+k_{sc}\frac{SA}{V}C_{ac,i}S_c-k_{cs,ir}\frac{SA}{V}C_{ac,i}C_c\left(1-\frac{S_{c,ir}}{S_{c,ir,max}}\right) \quad (2\text{-}6)$$

Solute Adsorbed onto Immobile Colloids in Fractures (ncolsites x 2 equations):

Reversibly-Filtered:
$$\frac{\partial C_{ac,i}S_c}{\partial t}=k_{ac,i}C_a S_c\left(1-\frac{C_{ac,i}S_c}{C_{ac,max,i}S_c}\right)-k_{ca,i}C_{ac,i}S_c - k_{cs}C_{ac,i}C_c\left(1-\frac{C_{ac,i}S_c}{C_{ac,max,i}S_c}\right)+k_{sc}C_{ac,i}S_c \quad (2\text{-}7)$$

Irreversibly-Filtered:
$$\frac{\partial C_{ac,i}S_{c,ir}}{\partial t}=k_{ac,i}C_a S_{c,ir}\left(1-\frac{C_{ac,i}S_{c,ir}}{C_{ac,max,i}S_{c,ir}}\right)-k_{ca,i}C_{ac,i}S_{c,ir} - k_{cs,ir}C_{ac,i}C_c\left(1-\frac{C_{ac,i}S_{c,ir}}{C_{ac,max,i}S_{c,ir}}\right) \quad (2\text{-}8)$$

Solute Diffusion and Reaction in Matrix (no Colloids assumed in Matrix):
$$\frac{\partial C_a}{\partial t}-D_{ma}\frac{\partial^2 C_a}{\partial y^2}=\sum_{i=1}^{nmatrixsites}\left[-k_{am,i}\frac{\rho_{Bm}}{\emptyset_m}C_a\left(1-\frac{S_{am,i}}{S_{am,max,i}}\right)+k_{ma,i}\frac{\rho_{Bm}}{\emptyset_m}S_{am,i}\right] \quad (2\text{-}9)$$

Solute Adsorbed to Immobile Surfaces in Matrix (nmatrixsites equations):
$$\frac{\partial S_{am,i}}{\partial t}=k_{am,i}C_a\left(1-\frac{S_{am,i}}{S_{am,max,i}}\right)-k_{ma,i}S_{am,i} \quad (2\text{-}10)$$

where, C_c = concentration of colloids in mobile phase, g/cm^3
S_c = colloid concentration on reversible filtration sites on fracture surfaces, g/cm^2
$S_{c,ir}$ = colloid concentration on irreversible filtration sites on fracture surfaces, g/cm^2
$S_{c,max}$ = maximum colloid concentration on reversible filtration sites on fracture surfaces, g/cm^2
$S_{c,max,ir}$ = maximum colloid concentration on irreversible filtration sites on fracture surfaces, g/cm^2
C_a = solution concentration of solute in fractures or matrix, g/cm^3
$S_{a,i}$ = adsorbed concentration of solute on fracture surface site *i*, g/g
$S_{am,i}$ = adsorbed concentration of solute on matrix surface site *i*, g/g
$C_{ac,i}$ = concentration of solute sorbed to colloid site *i*, g/g colloid
$S_{a,max,i}$ = maximum adsorbed concentration of solute on fracture surface site *i*, g/g
$S_{am,max,i}$ = maximum adsorbed concentration of solute on matrix surface site *i*, g/g
$C_{ac,max,i}$ = maximum concentration of solute sorbed to colloid site *i*, g/g colloid

P_c = colloid production rate in fractures, g/cm^2-hr
v_c = advective velocity of colloids in fractures, cm/hr
v_a = advective velocity of solutes in fractures, cm/hr
D_a = solute dispersion coefficient in fractures, cm^2/hr
D_c = colloid dispersion coefficient in fractures, cm^2/hr
D_{ma} = solute molecular diffusion coefficient in matrix, cm^2/hr
ρ_B = effective bulk density within fractures, g/cm^3
ρ_{Bm} = bulk density in matrix, g/cm^3.
$\emptyset$ = porosity within fractures
$\emptyset_m$ = matrix porosity
b = fracture half aperture, cm
$\frac{SA}{V}$ = surface area to volume ratio in fractures, cm^2/cm^3
k_{cs} = colloid filtration rate constant, cm^3/cm^2-hr
$k_{cs,ir}$ = irreversible colloid filtration rate constant, cm^3/cm^2-hr
k_{sc} = reverse colloid filtration (detachment) rate constant, 1/hr
$k_{as,i}$ = rate constant for sorption of solute onto fracture surface site i, cm^3/g-hr
$k_{sa,i}$ = rate constant for desorption of solute from fracture surface site i, 1/hr
$k_{am,i}$ = rate constant for sorption of solute onto matrix surface site i, cm^3/g-hr
$k_{ma,i}$ = rate constant for desorption of solute from matrix surface site i, 1/hr
$k_{ac,i}$ = rate constant for sorption of solute onto colloid site i, cm^3/g-hr
$k_{ca,i}$ = rate constant for desorption of solute from colloid site i, 1/hr

This model can be applied to identify and evaluate the conditions under which colloid-facilitated radionuclide transport is likely to contribute to nuclear waste repository risk assessment calculations. To do this, we simplify the model by reducing the number of different types of radionuclide adsorption sites on both colloids and immobile surfaces to one each, and we ignore any secondary porosity (assume $\emptyset_m$ = zero). We also assume that there are effectively no sorption site limitations (S_{max} values are very large) for the sorption reactions on both fracture surfaces and colloids, and we assume that colloids undergo only irreversible filtration (no resuspension or detachment from immobile surfaces). We further assume one-dimensional flow with a steady input of both colloids and radionuclides at the entrance to the domain starting at time zero (i.e., a step function input, rather than a pulse). Such an input function is reasonable for a breached repository, which will presumably release colloids and radionuclides indefinitely once it is compromised. We also assume steady-state flow with a fixed dispersion coefficient for both colloids and solutes. These simplifications and assumptions allow us to reduce equations (1) to (10) to the following six equations (where we now refer to flow domain instead of fractures and immobile surfaces instead of fracture surfaces because the fracture designation no longer has direct relevance):

Mobile and Immobile Colloids in Flow Domain:

$$\frac{\partial C_c}{\partial t} + v_c \frac{\partial C_c}{\partial x} - D_c \frac{\partial^2 C_c}{\partial x^2} = -k_{cs,ir} \frac{SA}{V} C_c + \frac{SA}{V} P_c \tag{2-11}$$

$$\frac{\partial S_{c,ir}}{\partial t} = k_{cs,ir} C_c \tag{2-12}$$

Mobile and Immobile Solute in Flow Domain:

$$\frac{\partial C_a}{\partial t} + v_a \frac{\partial C_a}{\partial x} - D_a \frac{\partial^2 C_a}{\partial x^2} = -k_{as} \frac{\rho_B}{\emptyset} C_a + k_{sa} \frac{\rho_B}{\emptyset} S_a - k_{ac} C_a C_c + k_{ca} C_{ac} C_c - k_{ac} C_a S_{c,ir} + k_{ca} C_{ac} S_{c,ir} \tag{2-13}$$

$$\frac{\partial S_a}{\partial t} = k_{as} C_a - k_{sa} S_a \tag{2-14}$$

Solute Adsorbed onto Mobile Colloids in Flow Domain:

$$\frac{\partial C_{ac}C_c}{\partial t} + v_c \frac{\partial C_{ac}C_c}{\partial x} - D_c \frac{\partial^2 C_{ac}C_c}{\partial x^2} = k_{ac}C_{ac}C_c - k_{ca}C_{ac}C_c - k_{cs,ir}\frac{SA}{V}C_{ac}C_c \quad (2\text{-}15)$$

Solute Adsorbed onto Immobile Colloids in Flow Domain:

$$\frac{\partial C_{ac}S_{c,ir}}{\partial t} = k_{ac}C_a S_{c,ir} - k_{ca}C_{ac}S_{c,ir} + k_{cs,ir}C_{ac}C_c \quad (2\text{-}16)$$

Before discussing the model further, we note that if we are dealing with a system where natural colloid concentrations are constant throughout the flow domain and there are no colloids being generated at the source, equations (11) and (12) can effectively be dropped from consideration and simply replaced with a constant colloid concentration, C_c, everywhere in the system. Furthermore, if solute reactions with immobile surfaces and colloids are fast relative to time scales of transport (both adsorption and desorption rates), then these reactions can be considered to be at equilibrium, and the rate expressions can be replaced with partition coefficient expressions in a single equation describes solute transport through the flow system. These simplifications allow equations (11) to (16) to be reduced to a single equation:

$$\frac{\partial C_a}{\partial t} + v_a \frac{\partial C_a}{\partial x} - D_a \frac{\partial^2 C_a}{\partial x^2} + \frac{\rho_B}{\emptyset}K_d \frac{\partial C_a}{\partial t} + K_c C_c \frac{\partial C_a}{\partial t} + K_c C_c \left(v_c \frac{\partial C_a}{\partial x} - D_c \frac{\partial^2 C_a}{\partial x^2}\right) = 0 \quad (2\text{-}17)$$

where, $K_d = k_{as}/k_{sa}$ = partition coefficient for solute on immobile surfaces, cm^3/g
$K_c = k_{ac}/k_{ca}$ = partition coefficient for solute on colloids, cm^3/g
$C_{ac} = K_c C_c C_a$, and
$C_{as} = K_d C_a$

If $v_a = v_c$ (solute and colloid velocities are equal) and $D_a = D_c$ (solute and colloid dispersion coefficients are equal), then equation (2-17) can be rearranged to yield:

$$\left(1 + \frac{\rho_B}{\emptyset}K_d + K_c C_c\right)\frac{\partial C_a}{\partial t} + (1 + K_c C_c)\left(v_a \frac{\partial C_a}{\partial x} - D_a \frac{\partial^2 C_a}{\partial x^2}\right) = 0 \quad (2\text{-}18)$$

or alternatively,

$$\left(\frac{1+\frac{\rho_B}{\emptyset}K_d + K_c C_c}{1+K_c C_c}\right)\frac{\partial C_a}{\partial t}\frac{\rho_B}{\emptyset} + v_a \frac{\partial C_a}{\partial x} - D_a \frac{\partial^2 C_a}{\partial x^2} = 0 \quad (2\text{-}19)$$

from which it is readily apparent that the term, $\frac{\mathbf{1+\frac{\rho_B}{\emptyset}K_d + K_c C_c}}{\mathbf{1+K_c C_c}}$, is an effective retardation factor for solute transport through the system. The implications of this effective retardation factor will be discussed in more detail later.

We present the results of a series of model calculations, using equations (11)-(16), as radionuclide breakthrough curves in which the dimensionless radionuclide concentration (C/C_0, where C_0 is the input concentration) is plotted vs. dimensionless time (t/τ, where τ is the mean groundwater residence time in the flow system). The mean groundwater residence time is equal to L/v, with L being the length of the flow domain and v the average velocity through the domain. The breakthrough curves are calculated for different values of dimensionless rate constants (effective rate constants multiplied by τ) or, when equations (17)-(19) apply, different values of the effective retardation factor, $\frac{\mathbf{1+K_d\frac{\rho_B}{\emptyset}+K_c C_c}}{\mathbf{1+K_c C_c}}$. In all calculations we assume a dimensionless dispersion coefficient, D_a/vL, of 0.02, which is equivalent to a Peclet number, vL/D_a, of 50. We also assume that solute adsorption to and desorption from the immobile surfaces is rapid and relatively strong, with $\frac{\boldsymbol{\rho_B}}{\boldsymbol{\emptyset}}\frac{\boldsymbol{k_{as}}}{\boldsymbol{k_{sa}}} = \frac{\rho_B}{\emptyset}K_d$ = 1000 (dimensionless). This assumption results in a solute retardation factor of 1001 in the absence of colloids, meaning that the breakthrough of the reactive solute is approximately 1000 times later than the breakthrough of a nonreactive species.

2.1 Radionuclides Released as Solutes: Early Breakthrough Behavior

We first consider a situation where a radionuclide is released as a solute at the entrance to the flow domain, with no initial association with colloids, but with a strong adsorption affinity to the colloids, which are present at constant concentration throughout the domain. This is equivalent to a scenario where natural colloids are assumed to be the colloids that facilitate the transport of the radionuclide. The colloids are assumed to be present at a concentration of 1 mg/L or 10^{-6} g/cm^3. To achieve this concentration while still assuming that there is a finite irreversible colloid filtration rate, we must assume that the irreversible filtration of colloids is balanced by a steady colloid production rate. Using the steady-state version of equation (11) (i.e., all derivatives set equal to zero), we see that this production rate must be given by:

$$P_c = k_{cs,ir} C_c \tag{2-20}$$

Fig. 2-1 shows the predicted breakthrough curves of colloid-associated radionuclide solute, free solute, and total solute when the solute association with colloids is given by an adsorption rate constant multiplied by τ, $k_{ac}\tau$, = 10^5 cm^3/g colloids, a dimensionless desorption rate constant $k_{ca}\tau$ = 0.1, and a dimensionless colloid filtration rate constant $\frac{SA}{V} k_{cs,ir}\tau$ = 0.1. Note that the upper plot of Fig. 2-1 has log axes whereas the lower plot has linear axes, and in both cases a curve for the radionuclide breakthrough in the absence of colloids is also shown. The partitioning of the radionuclide solute to the colloids, given by the ratio of the adsorption to desorption rate constants is 10^6 cm^3/g colloids, which is significantly stronger on a unit mass basis than the partitioning to the immobile surfaces (note that we have specified a dimensionless partitioning to immobile surfaces, $\frac{\rho_B}{\emptyset} K_d$, of 1000, so the actual partitioning will depend on the value of $\frac{\rho_B}{\emptyset}$ in the flow domain, but in all reasonable cases it will be much less than the partitioning to colloids on a mass basis). However, because the concentration of colloids is only 10^{-6} g/cm^3, the dimensionless partitioning to colloids $\frac{k_{ac}}{k_{ca}} C_c$ = 1, which is 1000 times less than the dimensionless partitioning to the immobile surfaces. Thus, at full equilibrium, we would expect 1000 times as much solute to be adsorbed to immobile surfaces as to colloids.

The upper plot of Fig. 2-1 shows that a very small fraction of the radionuclide breaks through at around t = τ, and that this fraction is essentially entirely associated with colloids. This radionuclide fraction that becomes associated with mobile colloids upon initial release and does not desorb from the colloids which in turn do not get filtered during their transit through the flow system. The fraction of radionuclide mass that becomes initially associated with colloids is approximately given by $\frac{k_{ac}C_c\tau}{1+k_{ac}C_c\tau+\frac{\rho_B}{\emptyset}K_d}$, which in this case is ~10^{-4}, although if the kinetics associated with desorption of the radionuclide from the immobile surfaces were slow, it would be given by $\frac{k_{ac}C_c\tau}{1+k_{ac}C_c\tau+\frac{\rho_B}{\emptyset}k_{as}}$. The fraction that remains associated with colloids during the transport of the colloids through the system is [exp(-$k_{ca}\tau$)][exp(-$\frac{SA}{V} k_{cs,ir}\tau$)], which in Fig. 2-1 is about 0.82. The product [exp(-$k_{ca}\tau$)][exp(-$\frac{SA}{V} k_{cs,ir}\tau$)][$\frac{k_{ac}C_c\tau}{1+k_{ac}C_c\tau+\frac{\rho_B}{\emptyset}K_d}$] is approximately the magnitude of C/C_0 at t/τ = 2 in Fig. 2-1, which is about the time that it takes for the initial concentration to be fully expressed at the discharge point of the flow system.

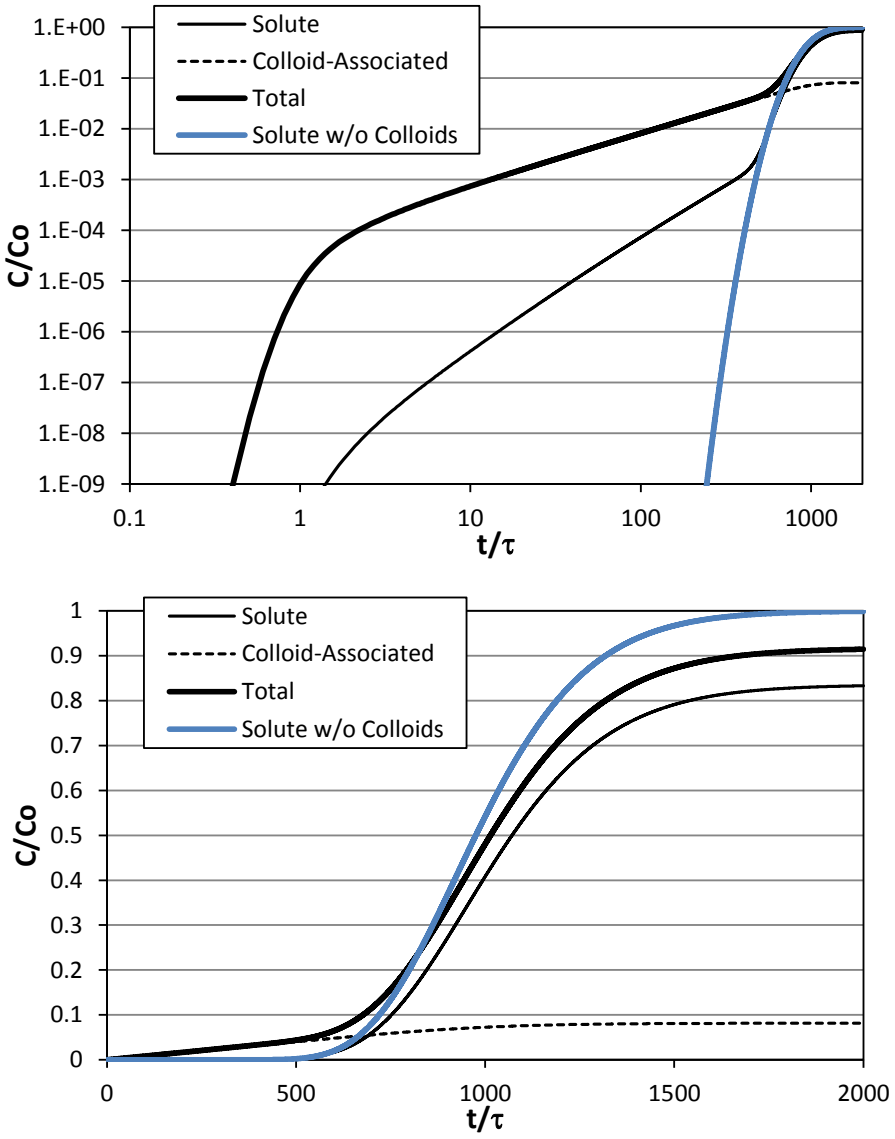

Figure 2-1. Solute, colloid-associated, and total breakthrough curves of a radionuclide assuming the following model parameter values: $k_{ac}\tau$, = 10^5 cm^3/g colloids, $k_{ca}\tau$ = 0.1, $\frac{SA}{V}k_{cs,ir}\tau$ = 0.1, $\frac{\rho_B}{\emptyset}K_d$ =1000, and C_c = 10^{-6} g/cm^3. The blue curve is the radionuclide breakthrough in the absence of colloids. Upper plot has logarithmic scales for axes, and lower plot has linear scales (same curves in each plot).

However, we note that the early colloid-associated radionuclide breakthrough concentration does not remain constant, but rather it increases steadily throughout the early breakthrough period (up until the time of the radionuclide breakthrough in the absence of colloids). This increase is approximately one order of magnitude for every order of magnitude increase in time. It occurs because the main radionuclide solute front advances linearly with time, and the colloid-associated concentrations increase at a nearly steady rate as long as the colloids remain in contact with the high solute concentrations behind the front. For a system in which radionuclide adsorption to and desorption from the immobile surfaces are considered to be at equilibrium (i.e., fast kinetics), the total increase in colloid-associated concentrations prior to the radionuclide breakthrough in the absence of colloids will be approximately $\frac{\rho_B}{\emptyset}K_d$, and the increase will be

linear in time up until $t = \frac{\rho_B}{\emptyset} K_d \tau$. In Fig. 2-1, $\frac{\rho_B}{\emptyset} K_d$ = 1000, and it is apparent that the colloid-associated concentrations indeed increase by about a factor of 1000 up until t/τ = 1000. However, it is also apparent in Fig. 2-1 that the colloids have the effect of 'dragging' solution-phase radionuclide mass along with them, causing some early breakthrough in the solution phase relative to the case with no colloids. This occurs because of the slow rate of desorption of radionuclides from the colloids. Note that if the radionuclide desorption rate from immobile surfaces is slow enough that equilibrium partitioning to immobile surfaces cannot be assumed, the rate of increase in colloid-associated concentrations prior to the colloid-free breakthrough will decrease. In the extreme case of no radionuclide desorption at all from immobile surfaces, there will be no increase in the early breakthrough concentration at all (i.e., the early breakthrough concentration will remain completely flat, and there will never be a main solute breakthrough).

The lower plot of Fig. 2-1 (linear axes) shows that the breakthrough of the bulk of the radionuclide mass is quite similar regardless of whether colloids are present or not, although the early breakthrough associated with colloids is still apparent. We note that the suppression of the late plateau of C/C_0 in the case of the colloid-associated breakthrough curve in Fig. 2-1 occurs because (1) the irreversibly-filtered colloids are still able to interact with the solute, (2) there is an unlimited number of colloid filtration sites on the immobile surfaces (allowing the colloids to accumulate indefinitely), (3) there is an unlimited number of adsorption sites on these colloids, and (4) the colloids generated to replace filtered colloids are assumed to have no radionuclides adsorbed to them. These assumptions all serve to suppress the transport of solution-phase radionuclide more than would likely be observed in a real system. It is more likely that the colloid-associated breakthrough curves would follow the colloid-free breakthrough curves once the two curves cross over, so the reader is advised to consider this to be the more plausible scenario in all remaining figures in this chapter. However, the assumptions are retained because they serve to illustrate the potential for strongly-adsorbing filtered colloids to retard radionuclide transport.

Fig. 2-2 shows what happens when $k_{ca}\tau$ is kept at a value of 0.1, but $\frac{SA}{V} k_{cs,ir}\tau$ is increased to 1 and 10. It is clear that the increase in colloid irreversible filtration rate constant results in significantly lower early breakthroughs of radionuclides associated with colloids. In these cases, the values of $[\exp(-k_{ca}\tau)][\exp(-\frac{SA}{V} k_{cs,ir}\tau)]$ are about 0.33 and 4 x 10^{-5}, respectively, and it is readily apparent in Figs. 2-1 and 2-2 that the magnitude of the early breakthroughs is roughly proportional to these values. Note that the fraction of radionuclide mass originally associated with colloids is still the same in Fig. 2-2 as in Fig. 2-1 (approximately 10^{-4}), and the rate of increase in colloid-associated breakthrough up until the time of the colloid-free breakthrough is also the same as in Fig. 2-1. We also note that the colloid-associated breakthrough curve at late times is orders of magnitude lower than the colloid-free breakthrough curve for the case of $k_{fc,ir}\tau$ = 10 because essentially all of the colloids are being filtered before passing through the system and therefore they are rapidly accumulating and adsorbing much of the radionuclide mass, which effectively imparts greater adsorption capacity to the immobile surfaces over time.

Fig. 2-3 shows a series of breakthrough curves where the value of $k_{ca}\tau$ is 1, and the values of $\frac{SA}{V} k_{cs,ir}\tau$ are, respectively, 0.1, 1, 3.16 and 10. Note that only the total radionuclide breakthrough curves are shown for these cases (not the solute and colloid-associated contributions). The values of $[\exp(-k_{ca}\tau)][\exp(-\frac{SA}{V} k_{cs,ir}\tau)]$ in these cases are, respectively, 0.33, 0.14, 0.016, and 1.7 x 10^{-5}. However, the fraction of radionuclide mass originally associated with colloids is still approximately 10^{-4}, and the rate of increase in colloid-associated concentrations is still the same because the value of $\frac{\rho_B}{\emptyset} K_d$ is unchanged. It is again clear that the magnitude of the early breakthrough is a strong function of the value of $[\exp(-k_{ca}\tau)][\exp(-\frac{SA}{V} k_{cs,ir}\tau)]$. Note that the colloid-associated breakthrough curve at late times for the case of $\frac{SA}{V} k_{cs,ir}\tau$ = 10 is considerably higher in magnitude than the corresponding case in Fig. 2-2 because the

radionuclide is desorbing ten times faster from the filtered colloids than in Fig. 2-2, which tends to keep the radionuclide mass from being retarded as much for the same value of $\frac{SA}{V}k_{cs,ir}\tau$.

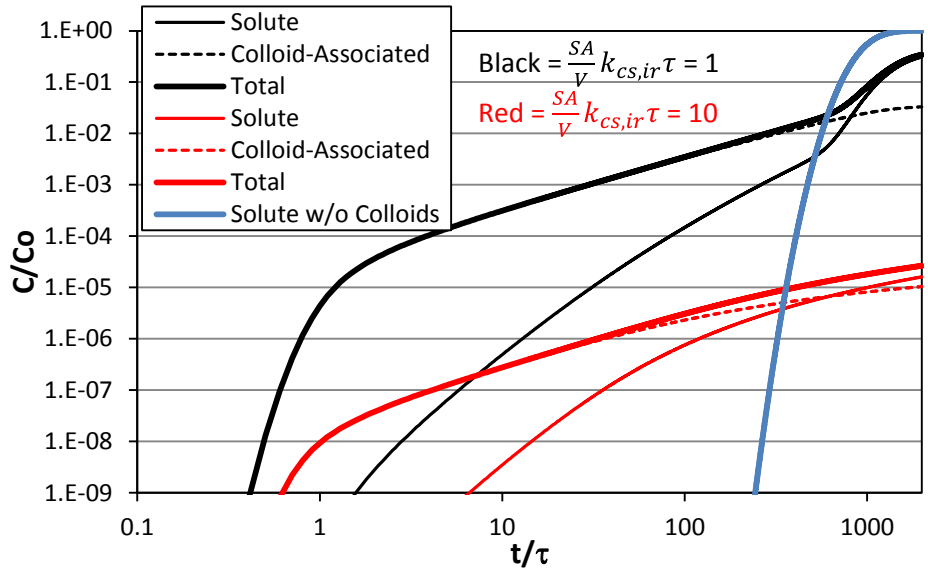

Figure 2-2. Solute, colloid-associated, and total breakthrough curves of a radionuclide assuming the same model parameters as Fig. 2-1 except with $\frac{SA}{V}k_{cs,ir}\tau$ = 1 (black) and 10 (red).

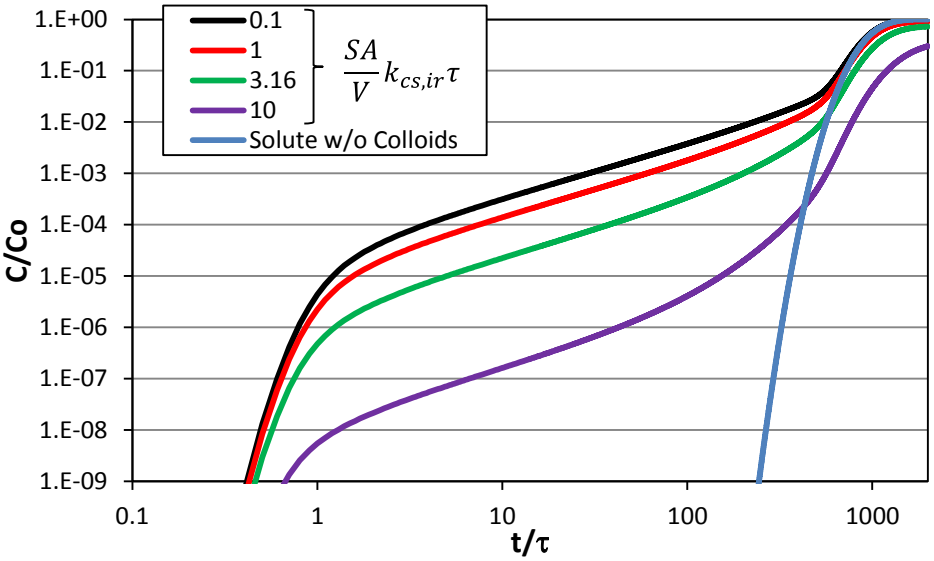

Figure 2-3. Breakthrough curves of a radionuclide (sum of solute and colloid-associated fractions) assuming $k_{ca}\tau$ is 1 (a factor of 10 higher than in Figs. 2-1 and 2-2) and the values of $\frac{SA}{V}k_{cs,ir}\tau$ are, respectively, 0.1, 1, 3.16 and 10. Other model parameters are same as in Fig. 2-1.

Fig. 2-4 is analogous to Fig. 2-3 except that in this case the series of breakthrough curves correspond to a fixed value of $\frac{SA}{V}k_{cs,ir}\tau$ = 1 and varying values of $k_{ca}\tau$ (0.1, 1, 3.16 and 10). The values of [exp(-$k_{ca}\tau$)][exp(-$\frac{SA}{V}k_{cs,ir}\tau$)] for the 4 sets of curves are the same as for the 4 sets in Fig. 2-4, and the fraction of radionuclide mass originally associated with colloids is still approximately 10^{-4}, with the value of $\frac{\rho_B}{\emptyset}K_d$ also unchanged. It is apparent that the early breakthroughs are essentially identical in Figures 2-3 and 2-4, which underscores that it is the product of the two exponential expressions that defines the magnitude of the early breakthroughs, not the individual values of either $\frac{SA}{V}k_{cs,ir}\tau$ or $k_{ca}\tau$.

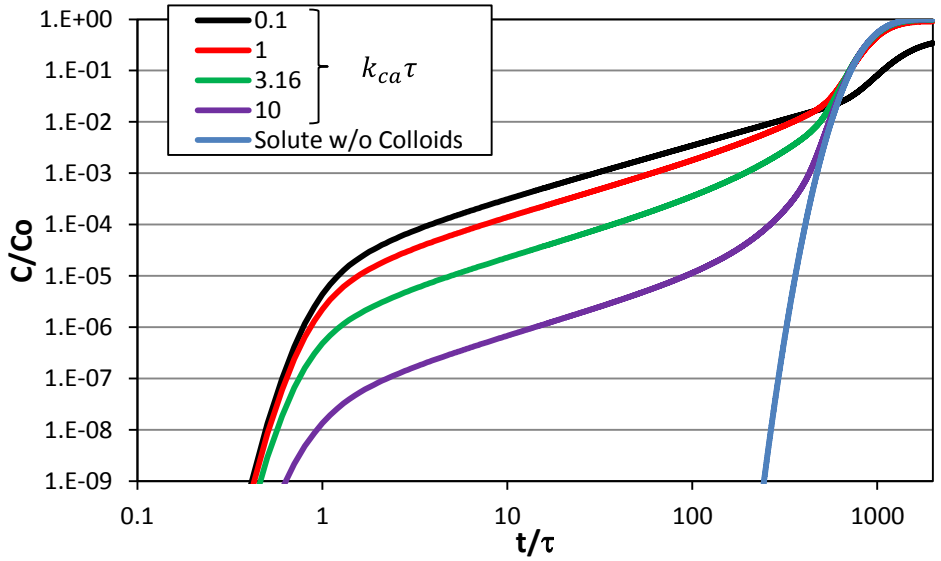

Figure 2-4. Breakthrough curves of a radionuclide (sum of solute and colloid-associated fractions) assuming $\frac{SA}{V}k_{cs,ir}\tau$ is 1 (a factor of 10 higher than in Fig. 2-1) and the values of $k_{ca}\tau$ are, respectively, 0.1, 1, 3.16 and 10. Other model parameters are same as in Fig. 2-1.

Fig. 2-5 shows the impact of increasing the rate constant for radionuclide adsorption to the colloids, k_{ac}, by one order of magnitude for $\frac{SA}{V}k_{cs,ir}\tau$ values of 0.1, 1, 3.16 and 10 while keeping the value of $k_{ca}\tau$ constant at 1. If the curves of Fig. 2-5 are compared with those of Fig. 2-3, it is apparent that the early breakthrough of the radionuclide is about one order of magnitude higher in concentration than in Fig. 2-3 for the same values of $\frac{SA}{V}k_{cs,ir}\tau$, but the shapes of the curves are otherwise very similar. This occurs because the value of $\frac{k_{ac}C_c\tau}{1+k_{ac}C_c\tau+\frac{\rho_B}{\emptyset}K_d}$ is one order of magnitude higher in Fig. 2-5 than in Fig. 2-3 (10^{-3} vs. 10^{-4}).

We note that the results of Fig. 2-5 can be reproduced almost exactly if all adsorption and desorption rate constants are kept the same as in Fig. 2-3, but the steady-state colloid concentrations are increased by an order of magnitude by increasing the steady production rate of colloids while keeping the values of $\frac{SA}{V}k_{fc,ir}\tau$ equal to 0.1, 1 and 10. Increasing the steady-state colloid concentration has exactly the same effect as increasing the radionuclide adsorption rate constant onto the colloids because it is the product of these two parameters that appears in the expression defining the initial fraction of radionuclides associated with colloids, i.e., $\frac{k_{ac}C_c\tau}{1+k_{ac}C_c\tau+\frac{\rho_B}{\emptyset}K_d}$. We do not show the results of increasing the steady-state colloid

concentrations by an order of magnitude because the curves are identical to Fig. 2-5 (other than minor changes at late times because more filtered colloids become associated with the immobile surfaces when colloid concentrations are higher, and these colloids exert a small influence on the late-time breakthrough by increasing the radionuclide retardation on the immobile surfaces).

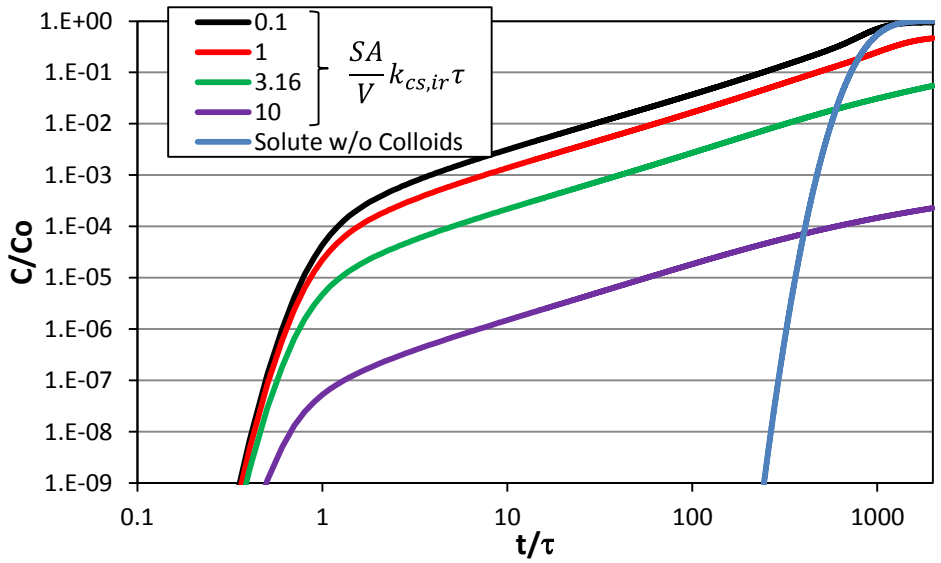

Figure 2-5. Breakthrough curves of a radionuclide (sum of solute and colloid-associated fractions) assuming $k_{ac}\tau$ is 10^6 cm^3/g colloids (a factor of 10 higher than in all previous figures) but the values of all other parameters are the same as in Fig. 2-3.

2.2 Radionuclides Released in Colloidal Form: Early Breakthrough Behavior

All of the model results presented and discussed in Section 2.1 consider the radionuclide mass to be released entirely in the solute form and that a small fraction (i.e., approximately $\frac{k_{ac}C_c\tau}{1+k_{ac}C_c\tau+\frac{\rho_B}{\emptyset}K_d}$) becomes rapidly associated with colloids. We next consider cases where the radionuclide is released entirely in colloidal form, either as an intrinsic colloid or as a waste-form degradation product or corrosion product colloid that has the radionuclide strongly associated with it when generated. In these cases, we assume that the colloidal fraction of the released radionuclide is 10^{-5}, and that no solute fraction is released, so the early breakthrough concentration can never exceed 10^{-5}. All other model parameters are the same as in the cases presented in Figs. 2-1 through 2-5.

Fig. 2-6 shows the results for a fixed value of $\frac{SA}{V}k_{cs,ir}\tau$ = 0.1 (a slow rate of colloid filtration) and varying values of $k_{ca}\tau$ (0.1, 1, 3.16 and 10, representing varying rates of radionuclide desorption from the colloids). In this case, we do not show a figure with linear axes because the values of C/C_0 always remain several orders of magnitude less than 1.0, although a colloid-free breakthrough curve is still shown for comparison on the log-log plot. Whereas in Figs. 2-1 through 2-5 the early radionuclide breakthroughs associated with colloids continually increased in concentration, the early breakthroughs in Fig. 2-6 remain essentially flat. This occurs because there is no movement of a solute front through the system as there was in Figs. 2-1 through 2-5, so the colloids do not pick up more radionuclide mass with time as they do in Figs. 2-1 through 2-5. The situation in Fig. 2-6 is essentially analogous to a case where there is no desorption at

all of radionuclides from immobile surfaces in Figs. 2-1 through 2-5. In Fig. 2-6, it is only after sufficient radionuclide mass has desorbed from the colloids that a solution phase component of radionuclide mass becomes evident, and the sum of the colloid-associated phase and the solution phase can still never exceed 10^{-5}. However, it is apparent that the product $[\exp(-k_{ca}\tau)][\exp(-\frac{SA}{V}k_{cs,ir}\tau)]$ still dictates the magnitude of the early breakthrough fraction in the same manner that it dictated the magnitude of the early breakthrough fraction in the case of solution-phase radionuclide releases. This product for the 4 curves of Fig. 2-6 is 0.82, 0.33, 0.038, and 4.1 x 10^{-5}, respectively, and it is always multiplied by the value of mass fraction initially associated with colloids to obtain the magnitude of the normalized early release concentration. For Fig. 2-6, the initial mass fraction is 10^{-5} for all cases (by assumption), and for the cases of Figs. 2-1 through 2-5 it is $\frac{k_{ac}C_c\tau}{1+k_{ac}C_c\tau+\frac{\rho_B}{\phi}K_d}$.

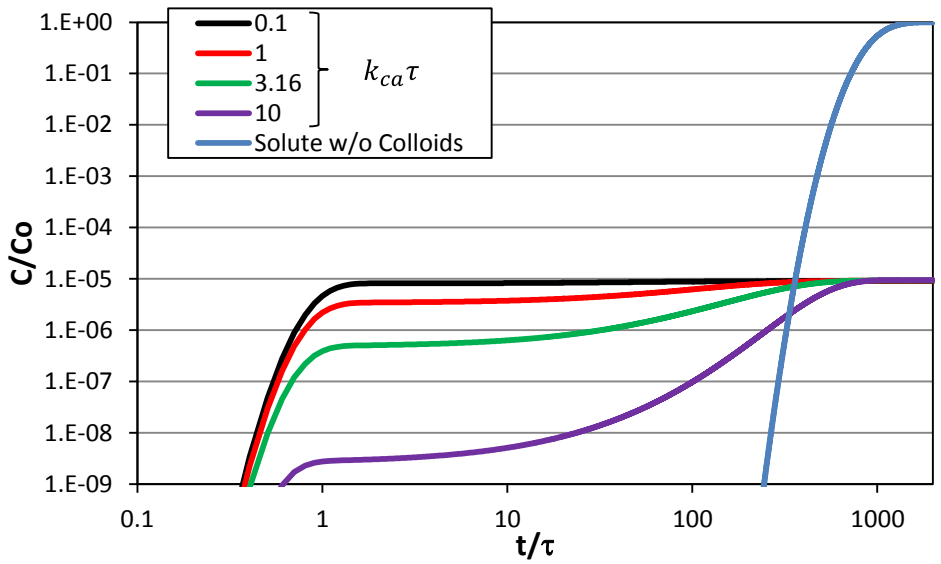

Figure 2-6. Breakthrough curves of a radionuclide (sum of solute and colloid-associated fractions) assuming a colloidal release fraction of 10^{-5}, with no solute release fraction. $\frac{SA}{V}k_{cs,ir}\tau$ is 0.1 for all cases. Other model parameters are same as in Fig. 2-4.

Fig. 2-7 shows results for a fixed value of $k_{ca}\tau$ = 0.1 (a slow rate of radionuclide desorption from colloids) and varying values of $\frac{SA}{V}k_{cs,ir}\tau$ (0.1, 1, 3.16 and 10, representing varying rates of colloid filtration). It is apparent that these breakthrough curves have essentially the same early breakthroughs as the corresponding cases in Fig. 2-6 that have the same values of the product $[\exp(-k_{ca}\tau)][\exp(-\frac{SA}{V}k_{cs,ir}\tau)]$. However, it is also apparent that the breakthroughs at late times in Fig. 2-7 are significantly lower for larger values of $\frac{SA}{V}k_{cs,ir}\tau$ than the breakthroughs at late times in Fig. 2-6 for larger values of $k_{ca}\tau$. The reason for these differences is the same as the reason for the differences observed in Figs. 2-1 through 2-5 for such combinations of $\frac{SA}{V}k_{cs,ir}\tau$ and $k_{ca}\tau$ values; i.e., larger values of $\frac{SA}{V}k_{cs,ir}\tau$ result in greater filtered colloid accumulation on the immobile surfaces, which suppresses radionuclide breakthroughs at late times because the filtered colloids impart additional retardation capacity to the immobile surfaces.

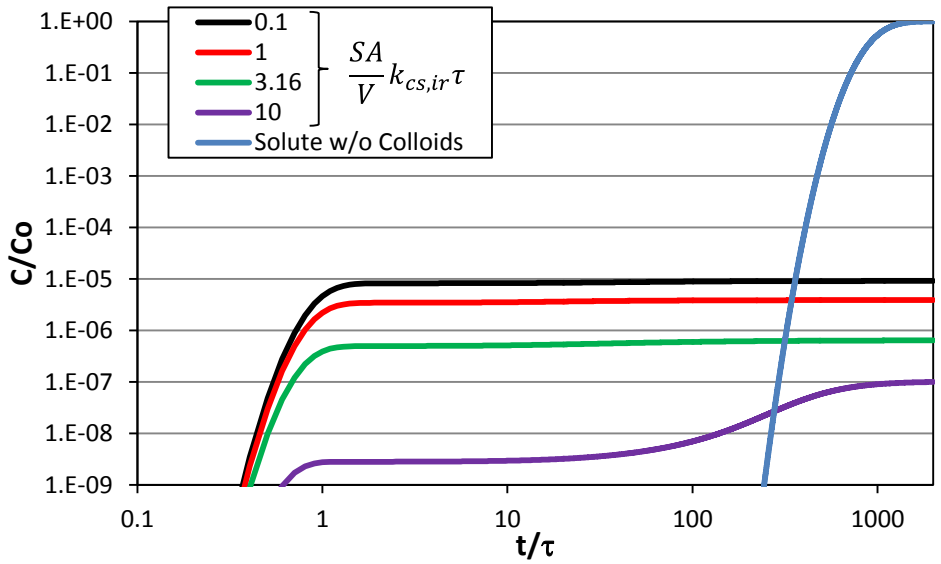

Figure 2-7. Breakthrough curves of a radionuclide (sum of solute and colloid-associated fractions) assuming a colloidal release fraction of 10^{-5}, with no solute release fraction. $k_{ca}\tau$ is 0.1 for all cases. Other model parameters are same as in Fig. 2-4.

2.3 Radionuclides Released as Solutes with Equilibrium Partitioning to Colloids: Reduced Retardation of a Large Fraction of Mass

We next consider cases where the radionuclide adsorption to and desorption from colloids is rapid relative to transport times so that equilibrium partitioning can be assumed for the radionuclide on the colloids as well as on the immobile surfaces. In this case, we revert back to the assumption that the radionuclide is released entirely in the solution phase, and it rapidly partitions between colloids, immobile surfaces and the solution phase. We assume an order of magnitude increase in steady-state colloid concentration, C_c, relative to the cases of Figs. 2-1 through 2-5, i.e. 10 mg/L or 10^{-5} g/cm^3 instead of 1 mg/L or 10^{-6} g/cm^3. We also assume the same value for K_c, or the ratio k_{ac}/k_{ca}, as in Figs. 2-1 through 2-4 (i.e., 100,000 ml/g colloid), but the rate constants are increased such that $k_{ca}\tau$ = 100, which is sufficient to approximate equilibrium partitioning onto the colloids. All other parameters are kept the same as in the cases of Figs. 2-1 through 2-5. For all of these parameter values, the effective retardation factor expression from equation (19), $\frac{1+\frac{\rho_B}{\emptyset}K_d+K_cC_c}{1+K_cC_c}$, is equal to $\frac{1+1000+1}{1+1}$ = 501. Fig. 2-8 shows that the breakthrough of the radionuclide for these parameter values indeed occurs at around t/τ = 500, which is about a factor of 2 faster than the colloid-free breakthrough at t/τ = 1000. It can also be shown that the value of $\frac{K_cC_c}{1+K_cC_c}$ is approximately the fraction of breakthrough that is predicted to be associated with colloids whereas the value of $\frac{1}{1+K_cC_c}$ is the fraction of breakthrough predicted to be in the solution phase. Both of these values are 0.5 for the parameter values selected, and Fig. 2-8 shows that the late-time colloid-associated and solute breakthroughs are both indeed C/C_0 = 0.5.

Fig. 2-9 shows the results of model calculations where the value of C_c is both increased and decreased by a factor of two relative to Fig. 2-8 while all other parameters are kept the same. The values of $\frac{1+\frac{\rho_B}{\emptyset}K_d+K_cC_c}{1+K_cC_c}$

for these two cases are 334 and 668 and the colloid-associated fractions $\frac{K_c C_c}{1+K_c C_c}$ are 0.67 and 0.33 for the increase and the decrease, respectively, in C_c. It is apparent in Fig. 2-9 that the colloid-associated, solute and total radionuclide breakthroughs conform exactly to the predictions based on these values.

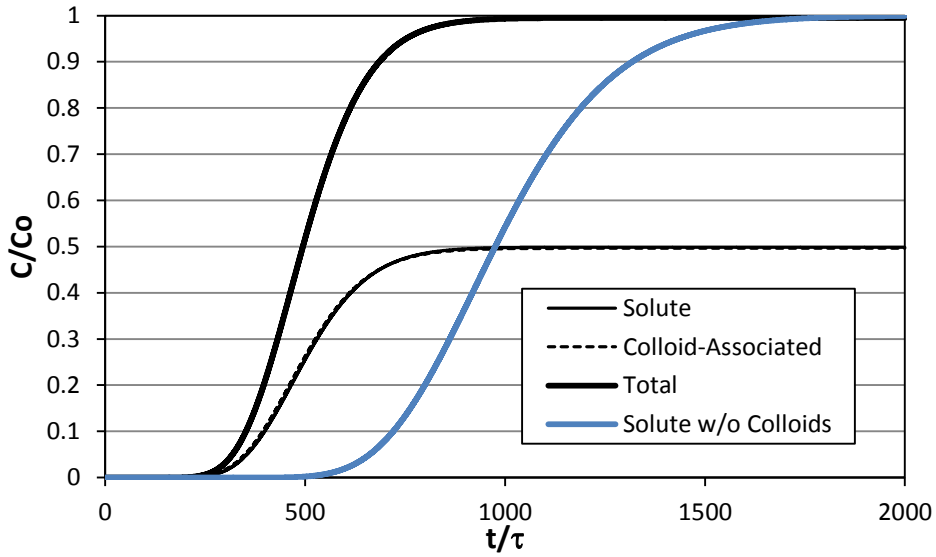

Figure 2-8. Solute, colloid-associated, and total breakthrough curves of a radionuclide assuming C_c = 10^{-5} g/cm^3, $k_{ac}\tau$, = 10^8 cm^3/g colloids, and $k_{ca}\tau$ = 100. The latter two values have the same ratio of k_{ac}/k_{ca} as in Figs. 2-1 to 2-4, but their values are large enough that equilibrium partitioning between the solute and the colloids can be assumed. The blue curve is the radionuclide breakthrough in the absence of colloids.

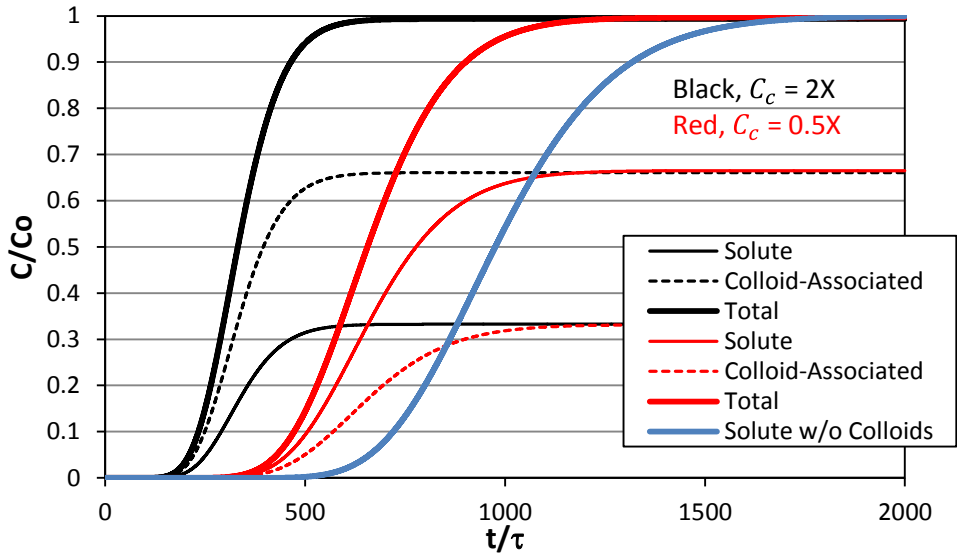

Figure 2-9. Solute, colloid-associated, and total breakthrough curves of a radionuclide assuming the same model parameters as in Fig. 2-8 except that C_c = 2 x 10^{-5} g/cm^3, or 2 times the value of C_c in Fig. 2-8 (black) and C_c = 5 x 10^{-6} g/cm^3, or half the value of C_c in Fig. 2-8 (red).

2.4 Hybrid Early Breakthrough and Reduced Retardation Behavior

One scenario that hasn't yet been discussed is a case where radionuclide adsorption to and desorption from colloids is slow enough relative to transport times that these reactions cannot be considered to be at equilibrium, yet the initial radionuclide association with colloids (i.e., $\frac{k_{ac}C_c\tau}{1+k_{ac}C_c\tau+\frac{\rho_B}{\emptyset}K_d}$) is large enough that the increase in early breakthrough concentrations of colloid-associated radionuclide approaches $C/C_0 = 1$ before a significant amount of solution-phase radionuclide breakthrough occurs. Fig. 2-10 shows the results of two model calculations where all model parameters are kept the same as in Fig. 2-1 except that C_c = 100 mg/L and 1000 mg/L, or 10^{-4} and 10^{-3} g/cm^3, respectively. Also, the dimensionless colloid filtration rate constant, $\frac{SA}{V}k_{cs,ir}\tau$, is set to a low value of 0.01, which results in minimal colloid filtration compared to other cases, and the quantity $P_c\tau$ was adjusted upward to 10^{-6} and 10^{-5} g/cm^3, respectively, so that the steady-state colloid concentrations were either 10^{-4} and 10^{-3} g/cm^3). The resulting values of the initial mass fractions of radionuclide mass associated with colloids ($\frac{k_{ac}C_c\tau}{1+k_{ac}C_c\tau+\frac{\rho_B}{\emptyset}K_d}$) are approximately 0.01 and 0.1 for these two cases, so if the colloid-associated radionuclide concentrations were to increase by an order of magnitude for every order of magnitude increase in time up until $t = \frac{\rho_B}{\emptyset}K_d\tau = 1000\tau$ (as they did in Figs. 2-1 through 2-5), the colloid-associated radionuclide concentrations would exceed $C/C_0 = 1$ long before the solute front arrives.

Fig. 2-10 shows that the increase in colloid-associated radionuclide concentrations during the early breakthrough period is initially about the same as in the cases of Figs. 2-1 through 2-5, but the concentrations level off once they approach $C/C_0 = 1$, and this leveling off occurs about an order of magnitude in time sooner for the case with the higher colloid concentrations. Thus, for scenarios such as those depicted in Fig. 2-10, it appears that the radionuclide concentrations approximately reach a value of $C/C_0 = 1$ at a time given by $t = [\frac{k_{ac}C_c\tau}{1+k_{ac}C_c\tau+\frac{\rho_B}{\emptyset}K_d}]\frac{\rho_B}{\emptyset}K_d\tau$. We note that the concentrations do not quite reach $C/C_0 = 1$ because of the retarding effect of the filtered colloids on the immobile surfaces at later times (even though the filtration rate constant was set to a low value, the high colloid concentrations in these simulations still result in a significant amount of colloid filtration).

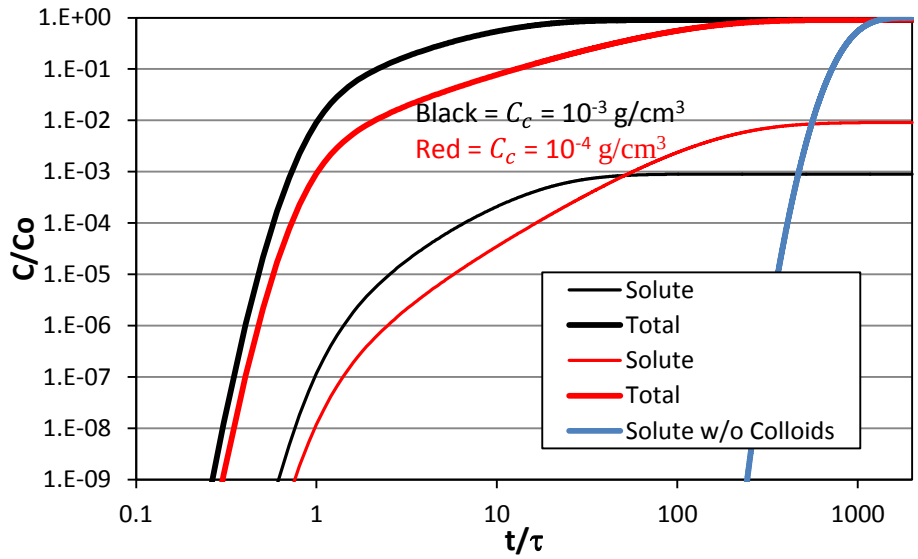

Figure 2-10. Solute, colloid-associated, and total breakthrough curves of a radionuclide assuming the model parameters of Fig. 2-1 except $\frac{SA}{V}k_{cs,ir}\tau$ = 0.01, C_c = 10^{-4} g/cm^3 (red), C_c = 10^{-3} g/cm^3 (black), which are 2

and 3 orders of magnitude greater than in Fig. 2-1. The blue curve is the radionuclide breakthrough in the absence of colloids.

2.5 General Considerations from Modeling

We can conclude that there are two primary regimes for significant colloid-facilitated radionuclide transport to be observed:

(1) A small fraction of radionuclide mass can transport essentially conservatively through a flow system if radionuclide desorption rates from colloids are slow enough that a measureable fraction of radionuclide mass remains associated with colloids during the travel time of a conservative species through the flow system *and* colloid filtration rates are slow enough that some fraction of the colloids that bear the slow-desorbing radionuclides transports through the system without filtration. If one of these conditions is not met, colloid-facilitated transport is not predicted to be observed. The radionuclide mass fraction transported conservatively will be approximately equal to $[\exp(-k_{ca}\tau)][\exp(-\frac{SA}{V}k_{cs,ir}\tau)][\frac{k_{ac}C_c\tau}{1+k_{ac}C_c\tau+\frac{\rho_B}{\emptyset}K_d}]$ if the radionuclide is initially released in the solution phase, and it will be $[\exp(-k_{ca}\tau)][\exp(-\frac{SA}{V}k_{cs,ir}\tau)]$[colloidal release fraction] if it is initially released in strong association with a colloid. In the former case, after the initial breakthrough, the concentration of the colloid-associated radionuclide will increase by approximately an order of magnitude for every order of magnitude increase in time up until the solute front of the radionuclide arrives. The latter time is given by $t = \frac{\rho_B}{\emptyset}K_d\tau$.

(2) A large fraction of radionuclide mass can be effectively transported through a flow system at a reduced retardation factor relative to transport in the absence of colloids if rates of radionuclide adsorption to and desorption from the colloids are rapid relative to conservative travel times through the flow system *and* the product of the mobile colloid concentration and the effective radionuclide partition coefficient onto the colloids is significantly greater than about 0.1. The effective retardation factor associated with the colloid-facilitated radionuclide transport in this case is $\frac{1+\frac{\rho_B}{\emptyset}K_d+K_cC_c}{1+K_cC_c}$. The breakthrough of radionuclide will consist of significant fractions that are associated with colloids and in solution, with the colloid-associated fraction being $\frac{K_cC_c}{1+K_cC_c}$ and the solution fraction being $\frac{1}{1+K_cC_c}$. For this transport regime, the filtration rate of colloids does not have an effect on radionuclide transport as long as the concentration of mobile colloids remains constant (the radionuclide adsorbs and desorbs rapidly enough from colloids that it is not affected at all by colloid filtration).

These two regimes are illustrated graphically in Figs. 2-11 and 2-12. A hybrid regime can develop if radionuclide adsorption to and desorption from colloids is slow (relative to transport times) but radionuclide concentrations are high enough and/or radionuclide adsorption rate constants onto colloids are fast enough that the fraction of radionuclide mass transported rapidly on colloids exceeds $1/(\frac{\rho_B}{\emptyset}K_d)$. In this case, there will be a relatively large conservative breakthrough fraction and an effective reduction in the retardation factor of the bulk of the radionuclide mass (relative to transport in the absence of colloids). The effective retardation factor of the bulk of the radionuclide mass in this case will be approximately $[\frac{k_{ac}C_c\tau}{1+k_{ac}C_c\tau+\frac{\rho_B}{\emptyset}K_d}]\frac{\rho_B}{\emptyset}K_d$, which represents a reduction in the colloid-free retardation factor of $\frac{k_{ac}C_c\tau}{1+k_{ac}C_c\tau+\frac{\rho_B}{\emptyset}K_d}$.

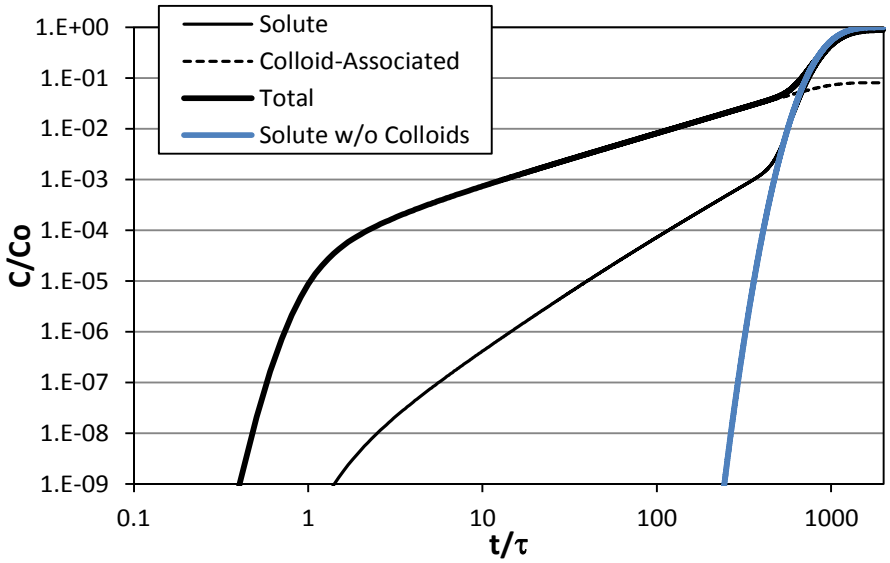

Figure 2-11. Colloid-facilitated transport regime (1): Early, essentially conservative, breakthrough of a small fraction of radionuclide mass associated with colloids.

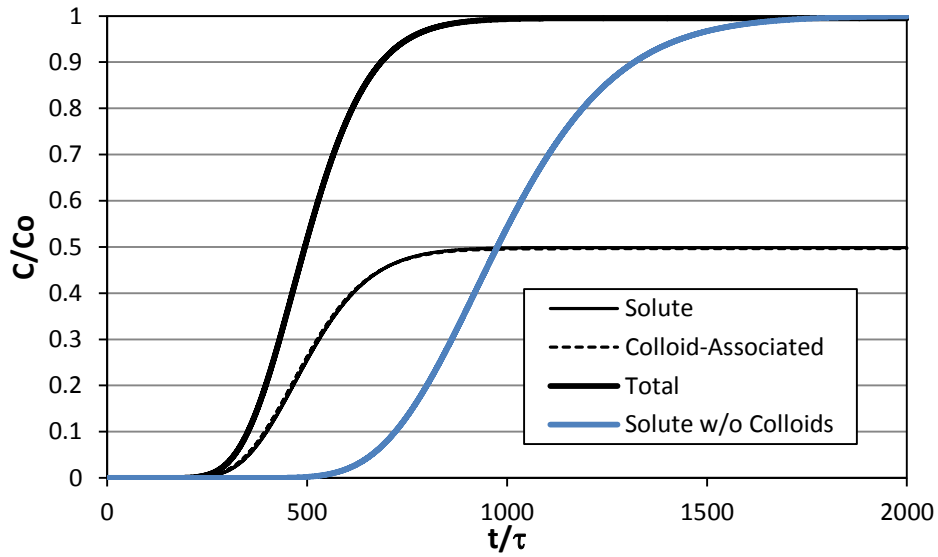

Figure 2-12. Colloid-facilitated transport regime (2): Early (but not conservative) breakthrough of a large fraction of radionuclide mass that transports with a reduced retardation factor because of colloid association.

2.6 More Complex Transport Scenarios

It must be acknowledged at this point that the concise expressions provided throughout this chapter for various mass fractions and effective retardation factors become less accurate if the simplifying assumptions used in the above model calculations are relaxed. For instance, reversible or partially reversible colloid filtration will have some effect on the shapes of the radionuclide breakthrough curves, as will slow radionuclide adsorption to and desorption from immobile surfaces. In the latter case, we have already mentioned that K_d should be replaced with k_{as} in the expression for the initial colloid-associated radionuclide fraction of transport regime (1). The situation becomes more complex when there are multiple radionuclide adsorption sites with different rate constants on both immobile surfaces and colloids, and when

the number of such sites are limited (i.e., adsorption capacity is finite rather than infinite). Furthermore, there can be a heterogeneous population of colloids that have a heterogeneous population of filtration and resuspension rate constants, and there can also be limitations on the number of either reversible or irreversible filtration sites on immobile surfaces. In dual-porosity systems, there will also be diffusive mass transfer of solute radionuclides between the primary (e.g., flowing) and secondary (e.g., nonflowing) porosity, which could significantly affect radionuclide solute transport through the flow system. Most of these processes or additional model complexities are represented in the general equations (1)-(10), but they were not considered in the model calculations used to generate the plots in this chapter or to develop the expressions for mass fractions and retardation factors.

Nevertheless, the model results and the resulting expressions are still useful for gaining perspective on what processes and parameters are important for colloid-facilitated radionuclide transport, and the overriding conclusion that radionuclide desorption rates from colloids and colloid filtration rates have the greatest impact on colloid-facilitated transport remains unchanged. Several model simulations were performed with some of the above simplifying assumptions relaxed, and the results and expressions discussed above were generally found to be still applicable, albeit with some minor deviations. These results are not presented here, but it can generally be said that in cases where multiple radionuclide adsorption sites of varying strengths or multiple colloid properties with multiple filtration rates were considered, only the radionuclide adsorption sites on colloids that had slow desorption rate constants relative to transport times (i.e., $k_{ca}\tau$ < 1-5) and the colloids that had slow filtration rate constants relative to transport times ((i.e., $\frac{SA}{V}k_{cs,ir}\tau$ < 1-5 and $\frac{SA}{V}k_{cs}\tau$ < 1-5 for all filtration sites) made a significant contribution to the early breakthrough fraction that transports conservatively in transport regime (1). All of the adsorption sites or colloids with faster rates effectively did not contribute to the early release fraction. Furthermore, these two conditions of slow desorption rates and slow colloid filtration rates were only important if they occurred *jointly* for radionuclide-colloid combinations. For instance, if slow radionuclide desorption was specified to occur only from colloids that had rapid filtration rate constants, or if slow colloid filtration occurred only for colloids that had rapid radionuclide desorption rate constants, the early breakthrough fraction was not observed (or was exceedingly small). It was only when these two conditions overlapped (i.e., radionuclides desorbed slowly from colloids that filtered slowly) that there was a significant early breakthrough fraction.

Also, the fraction of radionuclide mass that became initially associated with colloids (and was thus available for early breakthrough) in the case of solution phase radionuclide releases was governed by a complex interplay of the various radionuclide adsorption rates and adsorption site densities on both colloids and immobile surfaces. The early breakthrough mass fraction could be somewhat suppressed but would increase with time at a rate faster than the one-order-of magnitude increase per order-of-magnitude in time (discussed above) if radionuclides initially became associated primarily with adsorption sites that had fast adsorption rate constants but also had relatively fast desorption rate constants, provided there were also adsorption sites with slower desorption rate constants that better met the criteria for early breakthrough. In these cases, there tended to be a gradual increase in radionuclide association with the colloid adsorption sites having the slowest desorption rates (i.e., the strongest adsorption sites) over both time and distance because the radionuclides eventually became associated with the sites that they had the greatest affinity for, and then they tended to stay associated with these sites. If these strongest sites happened to be on colloids that had slow filtration rates, then the early breakthrough fraction increased significantly with time, but if the strongest sites were on immobile surfaces, then the early breakthrough fraction tended to not increase as rapidly.

For cases where transport regime (2) applied, the most important consideration when there were multiple radionuclide adsorption sites on colloids and immobile surfaces was that the existence of any very strong adsorption site or any site with a very slow desorption rate on immobile surfaces could greatly suppress the early breakthrough of the radionuclide (i.e., increase the value of the effective retardation factor and/or decrease the fraction of radionuclide mass that transported with the smaller effective retardation factor).

Essentially, any adsorption site on immobile surfaces with a slow desorption rate constant relative to transport times could effectively negate the early breakthrough behavior in regime (2). Colloid filtration rate constants had no effect on the observed breakthrough behavior in this regime unless there was also at least one adsorption site on colloids that had a very slow desorption rate constant relative to transport times. In this case, if colloid filtration occurred, the radionuclide mass fraction that transported with the smaller effective retardation factor decreased, but the retardation factor associated with this mass fraction was not affected. In general, if all radionuclide adsorption reactions were fast relative to transport times in the system, then the effective retardation factor expression could be expanded to include multiple sites on both colloids and immobile surfaces as follows:

$$R_{effective} = \frac{1+\sum_i^{nsites}\left(\frac{S_{a,max,i}}{\sum_i^{nsites} S_{a,max,i}}\right)\frac{\rho_B}{\emptyset}K_{d,i}+\sum_i^{ncolsites}\left(\frac{S_{ac,max,i}}{\sum_i^{ncolsites} S_{ac,max,i}}\right)K_{c,i}C_c}{1+\sum_i^{ncolsites}\left(\frac{S_{ac,max,i}}{\sum_i^{ncolsites} S_{ac,max,i}}\right)K_{c,i}C_c} \quad (2\text{-}21)$$

We note here that equation (21) does not allow for the possibility that different types of adsorption sites could occur on different types of colloids (the colloid population is treated as homogeneous). A heterogeneous colloid population would be addressed by using a double summation over both the number of adsorption sites on colloids and the number of different types of colloids in the last terms of both the numerator and denominator.

2.7 Implications for Risk Assessments and for Key Process/ Parameter Interrogations

There are many implications of the modeling results presented in the preceding sections for nuclear waste repository risk assessments. We start by discussing colloid-facilitated radionuclide transport regime (2), which is inherently the much easier regime to evaluate for its potential to contribute to radionuclide concentrations or fluxes at a compliance boundary. This regime generally requires large colloid concentrations and/or relatively strong equilibrium partitioning of radionuclides to the colloids relative to partitioning to immobile surfaces in a flow system to result in significant colloid-facilitated transport.

In principle, it should be possible to determine steady-state colloid concentrations by sampling wells, ideally at a range of sampling rates, to obtain upper bound estimates of colloid concentrations that are likely to exist over long periods in a repository system. Furthermore, because regime (2) is dominated by equilibrium partitioning of radionuclides to surfaces, it should be possible to conduct experiments to obtain estimates of bulk radionuclide partition coefficients to both colloids and immobile surfaces under appropriate geochemical conditions. These experiments need not be concerned with multiple different types of radionuclide adsorption sites, with a heterogeneous population of colloids, or with colloid filtration rates. However, they should be conducted with both representative colloids and immobile surfaces in the experimental system because the primary concern is whether enough radionuclide mass can be partitioned to colloids in the presence of representative immobile surfaces to result in a significant mass fraction of radionuclide mass being transported in accordance with a reduced retardation factor given by equation (21). If the fraction of radionuclide mass associated with colloids under equilibrium partitioning conditions is shown to be less than about 0.01, then transport regime (2) can be dismissed as being a concern. These experiments should be conducted over a sufficient range of conditions, including radionuclide concentrations, to address all potential geochemical conditions and colloid types that may occur in the repository system.

Consideration should be given to conducting experiments at successively higher colloid concentrations to try to determine a threshold colloid concentration at which partitioning to the colloids exceeds 0.01. Such experiments may show that colloid concentrations have to be so much higher than can be reasonably expected in a repository system that even if there is considerable uncertainty associated with the partitioning measurements, it is very unlikely that transport regime (2) will be a concern. Consideration might also be given to "stacking the deck" in favor of colloid partitioning by first associating the radionuclide with

colloids and then introducing the colloid-associated radionuclides to an experimental system containing the immobile surfaces. If longer-term partitioning to colloids can be shown to be below a threshold of concern (such as 0.01) in such an experiment, then it would be more defensible to eliminate transport regime (2) as a concern.

Transport regime (1) is the much more difficult regime to evaluate and parameterize for repository risk assessment scenarios than transport regime (2), and even if the results of the above-suggested experiments indicate that regime (2) is not a concern, regime (1) may still be a concern under exactly the same conditions. The primary problem with addressing transport regime (1) is that the radionuclide desorption rate constants from colloids and the colloid filtration rate constants that are slow enough to make this regime a concern are typically much too slow to be fully interrogated in experiments of reasonable duration. Analytical limitations and other random experimental errors typically make it very difficult to distinguish a first-order rate constant less than 1% of the inverse of the time scale of an experiment from a rate constant of zero, and 1% is even quite optimistic. Thus, if a measurable mass of radionuclide still remains adsorbed to colloids or a measurable mass of colloids remains unfiltered at the end of an experiment, we cannot say whether this remaining mass has a desorption rate constant or a filtration rate constant that is just barely less than 1% of the inverse time scale of the experiment or if it has a desorption rate constant of zero. From a practical standpoint, this means that if an experiment lasts one year, we will not be able to effectively distinguish a rate constant less than 0.01 yr^{-1} from zero. However, if we are dealing with a repository risk assessment where time scales for flow and transport may be several hundreds or thousands of years or more, then a rate constant of 0.01 yr^{-1} vs. a rate constant of zero will be the difference between virtually no colloid-facilitated radionuclide transport (0.01 yr^{-1}) and a considerable amount of colloid-facilitated transport (zero) according to transport regime (1). The only way we can eliminate transport regime (1) as a concern in this case, barring an experiment lasting several decades or longer, is if *all* the radionuclide mass desorbs from colloids or *all* the colloid mass filters during an experiment. Alternatively, it might be possible to show that the *joint* colloid-facilitated radionuclide mass fraction (i.e., the product of the radionuclide fraction that does not desorb from colloids and the fraction of colloids hosting such non-desorbing radionuclides that do not filter) can be tolerated in a repository risk assessment. That is, if a risk threshold is not exceeded if this entire joint radionuclide mass fraction were assumed to transport conservatively, then it may be possible to eliminate colloid-facilitated radionuclide transport by regime (1) as a concern.

Failing that, we are left with inconclusive results about the potential for a small amount of colloid-facilitated transport according to regime (1). However, we can at least place an upper bound on the radionuclide mass that may potentially be involved in such transport (i.e., the mass fraction recovered in a given experiment). We also can assign a lower bound to either the radionuclide desorption rate constant from colloids or the colloid filtration rate constant for the fraction of radionuclide or colloid mass that *did* desorb or filter during an experiment. Another experimental option is to evaluate colloid facilitated transport at natural analog sites that may provide evidence for the presence or absence of regime (1) at repository timescales.

The above dilemma would be less of a problem if a system were entirely homogeneous with a single type of adsorption site on colloids and on immobile surfaces and a single type of colloid with a single set filtration rate constants because then any observed desorption or filtration could be assumed to be part of a first-order process that could be extrapolated beyond the end of the experiment. However, such homogeneity is almost never observed in complex real systems, and we must therefore consider any observation of radionuclide desorption rates or colloid filtration rates in a heterogeneous system to be a composite expression of the behavior resulting from many different types of sites and colloids. This means that if there is *any* remaining undesorbed radionuclide mass or unfiltered colloid mass at the end of an experiment, we cannot rule out the possibility that there are some adsorption sites with extremely slow desorption rate constants or some colloids with extremely slow filtration rate constants. In fact, some fraction of the radionuclide mass may be associated with the colloid by mechanisms other than strict surface adsorption (e.g. coprecipitation, surface precipitation) and may lead to drastically lower apparent desorption rates.

2.8 Potential Experimental Approaches to Interrogate Colloid-Facilitated Radionuclide Transport Parameters for Transport Regime (1)

In this section, some potential approaches are discussed for addressing the significant challenges associated with interrogating the very slow radionuclide desorption or colloid filtration rate constants that typify colloid-facilitated transport regime (1). While it is not possible to address all potential experimental methods that may be relevant, we cover many that have been pursued as well as a few ideas for extending these methods. Case studies of a few selected methods are presented in subsequent chapters of this report.

One potential approach to addressing the problem of interrogating the very slow radionuclide desorption or colloid filtration rate constants that are the hallmarks of colloid-facilitated transport regime (1) is to conduct similar experiments to interrogate the rate constants over different time or distance scales. This approach cannot rule out the possibility of very slow rate constants that could be problematic (assuming some mass remains adsorbed or unfiltered), but it can establish whether a favorable scaling trend occurs that, if extrapolated, would result in a fast enough rate constant relative to the time scale of interest that an acceptably small mass fraction of radionuclide would be predicted to be transported according to regime (1) – or alternatively, it could help place upper bounds on mass fractions that may transport according to regime (1). An example of such an approach is discussed in Chapter 3 of this report, where a total of six colloid-facilitated radionuclide or homologue transport experiments are evaluated for their time-scale dependence of both solute desorption rate constants from colloids and colloid filtration rate constants to gain insights into the potential for colloid-facilitated transport by regime (1). (Note that a 'homologue' is a nonradioactive surrogate for a radionuclide.) These experiments were conducted in a fractured granodiorite at the Grimsel Test Site in Switzerland, and while the time scales of the tests fell well short of the time scales relevant to repository risk assessments, the trends suggest that there is a potential for radionuclide desorption rate constants from colloids to be slow enough (from some adsorption sites) that transport regime (1) might be a concern, depending on repository time scales.

Another approach, which represents a variation of the above approach, is to conduct colloid-facilitated transport experiments, such as column experiments, in series, where the effluent from one column is injected into the next column. With this approach, the strong influence of the faster rates can be effectively removed in the first column, and the second column can be used to interrogate slower rates, and the process can be continued for as long as colloids or radionuclides remain above detection limits in the effluent of each successive column. A couple of case studies of this approach are discussed in Chapter 4. A logical alternative to this approach would be to set up a very long column that can be sampled at different distances along its length. The principal limitation with this approach would be the ability to obtain samples large enough to analyze for low concentrations of colloids and/or radionuclides without disturbing flow in the column.

For interrogating very slow radionuclide desorption rates from colloids, a popular technique is to first adsorb the radionuclides onto the colloids and then conduct long-duration desorption experiments in which the radionuclide-bearing colloids are continually exposed to radionuclide-free water. These types of experiments can also be conducted on radionuclide-bearing colloids taken from either field or laboratory systems where the strong association with colloids may be a result of processes in which the radionuclides became incorporated into the colloid structure or possibly even as a result of intrinsic colloid formation (e.g., waste form degradation/alteration experiments, or samples taken from contaminated field sites).

The exposure to radionuclide-free water in these experiments can be accomplished by successive batch replacements (or partial replacements) of the water after centrifugation and decantation to remove radionuclide-bearing but colloid-free water from a batch reactor. It can also be accomplished by using a continuous-flow reactor where the radionuclide-free water is continuously introduced while radionuclide-bearing water is removed at the same rate by passing it through an ultrafine membrane filter while the contents of the reactor are kept stirred to avoid colloid settling or filtration on the filter. Aliquots of the

removed solution in either case are analyzed for radionuclide concentrations to provide detailed estimates of time-dependent rate constants for desorption from colloids (which in turn can be translated into multiple desorption rate constants from multiple adsorption sites). These experiments provide no information on colloid filtration in a representative flow system, but they have the advantage that they can be conducted for very long time scales – generally longer than can be accomplished in a column or field experiment. A case study of a set of continuous-flow reactor experiments in which slow plutonium desorption from clay colloids was interrogated is included in Chapter 6. These experiments are of particular interest because they illustrate that transformations of the sorbed radionuclide on colloid surfaces (in this case reduction of Pu(V) to the much more strongly-adsorbing Pu(IV)) can have a significant influence on colloid-facilitated transport.

Desorption experiments such as those described above can also be conducted in batch or flow reactors that include the immobile surfaces that occur in the repository system being studied. Huber et al. (2011) conducted such a set of "ternary" system experiments in which radionuclide desorption rates from colloids were measured in the presence of competing mineral surfaces present in the Grimsel Test Site system. These experiments should in principle maximize the potential for radionuclide desorption from colloids relative to a "binary" system that has only suspended colloids, thus providing a more realistic representation of the system that will be encountered in a repository setting. Xie et al. (2014) also recently conducted some ternary adsorption and desorption experiments with plutonium.

An additional experimental technique that could yield valuable insights into colloid-facilitated radionuclide transport is to purposely introduce flow or geochemical perturbations into any of the above experiments to induce radionuclide desorption from colloids or resuspension of filtered colloids. Such experiments may provide information that allows distinction between truly irreversible adsorption of radionuclides onto colloids (i.e., zero desorption rates) and just very slow desorption that is otherwise difficult to observe without the perturbations. Likewise, experiments with perturbations may allow distinction between truly irreversible colloid filtration and just very slow resuspension rates, which could have significant implications for transport behavior over long time and distance scales. If mechanistic underpinnings are known for the effects of the transient conditions imposed, it may be possible to effectively translate the rates observed under these imposed conditions to rates that would be observed (but are too slow to observe) under more steady conditions. This technique has not been fully exploited to our knowledge, although there are undoubtedly challenges with making defensible translations of observations under perturbed conditions to predictions under more steady conditions. However, flow and geochemical perturbations will also potentially occur in repository environments, and in fact, can probably be expected to occur over the long time scales of interest for repository risk assessments, so the response to perturbations may be directly applicable to certain scenarios.

Finally, it is important to couple any of the above experimental approaches with state-of-the-art colloid and radionuclide surface characterization methods to obtain valuable complementary information for estimating/bounding colloid-facilitated radionuclide transport or for suggesting more focused experiments to tease out important behavior. These characterization methods take on special importance when one considers that it is only the *joint* occurrence of very slow radionuclide desorption rates from colloids and very slow colloid filtration rates that result in significant colloid-facilitated transport according to transport regime (1). For instance, it would be very important to know if colloids that tend to be resistant to filtration fall within a certain size range or have a certain mineralogy or surface charge characteristics. If such knowledge is gained, then more focused experiments can be conducted with colloids having these characteristics to better understand their interactions with radionuclides and determine if their favorable transport characteristics also coincide with strong radionuclide affinities (i.e., slow desorption rates). Similarly, it would be very important to know the radionuclide surface species and mineral associations corresponding to adsorption sites that have very slow desorption rates, so that more focused experiments could be conducted using colloids that have a greater abundance of such sites to determine if such strong adsorption sites occur on colloids with favorable transport characteristics.

3. RADIONUCLIDE AND NONRADIOACTIVE HOMOLOGUE COLLOID-FACILITATED TRANSPORT AT THE GRIMSEL TEST SITE, SWITZERLAND

The Grimsel Test Site (GTS) in Switzerland has hosted the most extensive and carefully-controlled set of colloid-facilitated solute transport experiments that have ever been conducted in a non-laboratory setting. The GTS is an Underground Research Laboratory situated in a crystalline granodiorite in the Swiss Alps. Three colloid-facilitated radionuclide transport experiments were conducted at the GTS between 2002 and 2013, and three additional colloid-facilitated homologue transport experiments were conducted between 2008 and 2010. The results and interpretations of all these experiments have been presented and discussed in previous Used Fuel Disposition project reports (Wang et al., 2013, Ch. 2; Wang et al. 2014b, Ch. 7, and Viswanathan et al. 2016, Ch. 2), so only a combined summary is provided here, with emphasis on what the results imply for colloid-facilitated radionuclide transport over long time and distance scales. These tests serve to illustrate the experimental approach of varying transport times in the same system to gain insights into the time-scale dependence of both radionuclide/homologue desorption rates from colloids and colloid filtration rates.

Fig. 3-1 shows the configuration of all the tests, which were conducted within a single highly-transmissive shear zone (a roughly planar flow feature or large fracture) at the GTS. All tests were conducted either in a dipole flow configuration between two boreholes located 2.23 m apart or from a borehole to a surface packer in the access tunnel wall, with a separation distance of 5.71 m. The tunnel serves as a hydrologic sink for the shear zone, so the surface packer actually holds back flow at a controlled rate, which allowed tests of different travel times to be conducted. The colloids used in all tests were generated by dispersing a bentonite taken from a Spanish mine in groundwater from the GTS; this bentonite (called FEBEX bentonite) was also used in a long-term heater test at the GTS that is currently undergoing a cool-down and mine-back phase. Solutes were placed in contact with the resulting colloids before being injected into the shear zone as a solute-colloid mixture, or "cocktail". The colloid associations of each solute were measured prior to (or in one case after) injection of the cocktail.

In the experiments, the transport of the radionuclides ^{137}Cs, Pu and Am (various isotopes of the latter two) were consistently shown to be governed by their association with the bentonite colloids. Additionally, the trivalent homologues Eu and Tb and the tetravalent homologues Hf and Th were also shown to be strongly associated with colloids. In all these cases, a majority of the solute (sometimes exceeding 99%) was associated with the colloids in the injection cocktails, and their observed breakthrough curves appeared to be governed mainly by their desorption rates from the colloids (i.e., according to colloid-facilitated transport regime 1). Fig. 3-2 shows the collective log time dependence of the log desorption rate constants from colloids for the trivalent radionuclides or homologues (Eu, Tb, and Am), as well as for ^{137}Cs. Fig. 3-3 shows the collective log time dependence of the log desorption rate constants from the colloids for the tetravalent radionuclides and homologues. Finally, Fig. 3-4 shows the collective log time dependence of the irreversible log colloid filtration rate constants ($\frac{SA}{V}k_{cs,ir}$) in all experiments. All of the rate constants were estimated with the assumption that there was only one type of adsorption site for solutes on colloids and only one irreversible filtration reaction for colloids. In Figs. 3-2 through 3-4, the rate constants with the greatest uncertainty are at the low end of the transport time scale, as these correspond to tests that were so short that it was difficult to distinguish between a finite colloid filtration rate constant or a finite solute desorption rate constant (for tetravalent species in particular) and a rate constant of zero. The values plotted in these cases are upper-bound estimates of rate constants that still match the observed data quite well.

Although lumping all the trivalent species (and ^{137}Cs) in Fig. 3-2 and all the tetravalent species in Fig. 3-3 is obviously taking some liberties in that it implicitly assumes that the different elements all behave similarly, it is nonetheless apparent from comparing the two figures that the tetravalent species appear to

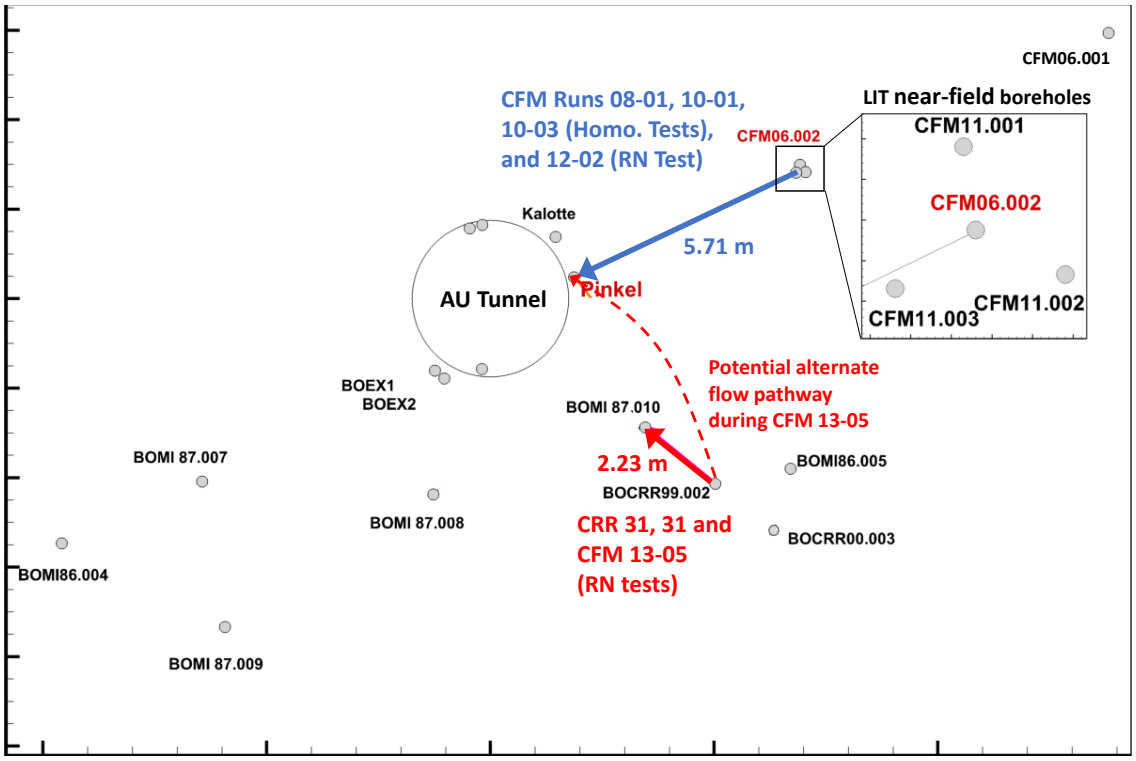

Figure 3-1. Configuration of colloid-facilitated radionuclide (RN) and homologue (Homo.) transport experiments at the Grimsel Test Site between 2002 and 2013. Boreholes and access tunnel are shown in the plane of the shear zone (shear zone is sub-vertical, tunnel and boreholes are sub-horizontal). "Pinkel" is a surface packer used for collection of water.

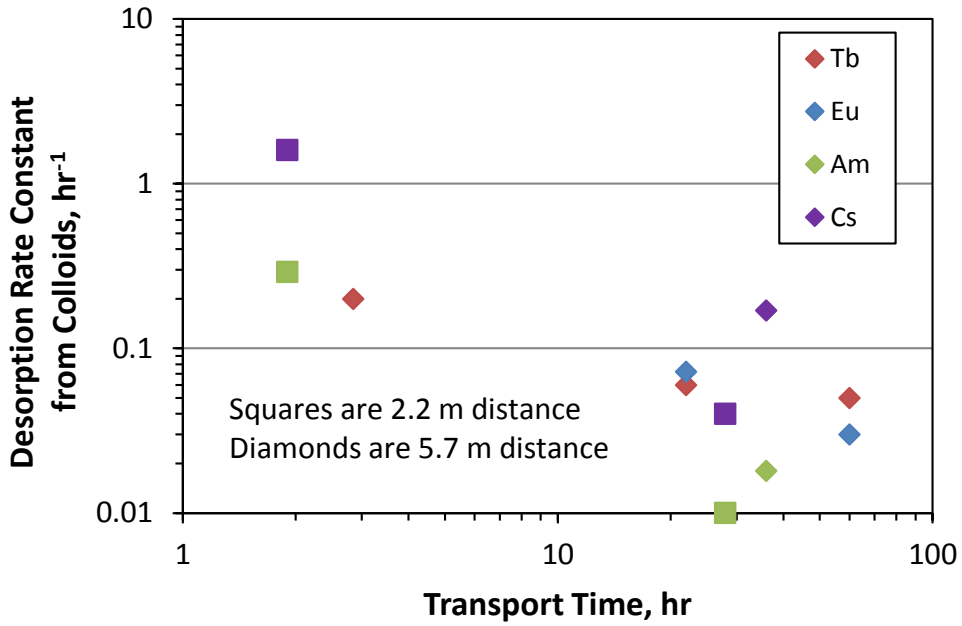

Figure 3-2. Log transport time dependence of desorption rate constants from colloids for the trivalent radionuclides or homologues Eu, Tb, and Am, and for ^{137}Cs in the GTS field experiments.

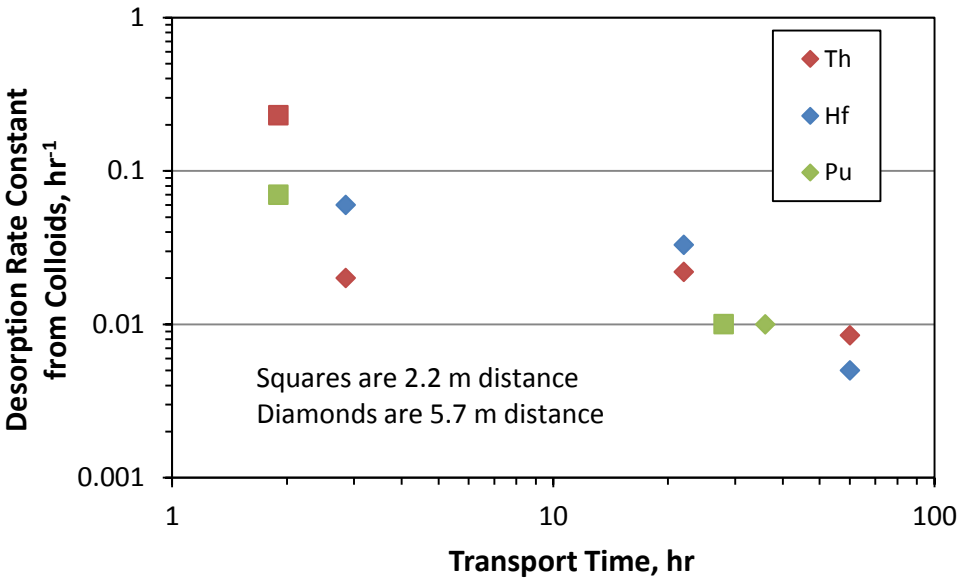

Figure 3-3. Log transport time dependence of desorption rate constants from colloids for the tetravalent radionuclides or homologues Th, Hf, and Pu for the GTS field experiments.

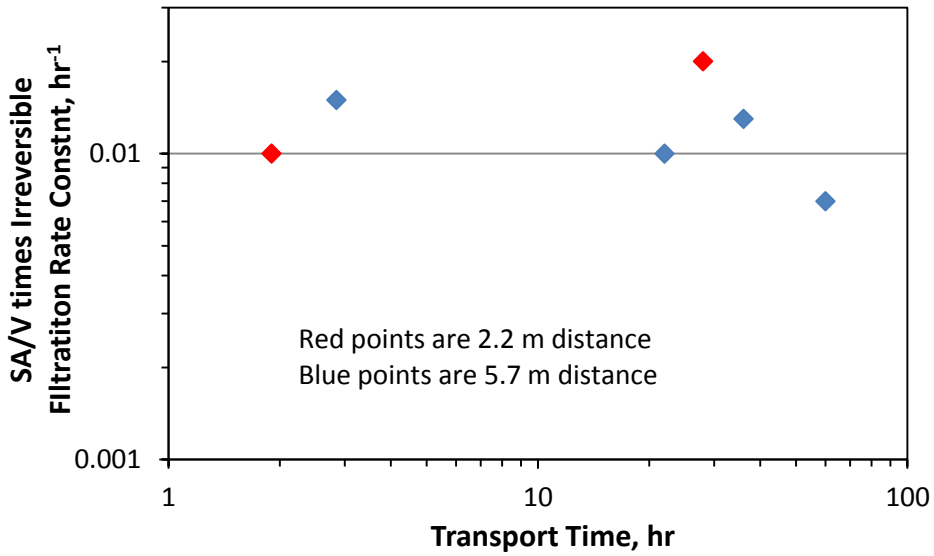

Figure 3-4. Log transport time dependence of irreversible colloid filtration rate constants ($\frac{SA}{V} k_{cs,ir}$) in the GTS field experiments.

have somewhat slower desorption rate constants from colloids than the trivalent species. It also appears that ^{137}Cs desorbs somewhat faster from colloids than the trivalent species (Fig. 3-3). Fig. 3-4 shows there is not nearly as strong of a time dependence for colloid filtration rate constants as there are for the radionuclide desorption rate constants. In fact, it would be hard to conclude that there is any time dependence.

Fig. 3-5 shows the deduced tetravalent solute desorption rate constant data plotted as a function of travel time with a linear extrapolation to longer times on the log-log plot. This figure also shows a range of potential extrapolations that could result in either no colloid-facilitated solute transport at longer times (if desorption rate constants do not decrease much more with time) or a considerable amount of colloid-facilitated transport at longer times (if desorption rate constants decrease more than the linear trend predicts with time). The dashed line in Fig. 3-5 is a fit to the log-log data, and it has a slope of -0.69, which indicates that the log of the desorption rate constant does not decrease as rapidly as the log of time increases. Thus, as time scales increase, the product $k_{ca}\tau$ will continually increase, and the fraction of solute remaining associated with colloids (exp(-$k_{ca}\tau$)) will decrease with time. For the dashed-line extrapolation of Fig. 3-5, it would be predicted that about 1% of the solute initially adsorbed to colloids would remain adsorbed after 100,000 hours, or 11.4 years, and less than 0.01% would remain adsorbed after 1,000,000 hours, or 114 years. While these are small fractions, they might still result in measurable radionuclide concentrations at a compliance boundary if transport time scales are on the order of 10 to 100 years.

However, if one considers the apparent lack of a time dependence of the colloid filtration rate constants ($\frac{SA}{V}k_{fc,ir}$) in Fig. 3-4, or even if one extrapolates a shallowly-sloping line through the data points, it would be concluded that the value of $\frac{SA}{V}k_{cs,ir}$ at about 100,000 hours or more would likely remain above 0.001 hr^{-1}. Thus, the value of $\frac{SA}{V}k_{cs,ir}\tau$ at 100,000 hrs (about 11.4 years) would be 100 or more. If we consider the product [exp(-$k_{ca}\tau$)][exp(-$\frac{SA}{V}k_{cs,ir}\tau$)] to be the fraction of colloid-associated radionuclide mass that can transport conservatively, then we would predict that this fraction would be only [0.01][4 x 10^{-44}] = ~1 x 10^{-46} for an 11.4-year travel time (even if essentially all the radionuclide mass were initially associated with colloids). Therefore, essentially no colloid-facilitated solute transport would be predicted for any of the tetravalent solutes. Although not shown in a plot, if we repeat the exercise of Fig. 3-5 above for the trivalent solutes (excluding ^{137}Cs), we would predict that only 0.0002% of these solutes would remain adsorbed to colloids after 11.4 years, so colloid-facilitated transport would be predicted to be even less likely for the trivalent species. However, it must be acknowledged that the uncertainty in the slope of the line of Fig. 3-5 is rather large, and if the slope were to approach -1, then the log solute desorption rate constants would be predicted to decrease nearly as rapidly as the log of time increases, and the implication would be that a similar fraction of radionuclide mass would remain adsorbed to colloids for very long times.

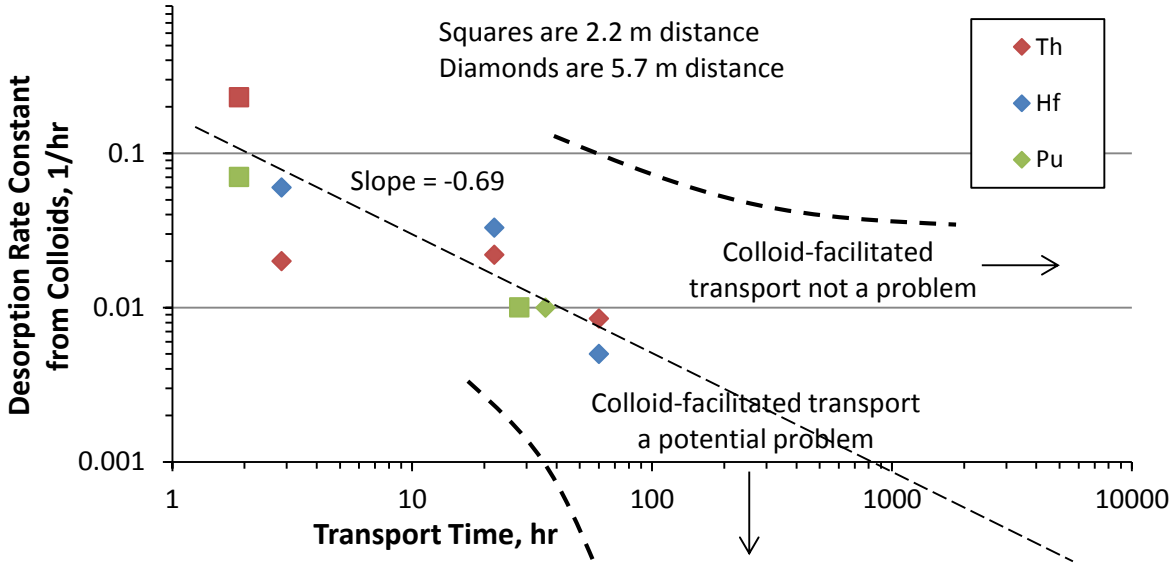

Figure 3-5. Extrapolation of log dependence of tetravalent solute desorption rate constants from colloids in GTS field experiments. Dashed line is a linear regression fit to the data.

One of the problems with drawing a conclusion of essentially no colloid facilitated transport over any repository-relevant time scale for the GTS system is that it hinges mainly on the observed colloid transport behavior because the $\exp(-\frac{SA}{V}k_{cs,ir}\tau)$ term dominates the product $[\exp(-k_{ca}\tau)][\exp(-\frac{SA}{V}k_{cs,ir}\tau)]$ that leads to the prediction of no colloid-facilitated transport of radionuclides. Given that there was never less than about 35% recovery of the colloids in any of the tests relative to the recovery of a conservative tracer (and essentially 100% recovery in the two shortest tests), it seems very tenuous to assume that 35% of the colloid mass will have filtration rate constants that are essentially the same as or only slightly smaller than all the colloids that were filtered. On the other hand, it seems very plausible that there may have been have been a few percent of colloids that had much smaller effective filtration rate constants than the rate constants deduced from the model interpretations. The assumption that all colloids in a given test had the same filtration rate constant has the effect of biasing the estimated filtration rate constants to larger values to accommodate the fraction that is filtered. Even if up to 10 percent of the colloids in each test had filtration rate constants of zero, the impact that these colloids would have on the model-estimated filtration rate constants would be very minimal because the *bulk observed* behavior still reflects a finite filtration rate constant. Furthermore, because there was essentially 100% colloid recovery in the two shortest-duration tests, the filtration rate constant estimates for these tests cannot be distinguished from zero.

Although it does not completely address the problem of the uncertainty in knowing what the true filtration rate constants are for the unfiltered colloids in any test, another way of assessing the potential for some colloids to remain unfiltered for long times is to extrapolate a plot of colloid recovery divided by conservative solute recovery vs. log travel time for a series of tests of different time scales. The colloid recovery relative to conservative solute recovery is not converted to log scale because, in principle, it is a function of $\exp(-\frac{SA}{V}k_{cs,ir}\tau)$, and if the natural log of this quantity is taken, it will translate to a non-log function. Such a plot is provided for the GTS tests in Fig. 3-6, and although the extrapolation is obviously somewhat tenuous, it would suggest that up to 10% of the colloid mass may remain unfiltered (or at least travel nearly conservatively) over time scales of up to 1000 hours, or about 0.11 years. In contrast, even if the plot of Fig. 3-4 is extrapolated to a relatively small value of 0.005 hr^{-1} at 1000 hours, the predicted unfiltered colloid mass would be only about 0.7%. Although neither of these calculated values would suggest a worrisome potential for colloid-facilitated transport over longer time scales, it is clear that the method of extrapolating the recoveries is a bit more conservative (more predicted colloid transport) than the method of extrapolating rate constants, at least for this particular case. Because of the nature of repository safety cases, which are meant to build confidence that risk is lower than a regulatory value, it would seem that Fig. 3-6 may be more appropriate to use than Fig. 3-4 for assessing the potential for bentonite colloid transport over long time scales in a system similar to the GTS shear zone. In particular, it represents a more conservative approach to estimating the amount of colloid-facilitated transport of radionuclides. We note that although the extrapolation line of Fig. 3-6 intersects zero recovery at around 2000 hours, it is probably more appropriate to assume that the time associated with some reasonable recovery, say 10%, is the additional time that it will take to for the recovery to drop another 10%. Thus, if there is 10% recovery at 1000 hours, there will be 1% recovery at 2000 hrs, and 0.1% recovery at 3000 hrs. This is a half-life (or 10%-life) concept that avoids having the extrapolated recovery drop below zero.

Of course, any extrapolation method is tenuous, particularly when it is based on extrapolating rate parameters from a modeling exercise that assumes only a single type of adsorption site on colloids or only a single type of colloid with a single colloid filtration rate constant. As the above discussion implies, the plots of Figs. 3-2 through 3-5 should not be considered to reflect a true time-scale dependence of either desorption or filtration rate constants, but rather they should be considered to reflect *distributions* of rate constants that reflect distributions of different types of adsorption sites on colloids or of different types of colloids that have different filtration properties. Just as one cannot rule out the possibility that up to 10% of the colloids in the GTS experiments may have been capable of transporting without filtration for extremely long times, it is not possible to rule out that some small fraction of radionuclide mass remaining

associated with colloids throughout the GTS experiments would not desorb from the colloids for very long times.

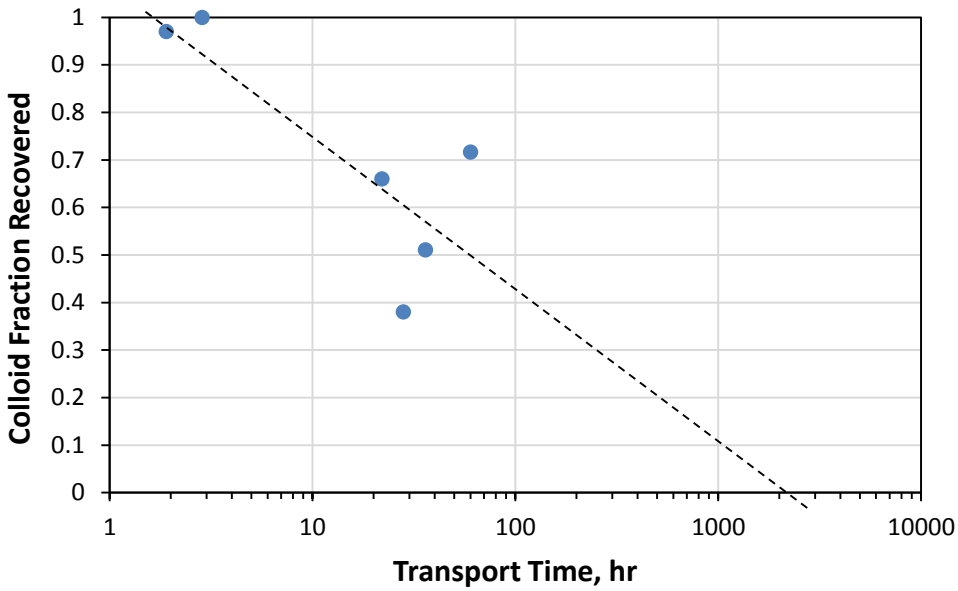

Figure 3-6. Extrapolation of colloid recoveries vs. log time for the GTS field experiments. Dashed line is a linear regression fit to the data.

In some cases, additional insights into multiple adsorption sites with different rates or multiple colloid types with different filtration properties can be obtained by extending the interpretive model to include multiple adsorption sites or multiple colloid types to see if these extensions offer a better match to the experimental data. This exercise was conducted for all 3 of the GTS colloid-homologue tests and for one of the GTS colloid-radionuclide tests in Ch. 2 of Wang et al. (2013), although it was limited to only considering additional solute adsorption sites on colloids. It was found that for 3 of the 4 tests, at least one solute data set was better matched (considering statistical significance) with a two-site solute adsorption model on colloids. Interestingly, the best model matches for all the solutes (both tri- and tetravalent) in the test with the longest travel time were obtained when a significant fraction (between 10 and 25%) of the solute mass was assumed to be associated with an adsorption site on colloids that had a desorption rate constant that could not be distinguished from zero. It was also of interest that this test had the smallest apparent colloid filtration rate constant of any of the tests. The implications are that predictions of colloid-facilitated transport of solutes based on this test alone would be significantly greater than if such predictions were based on the data from any other test.

4. LABORATORY COLUMN EXPERIMENTS TO INTERROGATE SLOW RADIONUCLIDE DESORPTION KINETICS OR SLOW COLLOID FILTRATION RATE

In this chapter, we summarize the results of some laboratory column experiments that were conducted with the intent of interrogating adsorption sites on colloids that have slow desorption kinetics and also with the intent of determining whether there is a subpopulation of colloids that have slow filtration rate constants. The common feature in these experiments is that multiple columns are used, and the effluent from one column is injected into a second column (and so on), so that the influence of rapid desorption or rapid colloid filtration is reduced in the subsequent columns, allowing a more focused interrogation of the adsorption sites and/or colloids that are more likely to contribute to colloid-facilitated transport over long time and distance scales. The underlying concept is that the adsorption sites with the fastest desorption kinetics and the colloids that are most likely to filter will tend to get "stripped out" in the first or second column so that observations in subsequent columns will more directly reflect the behavior of the stronger adsorption sites or the more filtration-resistant colloids. This stripping effect does not occur when experiments are simply repeated at different time scales, although as was illustrated in the previous chapter, some insights can still be gained in such experiments despite the fact that the faster adsorption sites or more easily-filtered colloids dominate the observed behavior at each time scale. With the sequential column approach, each successive column interrogates a smaller subpopulation of adsorption sites or colloids that are the ones of greatest interest for colloid-facilitated transport.

We first present an example involving evaluation of the colloid-facilitated transport of ^{137}Cs at the Nevada Nuclear Security Site. These experiments clearly show the potential for facilitation of ^{137}Cs transport by the NNSS colloids, although this potential would not have been apparent from running just a single column experiment. We next present an example involving the evaluation of colloid-facilitated transport of Am in the Grimsel Test Site system; these experiments do not show any evidence of stronger adsorption sites on colloids that would suggest facilitation of Am transport over long time and distance scales. The latter example appeared in Wang et al. (2014a), Ch. 6. The first example, involving ^{137}Cs transport in the NNSS system, is fully documented in Reimus and Boukhalfa (2014).

4.1 Evaluating the Potential for Colloid-Facilitated Transport of ^{137}Cs at the NNSS

Groundwater collected from the Chancellor nuclear test cavity, which had an unusually high concentration of colloids (~120 mg/L) and measurable concentrations of ^{137}Cs (1.3×10^{-12} mol/L), was used in an experiment involving 3 sequential injections into the same column, with a portion of the effluent from earlier column injections being re-injected into the column. The colloids were determined by qualitative XRD analysis to consist predominantly of smectite and illite clay (Reimus and Boukhalfa, 2014). The water was spiked with additional Cs to a concentration of 2.24×10^{-7} mol/L, although the majority of the spiked Cs was nonradioactive, so the resulting ^{137}Cs concentration was only about 18% higher than in the unspiked water. This was done in part to see if the five-order-of-magnitude increase in total Cs concentration would induce some of the ^{137}Cs that was initially adsorbed to the colloids to desorb, which would provide some indication of how strongly associated with the colloids the original ^{137}Cs was. It was found that the ^{137}Cs association with the colloids was nearly the same before and after the spike (about 50% partitioned to colloids), so it was apparent that the spike did not result in significant exchange of nonradioactive Cs with colloid-bound ^{137}Cs, and therefore the original ^{137}Cs was quite strongly associated with the colloids.

After the first column injection, breakthrough curves were obtained for both the ^{137}Cs and the colloids, as well as for ^{3}HHO, which was used as a conservative tracer. The high-concentration column effluent that was not used for radionuclide or colloid analysis was then reinjected into the same column (there was not enough material available to prepare multiple columns). This process was repeated twice for a total of three

successive column injections. The normalized breakthrough curves of ^{3}HHO, ^{137}Cs, and colloids (C/C_0 vs. volume eluted) for each of the injections are shown in Figs. 4-1 through 4-3 along with model fits to the data, and the best fitting model parameters are listed in Table 4-1. Details of the experiments and the interpretive procedure are provided in Reimus and Boukhalfa (2014).

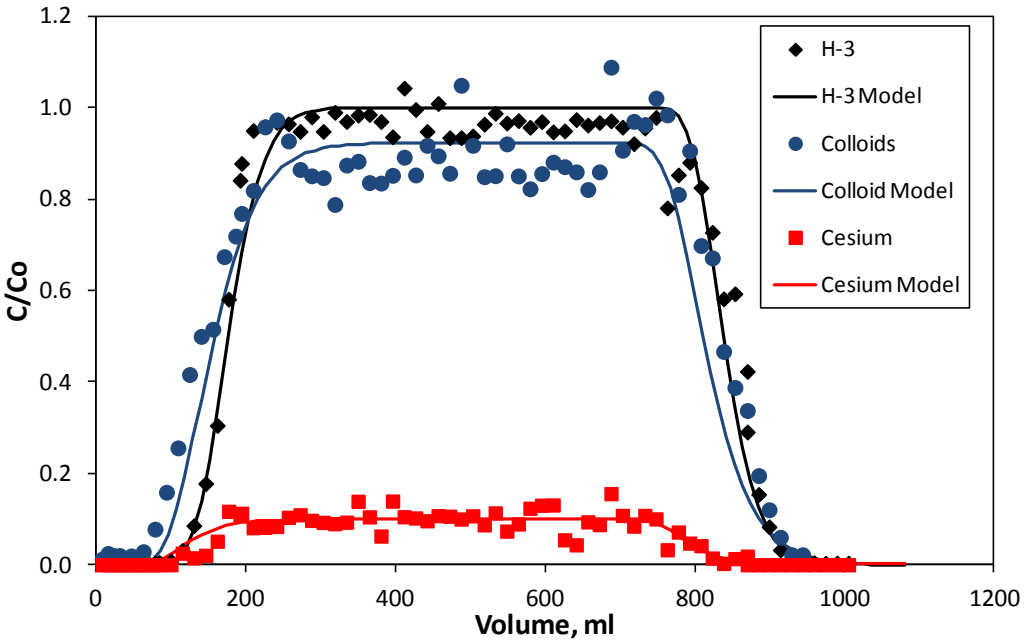

Figure 4-1. Breakthrough curves and model fits for the first injection in the Cs-spiked Chancellor water column experiment. Concentrations are normalized to injection concentrations. See Table 4-1 for best-fitting model parameters.

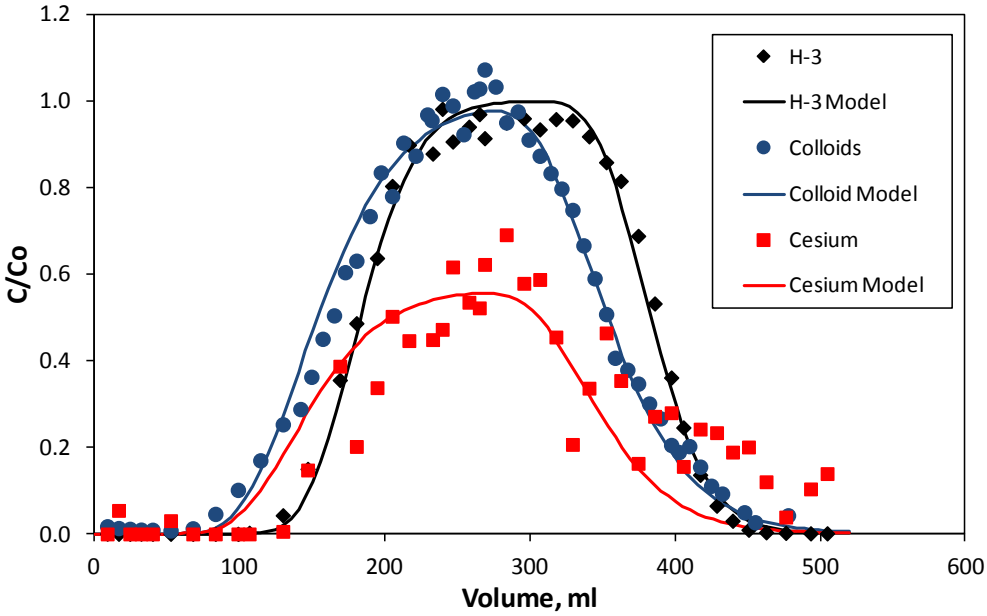

Figure 4-2. Breakthrough curves and model fits for the second injection in the Cs-spiked Chancellor water column experiment. Concentrations are normalized to injection concentrations. See Table 4-1 for best-fitting model parameters.

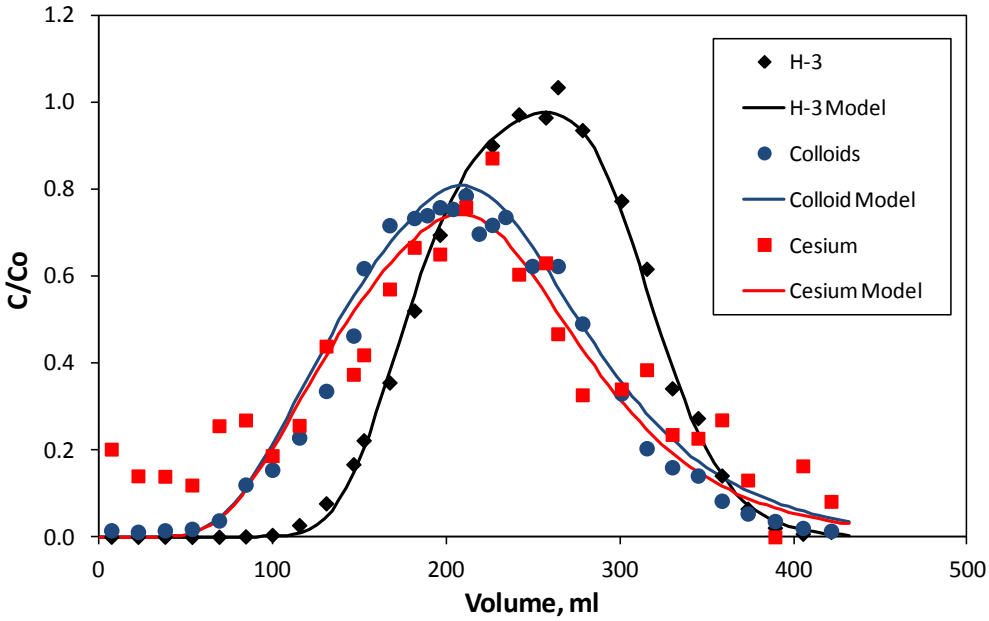

Figure 4-3. Breakthrough curves and model fits for the third injection in the Cs-spiked Chancellor water column experiment. Concentrations are normalized to injection concentrations. See Table 4-1 for best-fitting model parameters.

Table 4-1. Best-fitting model parameters for the Cs-spiked Chancellor water column injections.

Parameter	Injection 1	Injection 2	Injection 3
Colloid Recovery	0.92	~100%	~100%
^{137}Cs Recovery	0.10	0.62	>0.95
^{137}Cs association with colloids in column injection solution	0.54	0.83	0.91
^{3}HHO mean residence time, hr	50	93(1)	50
^{3}HHO Peclet number(2)	46	71	61
Colloid mean residence time, hr	45	80(1)	42
Colloid Peclet number(2)	19	25	11
Colloid filtration rate constant, $(SA/V)k_{cs,ir}$, hr^{-1}	0.0018	0	0
^{137}Cs desorption rate constant from colloids, k_{ca}, hr^{-1}	0.033	0.0048-0.0073(3)	0.0009-0.0023(3)

(1)Mean residence time is longer for Injection 2 than the other injections because column flow rate was inadvertently reduced by nearly a factor of 2.

(2)Peclet number is L/α, where L is column length, and α is longitudinal dispersivity.

(3)First number assumes that fraction ^{137}Cs adsorbed to colloids in injection solution is the fraction measured after the injection; second number assumes 100% ^{137}Cs sorption to colloids in injection solution at time of injection.

Figs. 4-1 through 4-3 show clearly that the ^{137}Cs recoveries steadily increased with each successive injection, and Table 4-1 shows that colloid-association of the ^{137}Cs also increased in each successive

injection solution. Whereas only about 10% of the ^{137}Cs was recovered after the first injection, over 95% was recovered after the third injection, and whereas about 54% of the ^{137}Cs was associated with colloids in the first injection solution, 91% was associated with colloids in the third injection solution. The breakthrough curves also suggest that essentially all of the ^{137}Cs that transported through the columns was associated with colloids (the ^{137}Cs and colloid breakthrough curves coincide exactly in timing), and the fraction that was later measured to be in the solution phase probably desorbed from the colloids between the time the column effluent was collected and the time that the partitioning was measured (which was often several days). It is also possible that the centrifugation process used to separate the solution phase from the colloid phase was not 100% efficient, so there may have been a small fraction of ^{137}Cs on very small colloids remaining in the supernatant from centrifuging.

These results clearly show the "stripping" effect mentioned in the introduction to this chapter; i.e., the ^{137}Cs in the solution phase and the fraction that is more weakly bound to colloids is being stripped off in the first two injections, leaving only ^{137}Cs that is very strongly bound to colloids in the last injection. The ^{137}Cs mass that transported essentially with complete recovery in the last injection was about 14.5% of the mass originally adsorbed to colloids in the first injection and about 7.5% of the total mass of ^{137}Cs in the first injection (since only about 50% of the ^{137}Cs was initially adsorbed to colloids). It would be impossible to deduce from just the first injection that as much as 14.5% of the original colloid-bound ^{137}Cs was this strongly associated with the colloids. If two experiments had been conducted with a factor of three difference in travel time (i.e., the difference between one and three columns), the recovery in the shorter experiment (one column) would have been about 24%, and in the longer experiment it would have been the 14.5% observed after the third column. That is, the majority of the ^{137}Cs would have desorbed from the colloids in both experiments, and the deduced difference in the ^{137}Cs desorption rate constants in the two experiments would have been about a factor of 2, with a smaller rate constant in the longer experiment, consistent with the observations in the GTS field experiments. In contrast, Table 4-1 shows that the ^{137}Cs desorption rate constant from colloids deduced from the last sequential column injection is over an order of magnitude smaller than the first injection, with a questionable ability to even be able to distinguish the rate constant from zero because of the nearly complete recovery of ^{137}Cs. Thus, the sequential column injections yielded a much better interrogation of the stronger, slower ^{137}Cs adsorption sites on the colloids than a single experiment of greater time scale would have been capable of doing.

We note that the stripping effect is also apparent for the colloids, which were not completely recovered after the first column injection, although they appeared to be completely recovered after each of the next two injections. Based on Table 4-1, it can be concluded that at least 92% of the colloids (the fraction recovered after the first injection) had an effective filtration rate constant ($\frac{SA}{V} k_{cs,ir}$) of less than 0.0018hr^{-1}. However, we can only place an upper bound on the effective filtration rate constant of this remaining 92% of colloids because of their complete recovery (within measurement capability) in the two subsequent injections. Assuming an ability to be able to distinguish 97.5% recovery from 100% recovery, the lower bound filtration rate constant would be about 0.0003 hr^{-1}.

We note that an additional insight provided by these experiments is that the presence of the immobile surfaces clearly had an enhancing effect on the desorption rate of ^{137}Cs from the colloids that was not apparent without the surfaces present. Although desorption experiments in the absence of immobile surfaces were not performed, the fact that the spiking of the Chancellor water with mostly nonradioactive Cs, discussed above, induced very little exchange of the ^{137}Cs on the colloids with nonradioactive Cs suggests that the original ^{137}Cs was strongly bound to the colloids. The ^{137}Cs measurement in this case was conducted about one week after spiking, and given the apparent lack of any shift in the ^{137}Cs partitioning before and after spiking, one would have to conclude that the ^{137}Cs exchange/desorption rate constant was less than about 0.0002 hr^{-1} (a rate constant that would result in about a 5% reduction in the partitioning in a week, which would be easily measurable). In contrast, the ^{137}Cs desorption rate constant from colloids after the first column injection was estimated to be 0.033 hr^{-1}, which represents a significant enhancement over the rate constant in the absence of the immobile surfaces present in the column.

The results from the sequential column experiments can be put into perspective with a plot such as that provided in Fig. 4-4. In this plot, the mass fraction of ^{137}Cs that was *initially associated* with colloids is plotted vs. the log of the apparent desorption rate constant from the colloids in each successive column injection. Note that a range of desorption rate constants is plotted for the second and third column injections; this is the range that results from assuming that the ^{137}Cs was either 100% associated with colloids in each successive injection (larger value) or that the ^{137}Cs association was given by the partitioning measured in the injection solutions and listed in Table 4-1 (smaller value). A range is plotted because there was not complete confidence that that centrifugations used for measuring the ^{137}Cs partitioning were 100% effective in removing all the small colloids from solution. Any given data point in Fig. 4-4 corresponds to the mass fraction of ^{137}Cs that has an apparent desorption rate constant from colloids that is *less than* the corresponding value on the x axis. In effect, the plot is a cumulative distribution function of ^{137}Cs desorption rate constants from colloids. It is apparent that while a majority of the ^{137}Cs initially associated with colloids has a relatively fast desorption rate constant under the conditions of the column experiments, there is a significant fraction that has much lower rate constants. The dashed vertical line indicates a somewhat arbitrary upper bound value for a desorption rate constant that cannot be distinguished from zero given the time scale of the column experiments (about 50 hours). This value will depend on the detection limits and precision of the analytical measurements, but it is believed to be about 0.001 hr^{-1} for these experiments (representing an ability to distinguish between a 95% recovery of ^{137}Cs and a 100% recovery). For a given set of analytical detection limits and precision, this value can be decreased only by increasing the time scale of the experiment, with the desorption rate constant that can be interrogated being roughly inversely proportional to the experiment time scale. The shaded-blue region at the lower left of the plot of Fig. 4-4 represents a region of uncertainty that must contain the extrapolation of the cumulative distribution function to smaller rate constants, but it is unknown exactly what the extrapolation looks like. The shaded region to the upper right is also a region of uncertainty, but it is much less important to know what the distribution looks like in this region because the desorption rate constants in this region are all large enough that colloid-facilitated transport would not be predicted to occur over long time and distance scales.

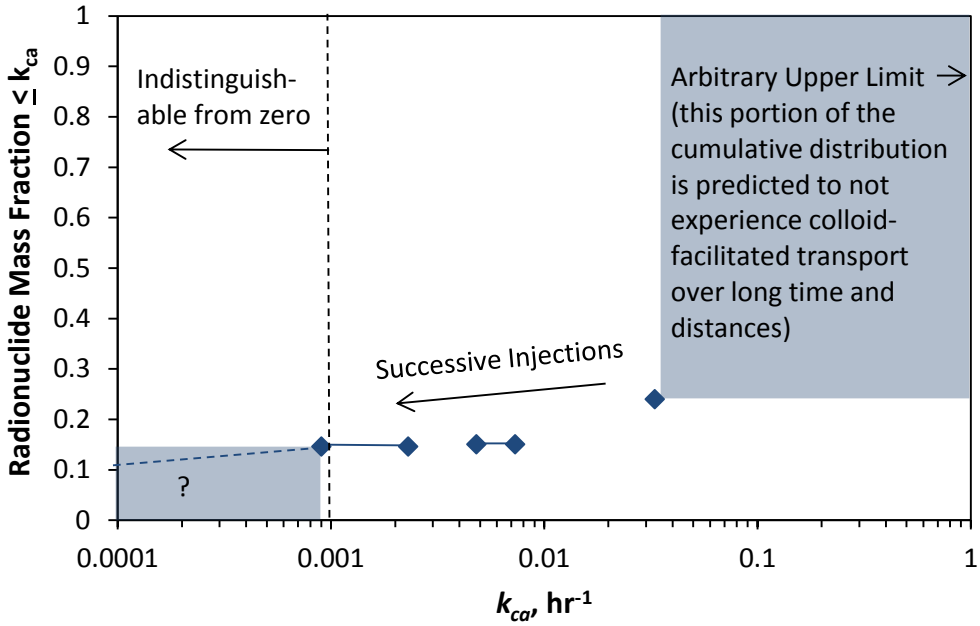

Figure 4-4. Cumulative mass fraction distributions of Cs desorption rate constants from Chancellor colloids deduced from the column transport experiments. Blue-shaded regions are regions of uncertainty.

4.2 Evaluating the Potential for Colloid-Facilitated Transport of Am in the Grimsel Test Site System

A similar set of experiments to the ones conducted for ^{137}Cs in the NNSS system were performed to evaluate the colloid-facilitated transport of Am in the Grimsel Test Site system. These experiments and their interpretations are described in detail in Ch. 6 of Wang et al (2014a) and also in Dittrich et al. (2015). The procedure in both sets of experiments was roughly identical, although the columns used for the Am experiments were much smaller and the injections were not repeated into the same columns but rather into fresh columns that had not been previously exposed to radionuclides or colloids. This is the preferred approach if sufficient material exists, as it avoids the potential for exhausting solute adsorption sites or colloid filtration sites in early injections and thus suppressing adsorption or colloid filtration in subsequent injections into the same column. We note that a simple calculation using reported values of cation exchange capacities indicated that the columns used in the ^{137}Cs experiments described in the previous section had orders of magnitude more adsorption capacity than the amount of Cs injected into them, but we cannot say the same thing with certainty about colloid filtration sites because little is known about colloid filtration site capacities in real systems.

The Am experiments used crushed fracture fill material from the GTS (containing an enrichment of fault gouge material from the shear zone), and bentonite colloids were generated using a similar procedure used to generate colloids for the GTS field experiments. Two columns packed with the fracture fill material were run in parallel for the first column injection so that more water could be collected for subsequent injections. Given the small size of the columns, a much larger percentage of a column pore volume of water had to be sacrificed for each analytical measurement than in the ^{137}Cs experiments. Partly because of this limitation, the injection pulses of Am-bearing colloids were much larger in terms of column pore volumes than in the ^{137}Cs experiments.

The results of the sequential injection experiments and the interpretive modeling matches to the data are shown in Fig. 4-5. In stark contrast to the ^{137}Cs results of the previous section, it is apparent that there seemed to be little difference in the observed transport behavior of the Am in each subsequent column injection. Indeed, as Table 4-2 shows, the model-estimated Am desorption rate constants from the colloids for each injection (or pass) are nearly identical, and they really cannot be claimed to be significantly different from one another. The colloids were filtered to a minor degree in each of the two parallel first injections, but thereafter there was no evidence of additional filtration. These results suggest that, unlike ^{137}Cs in the experiments of the previous section, there appears to be only one dominant Am adsorption site on the bentonite colloids. Of course, as is always the case, we cannot rule out the possibility that some of the approximately 15% of the Am that remained associated with the colloids after three injections was much more strongly associated with the colloids than the 85% that desorbed from the colloids. Nonetheless, it would appear from these results that the potential for colloid-facilitated transport of Am by bentonite colloids over long time and distance scales in the GTS system is quite small.

We note that these experimental results for Am are in good qualitative agreement with observations at the GTS and with laboratory experiments conducted by Huber et al. (2011). First, the colloid-facilitated transport of Am at the GTS could be explained very well in all experiments in which Am was injected by assuming only a single type of adsorption site on the colloids, which is consistent with the single-site behavior observed in the column experiments. Second, the colloid filtration rate constants deduced for the first injections in the column experiments are similar to those in the GTS field experiments despite the fact that the packed columns certainly had different solid surface area to solution volume ratios than the shear zone. Third, the desorption rate constants from colloids measured by Huber et al. (2011) for Am in their ternary system batch experiments (using bentonite colloids and fracture fill material) are in relatively good agreement with those deduced from the column experiments when one makes adjustments for the relative surface area to volume ratios in the two sets of experiments. The raw estimates of the desorption rate constants were much higher in the column experiments, but the column experiments also had much higher

surface area to volume ratios of fracture fill material, and when the additional surface area is taken into account and the desorption rate is considered to be a function of competing surface area to volume ratio, the rates are in good agreement (Wang et al. 2014a, Ch. 6; Dittrich et al., 2015).

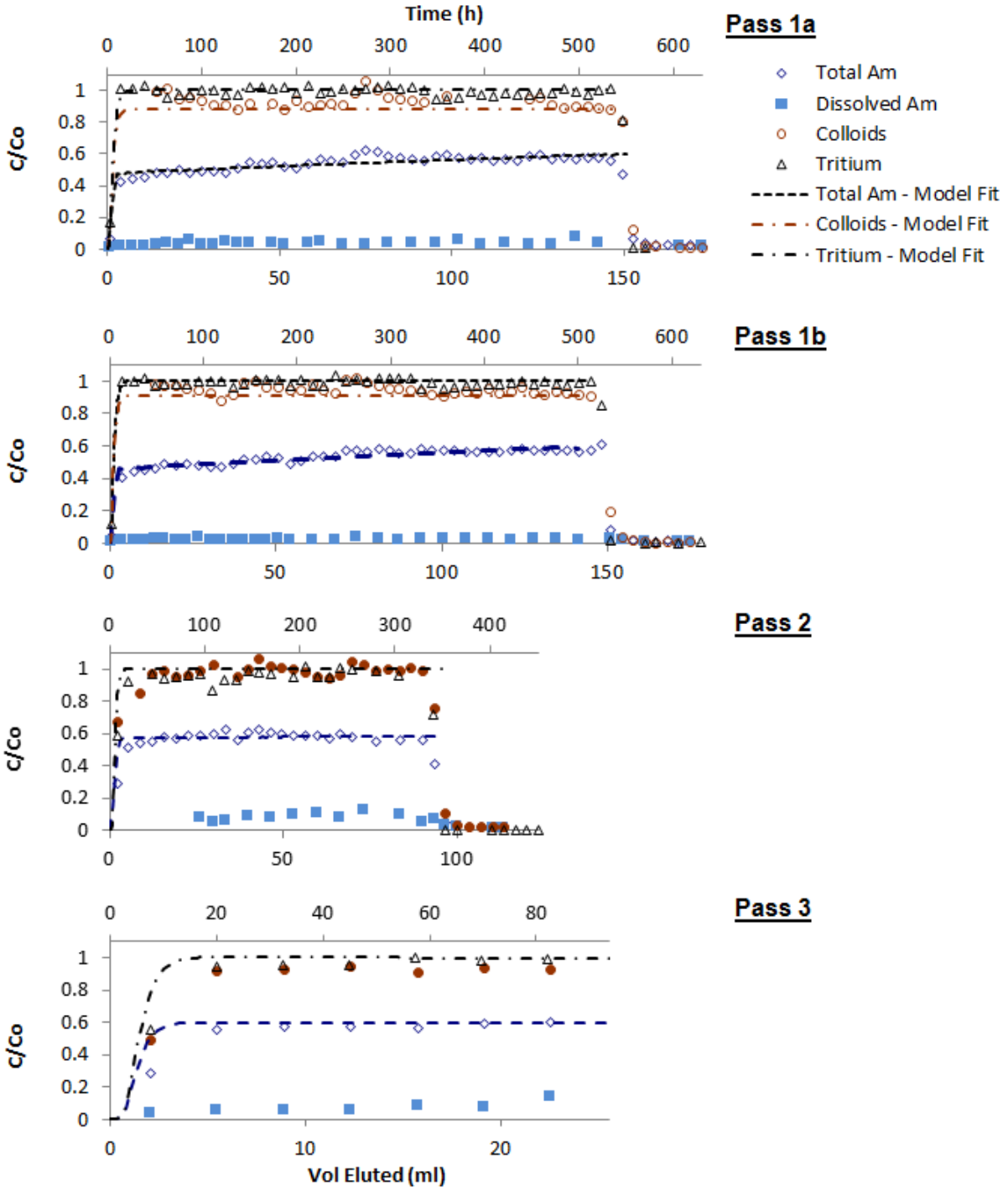

Figure 4-5. Breakthrough curves and model fits for colloid-facilitated Am transport experiments with bentonite colloids. Results are shown for the first injection (Passes 1a and 1b in parallel columns), second injection (Pass 2), and third injection (Pass 3).

Table 4-2. Parameters deduced from model fits to Am column breakthrough curves.

Parameter	Pass 1a	Pass 1b	Pass 2	Pass 3
Colloid filtration rate constant, $(SA/V)k_{cs,ir}$, hr^{-1}	0.01	0.02	-	-
Am desorption rate constant from colloids, k_{ca}, hr^{-1}	0.094(1)	0.097(1)	0.098	0.091
Mean residence time, hr	6.5	6.5	6	6
Peclet number(2)	5	5	10	10

(1)These rate constants were estimated by matching the final Am C/C_0 values in the first pass (first column) just before the colloid and Am-free water was injected.

(2)Peclet number is L/α, where L is column length, and α is longitudinal dispersivity.

5. COLUMN TRANSPORT EXPERIMENTS DEMONSTRATING TRANSPORT REGIME (2) FOR ^{137}CS IN THE GRIMSEL TEST SITE SYSTEM

A third set of experiments was conducted with the intention of interrogating slow desorption rate of ^{137}Cs from bentonite colloids in the Grimsel Test Site system. These experiments and their interpretation are described in detail in Ch. 8 of Wang et al. (2015). The experiments were planned to be conducted in nearly identical fashion to the Am experiments described in the preceding section. The expectation was that because the colloid-facilitated transport of ^{137}Cs in the field experiments at the GTS appeared to be governed by transport regime (1), this transport regime would also be observed in the laboratory experiments. However, when the first column injection was conducted, it was apparent that the ^{137}Cs did not break through with the bentonite colloids at all, and in fact the breakthrough of ^{137}Cs was significantly delayed relative to both colloids and ^{3}HHO (used as a conservative tracer). This was unexpected, particularly after batch experiments had indicated a significant amount of ^{137}Cs adsorption to the colloids, although it was a bit surprising that the Cs partitioning to colloids (about 25%) was significantly less than had been reported for the injection cocktails in the two most recent field experiments at the GTS (64% and 97%). An experiment without colloids was then conducted in a second column to assess the transport behavior of ^{137}Cs in the absence of colloids.

The ^{137}Cs breakthrough curves from the two experiments are shown in Fig. 5-1 along with model curves that match the data. The ^{3}HHO and colloid breakthrough curves are not shown in Fig. 5-1 because they were almost identical (indicating very little filtration of the colloids), and they broke through and rose to C/C_0 = 1 within the first ml eluted through the column because of its very small size. They also decreased to zero immediately when the two injection pulses ended.

In looking at the rising limbs of the breakthrough curves, it is immediately apparent the ^{137}Cs breakthrough curves with and without colloids almost classically follow the expectation for transport regime (2), as discussed in Chapter 2 of this report. The ^{137}Cs arrival with the colloids is earlier in time/volume relative to the arrival without colloids, but it is not a conservative breakthrough (i.e., nearly coincident with the ^{3}HHO), and it is also not a partial breakthrough (it rises effectively to C/C_0 = 1). The model in this case assumes two ^{137}Cs adsorption sites on both the colloids and the fracture fill material in the columns. The fits to the breakthrough curves were relatively insensitive to whether there was one or two adsorption sites on the colloids, but they were very much improved by assuming two adsorption sites on the fracture fill surfaces instead of one. This was particularly true in the tails of the breakthrough curves (Wang et al., 2015, Ch. 8). Two-site modeling of ^{137}Cs adsorption to the fracture fill material was also strongly suggested in the interpretation of batch adsorption and desorption experiments using this material (Wang et al., 2015, Ch. 8).

The adsorption and desorption rates constants for ^{137}Cs adsorption to and desorption from the more abundant adsorption sites on both the colloids and the fracture fill material were assumed to be fast relative to transport times through the columns. Under these conditions, the effective retardation factor for colloid-facilitated transport regime (2), $\frac{1+\frac{\rho_B}{\emptyset}K_d+K_cC_c}{1+K_cC_c}$, should apply. For the ^{137}Cs experiments, independent measurements of K_c and K_d were made in batch experiments, and the values of C_c and $\frac{\rho_B}{\emptyset}$ were known from the preparation of the colloid solutions and columns, respectively. These values were K_c = 3700 ml/g, K_d = 51 ml/g, C_c = 100 mg/L = 0.0001 g/ml, and $\frac{\rho_B}{\emptyset}$ = ~4 g/ml (Wang et al., 2015, Ch. 8). If these values are inserted into the retardation factor expression, the result is $\frac{1+(4)(51)+(3700)(0.0001)}{1+(3700)(0.0001)} = \frac{205.37}{1.37}$ = 149.9. The retardation factor without colloids is given by $1+\frac{\rho_B}{\emptyset}K_d$ = 1 + (4)(51) = 205. Fig. 5-2 shows the results of a simple 1-D model that uses these two retardation factors to predict the ^{137}Cs breakthrough curves with and without colloids (using the mean water residence time and dispersion coefficient determined from

fitting the ^{3}HHO breakthrough curves). It is apparent that the independently measured values of the parameters used in the retardation factor expressions yield excellent predictions of both the colloid-free transport of ^{137}Cs and the colloid-facilitated transport of ^{137}Cs in accordance with transport regime (2).

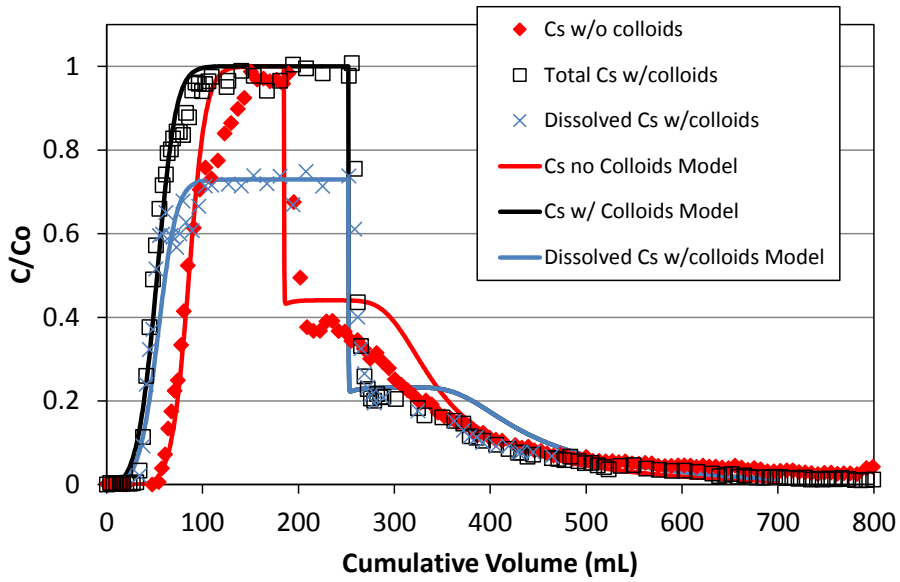

Figure 5-1. Normalized breakthrough curves of ^{137}Cs in experiments with and without bentonite colloids showing model matches to the data assuming two types of sorption sites on both the colloids and the fracture fill material used to pack the columns.

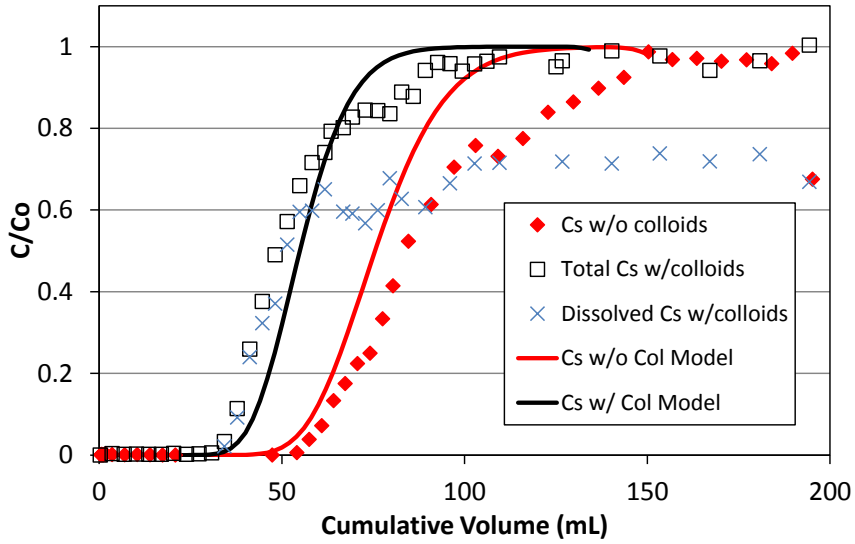

Figure 5-2. Predictions of the rising portion of the ^{137}Cs breakthrough curves of Fig. 5-1 using a 1-D advection-dispersion analytical model with $\frac{1+\frac{\rho_B}{\emptyset}K_d+K_cC_c}{1+K_cC_c}$ as the retardation factor for colloid-facilitated transport and $1+\frac{\rho_B}{\emptyset}K_d$ as the retardation factor for colloid-free transport. The K_d and K_c values were independently measured in batch experiments.

The question still remained as to why the colloid-association of the ^{137}Cs was so much less in the lab experiments than in the GTS field experiments, and also why transport regime (1) was observed in the field experiments whereas transport regime (2) was apparent in the lab experiments. The explanation lies in the concentrations of ^{137}Cs used in the two experiments and the fact that the more abundant adsorption site on the colloids is a much weaker site than the less abundant site.

In the field experiments, the injection concentration of Cs was about 3 x 10^{-11} M, whereas in the lab it was about 9 x 10^{-7} M. It was originally intended that the Cs concentration in the lab experiments be about the same as in the field experiments, but the ^{137}Cs stock solution used for the lab experiments contained a large amount of nonradioactive Cs, whereas carrier-free ^{137}Cs was used for the field experiments ("carrier" refers to nonradioactive isotopes of the same element as the radioisotope of interest). Thus, even though the ^{137}Cs concentrations were similar in the two sets of experiments, the total Cs concentrations were vastly different. The importance of this difference for colloid-facilitated transport lies in the two-site adsorption behavior on the colloids. Fig. 5-3 shows the adsorption "isotherm" reported by Missana et al. (2004) for ^{137}Cs onto FEBEX bentonite colloids as a function of ^{137}Cs concentration. The shape of isotherm reflects a more abundant weak adsorption site, which is expressed at the higher concentrations, and a less abundant strong site, which is expressed at the lower concentrations. The strong sites are almost entirely occupied by ^{137}Cs at the higher concentrations, but their effect is swamped by the much greater abundance of the weak sites, which account for the majority of the adsorbed ^{137}Cs mass at these concentrations. In Fig. 5-3, the injection concentrations in the lab and field experiments are shown as vertical lines, and it is apparent that the colloid-facilitated transport behavior in the lab experiments would be expected to be dominated by the adsorption characteristics of the weak sites while the behavior in the field experiments should be dominated by the stronger sites.

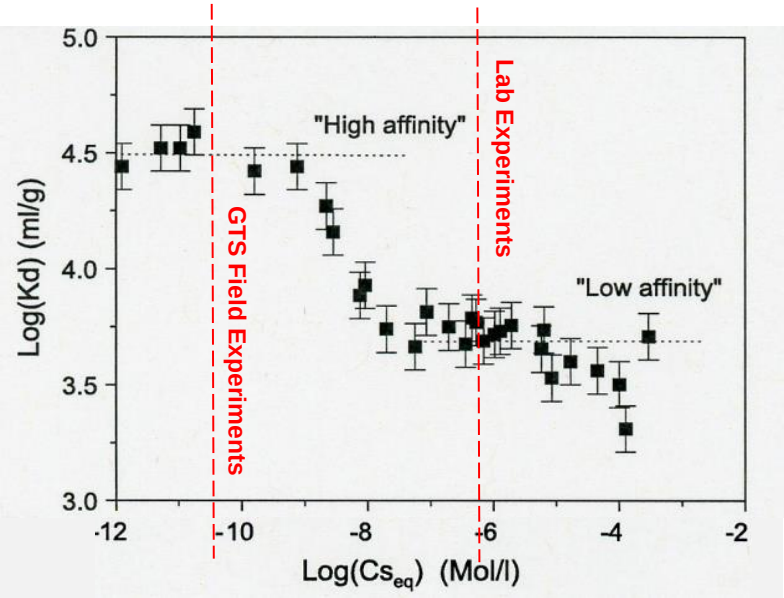

Figure 5-3. ^{137}Cs adsorption isotherms on FEBEX bentonite colloids (expressed as log K_d value vs. log Cs concentration after equilibration) measured by Missana et al. (2004). The total Cs concentrations in the GTS field experiments and in the lab experiments of Wang et al. (2015), Ch. 8 are indicated by the vertical dashed lines.

The adsorption site parameters used in the modeling of colloid-facilitated transport in the column experiments were selected to be consistent with this isotherm, and it is apparent that they provided an

excellent match to the colloid-facilitated ^{137}Cs breakthrough curves. Thus, in the end, the lab and field transport behavior of the ^{137}Cs are entirely consistent when one considers the large differences in Cs injection concentrations in the two sets of experiments and the two-site ^{137}Cs adsorption characteristics of the bentonite colloids.

6. BATCH AND FLOW CELL EXPERIMENTS OF PU SORPTION/DESORPTION FROM CLAY COLLOIDS

Due to their importance as backfill material and repository host rock, the interaction of radionuclides with aluminosilicate clay minerals has been the subject of intense study. Recent efforts at Lawrence Livermore National Laboratory have focused on the potential role of montmorillonite colloids in facilitating Pu migration. In these studies, the focus has been on understanding both the mechanisms and rates of Pu sorption and desorption from montmorillonite clay (Begg et al., 2014; Begg et al., submitted; Begg et al., 2015; Begg et al., 2013; Benedicto et al., 2014; Zavarin et al., 2008). In the following section, we summarized the experimental results and numerical modeling approach used to quantify the observed behavior. Importantly, the approach in these experiments was focused on adsorption and desorption processes rather than transport behavior. The equations do not include processes associated with colloid transport or filtration. However, the adsorption and desorption processes were based on the same simple first order reaction equations that have been employed to describe radionuclide behavior in the earlier chapters. Thus, values determined in these experiments may be applied and compared to the values reported in earlier chapters.

6.1 Sorption Linearity and Surface Mediated Reduction of Pu(V)

As stated earlier, the potential for colloid-facilitated radionuclide transport is intimately tied to the adsorption affinity of a radionuclide for clay colloids and the reversibility and ratesa of radionuclide desorption. As was shown for the case of Cs on bentonite, higher affinities at low radionuclide concentrations can lead to greater colloid facilitated transport than might be predicted from high concentration experiments. This same question was asked in the case of Pu sorption to montmorillonite colloids (Begg et al., 2015; Begg et al., 2013).

In the case of Pu(V) sorption to SWy-1 montmorillonite, Begg et al. (2013) determined that sorption across a 10 order of magnitude Pu concentration range was linear (Fig. 6-1). This implies that increased adsorption affinity of Pu for the montmorillonite surface at low radionuclide concentrations is not present under these experimental conditions. Furthermore, it suggests that a single sorption site will likely be sufficient to simulate the sorption behavior of Pu(V) on montmorillonite colloids.

The adsorption affinity of Pu(V) was compared to that of Pu(IV) under identical solution conditions. While these experiments were only performed over a 5 order of magnitude concentration range and at generally higher Pu concentrations, linear behavior was observed in this case as well. Importantly, the adsorption affinity of Pu(IV) for the montmorillonite surface was clearly higher than Pu(V) after a 30 day equilibration time period. However, the adsorption affinity of Pu(V) increased with time such that it matched that of Pu(IV) after a 1 year equilibration time period. This was attributed to the slow surface mediated reduction of Pu(V) which has been observed on a number of mineral surfaces (Begg et al., 2013; Powell et al., 2004; Powell et al., 2005; Sanchez et al., 1985).

To further examine the linearity of Pu sorption to clay colloids, Begg et al. (Begg et al., 2015) repeated the same experiments on FEBEX bentonite colloids which is dominated by montmorillonite but may include trace quantities of other minerals. In this case, Pu(IV) sorption after a 120 day equilibration time period was again linear across a 9 order of magnitude concentration range (Fig. 6-2) with non-linear behavior occurring only at the highest Pu concentration samples which were above the solubility limit of PuO_2(am,hyd). The time dependence of sorption was found to be on the scale of months and attributed to either the slow surface mediated reduction of trace amounts of Pu(V) in the sample or other aging processes. Nevertheless, the sorption appeared to be linear which suggests that one adsorption site dominates the observed sorption behavior of Pu to bentonite colloids under these solution conditions. A small set of desorption experiments included in this work also suggested that the Pu desorption rates from montmorillonite and bentonite are comparable, though a detailed modeling effort was not performed.

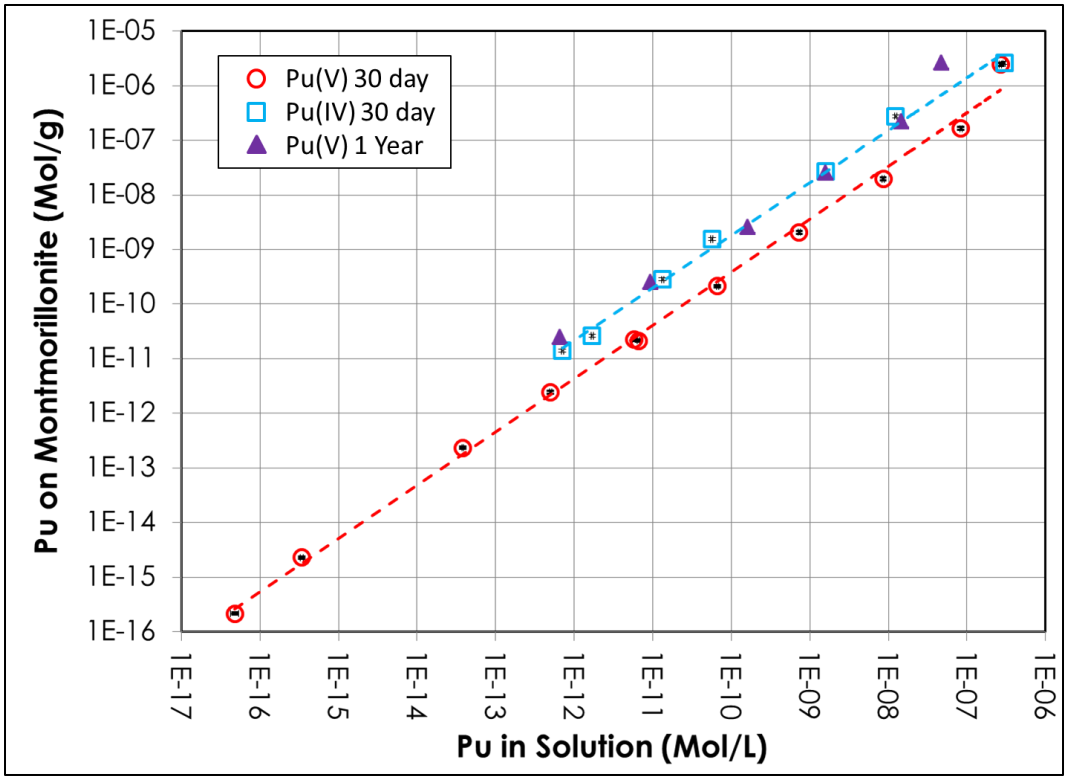

Figure 6-1. 30 day Pu(V) (circles), 30 day *high concentration* Pu(IV) (squares) and 1 year *high concentration* Pu(V) (triangles) sorption isotherm for SWy-1 Na-montmorillonite (1 g L^{-1}) in 0.7 mM $NaHCO_3$, 5 mM NaCl buffer solution at pH 8.

6.2 Pu Desorption Rates from Montmorillonite

A detailed study of Pu desorption rates from montmorillonite was recently completed by Begg et al. (submitted). In these experiments, Pu was pre-equilibrated with montmorillonite for a specified time and a desorption experiment followed using a continuously stirred reactor cell (Fig. 6-3). The desorption of Pu was monitored in the effluent and the resulting desorption data were modelled using a series of first order reactions that are comparable to those described in earlier chapters of this report (Fig. 6-4). Importantly, the first order reactions were written so as to account for the known surface mediated reduction of Pu(V). The model also attempted to honor the rates of Pu sorption and equilibrium sorption affinities available in the literature. The manuscript provides detailed information regarding the data and modeling efforts and will not be reproduced here. However, a typical dataset is shown in Fig. 6-5 and the rate constants produced as a result of our data fitting effort are reported in Table 6-1.

While a detailed analysis of the rate constants associated with our modeling effort is beyond the scope of this summary report, it is valuable to compare rate constants from these experiments to those reported for column and field experiments described earlier. The net K_d values ($10^{5.1}$ at pH 8 to $10^{6.3}$ ml/g at pH 4) are one to two orders of magnitude higher than those reported for Cs on bentonite (Fig. 5-3) and reflect the very high adsorption affinity of Pu for the montmorillonite surface. The net K_d values are controlled by oxidized Pu(V) in solution and the reduced Pu(IV) on the surface. If we presume that solution conditions at a repository would tend towards reducing conditions, we may expect that Pu(V) would not be stable in solution. This would further increase the net K_d values for Pu sorption to montmorillonite. Based on the parameters in Table 6-1, the absence of Pu(V) would lead to a net K_d of $10^{6.4}$ at pH 8 to $10^{7.8}$ ml/g at pH 4

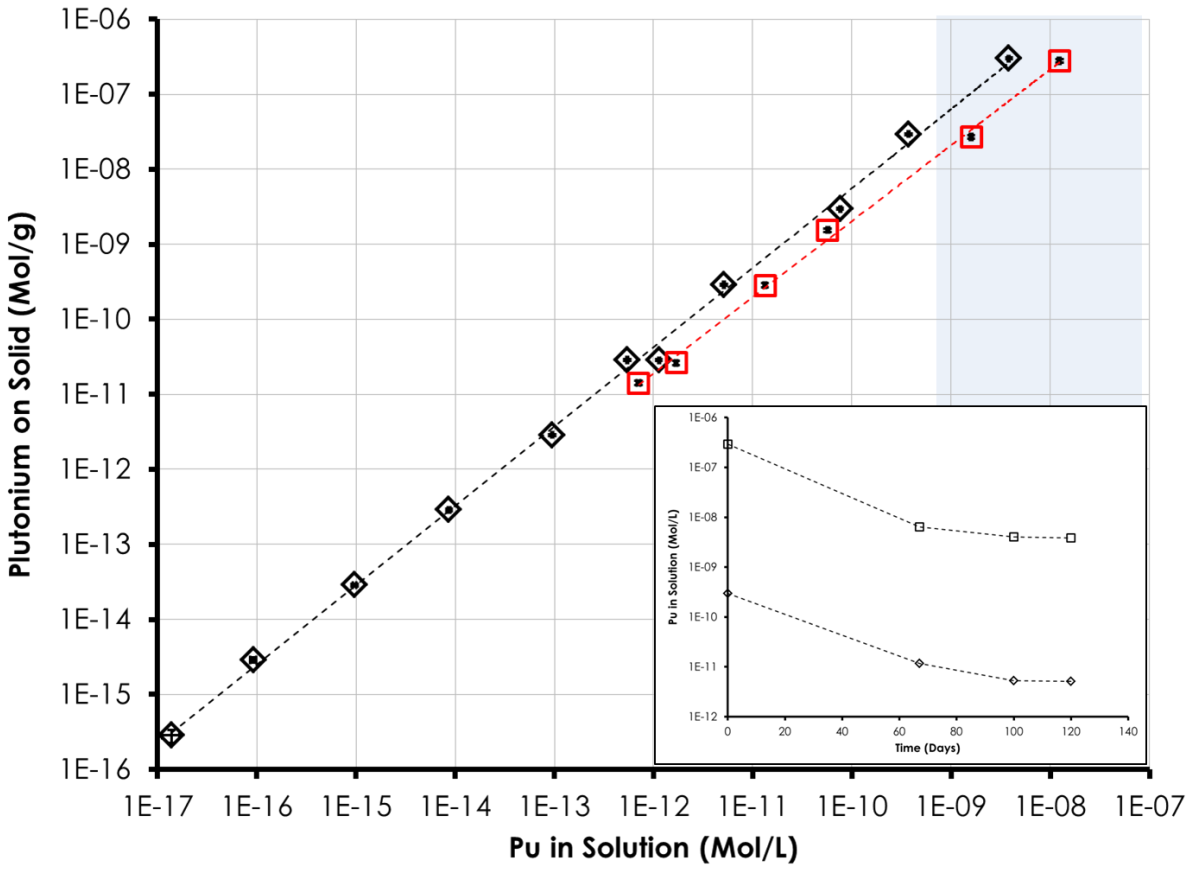

Figure 6-2. 120 d Pu(IV) sorption isotherm for FEBEX bentonite (1 g L^{-1}) in 0.7 mM $NaHCO_3$, 5 mM NaCl buffer solution at pH 8 (black diamonds). Inset shows time series data for experiments at 10^{-7} and 10^{-10} M initial Pu(IV) to indicate apparent adsorption equilibrium at 120 d. Also shown are data for 30 d Pu(IV) adsorption isotherm for SWy-1 Na-montmorillonite (1 g L^{-1}) in 0.7 mM $NaHCO_3$, 5 mM NaCl buffer solution at pH 8 (red squares) (Begg et al., 2013). Lines are shown to guide the eye only. Blue shaded area represents expected concentration for Pu(IV) colloid formation (Neck et al., 2007). Error bars based on LSC counting uncertainties (1σ) for bentonite experiments and 1σ for quadruplicate montmorillonite experiments are within range of the symbols used.

under reducing conditions. This extreme adsorption affinity of Pu for the surface of montmorillonite, in part, explains the observed colloid facilitated Pu transport that has been reported in the field.

Based on our modeling approach, it appears that the rate limiting step to Pu desorption is Reaction 4 (Fig. 6-4). Reaction 4 was included in our model to effectively simulate the flow cell data. It has been attributed to an aging phenomenon (Begg et al., submitted) and may relate to changes in the bonding of Pu(IV) on the mineral surface (e.g. monodentate to bidentate adsorption). However, the mechanistic nature of this phenomenon is purely speculative. Presently, Reaction 4 is implemented simply because it is necessary for the model to adequately represent these data. The Reaction 4 rate constants (for all pH's) suggest a rate-limiting desorption rate constant on the order of 10^{-4} to 10^{-5} hr^{-1}. These values are substantially lower than those reported for Am column flow through experiments (10^{-1} hr^{-1}, Table 4-2) but are closer to the lowest values reported for Cs (10^{-3} hr^{-1}, Table 4-1). The lower desorption rate constants of Pu relative to Cs (one to two orders of magnitude) correlate with the higher equilibrium K_d value of Pu on bentonite/montmorrllonite colloids relative to Cs (also one to two orders of magnitude). The Pu rate

constants better reflect the long-term desorption rates that have been observed in the field for tetravalent radionuclides (Fig. 3-5).

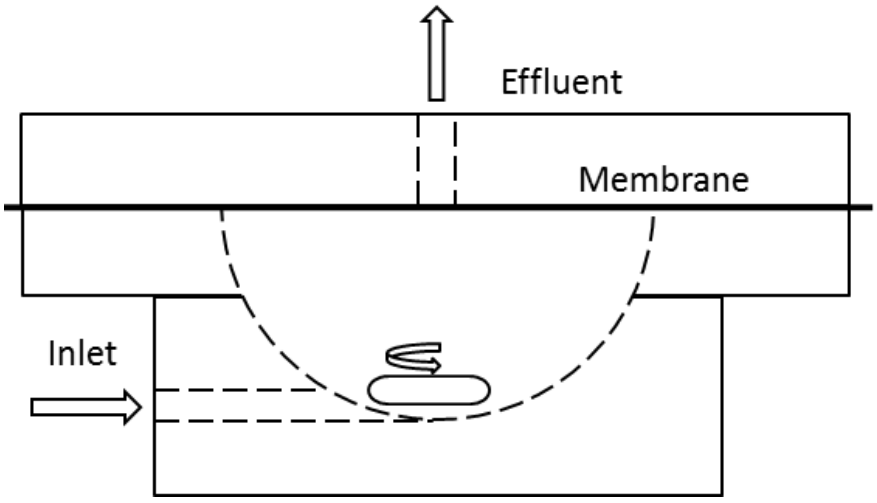

Figure 6-3. Flow cell set up. Cell provided by Dr Brian Powell (Environmental Engineering and Earth Sciences, Clemson University). Figure provided by Jennifer Wong (Environmental Engineering and Earth Sciences, Clemson University).

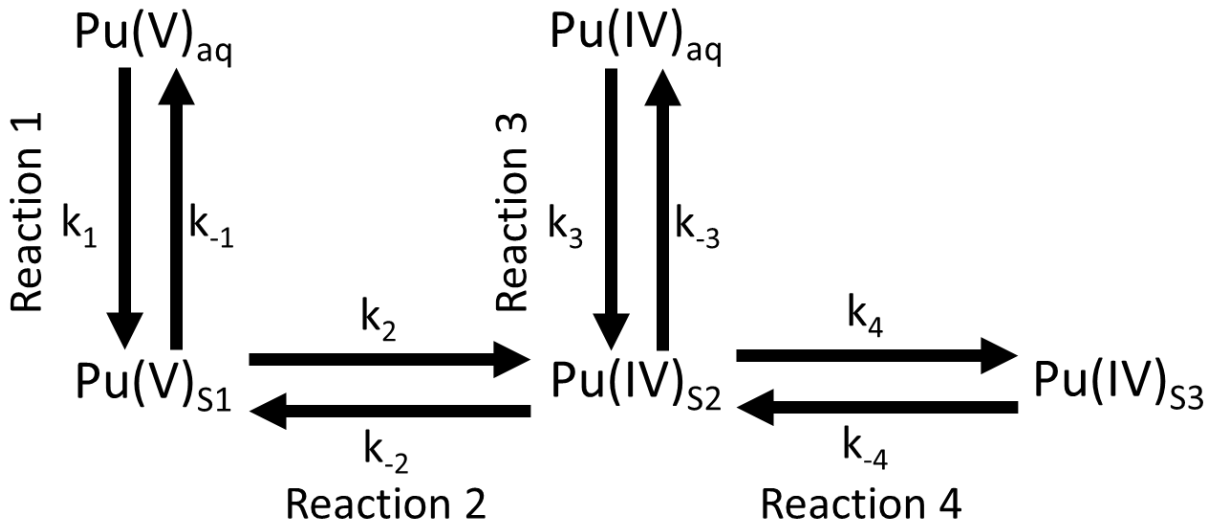

Figure 6-4. Conceptual model used for the simulation of Pu desorption kinetics from montmorillonite. In this model, sites 1, 2, and 3 represent unique states of adsorbed Pu and not necessarily unique surface sites. Sites 1 and 2 refer to Pu(V) and Pu(IV) sorbed to the surface; site 3 represents an aging phenomenon that is included strictly to facilitate modeling (it was necessary to effectively simulate the observed behavior of Pu sorbed to montmorillonite).

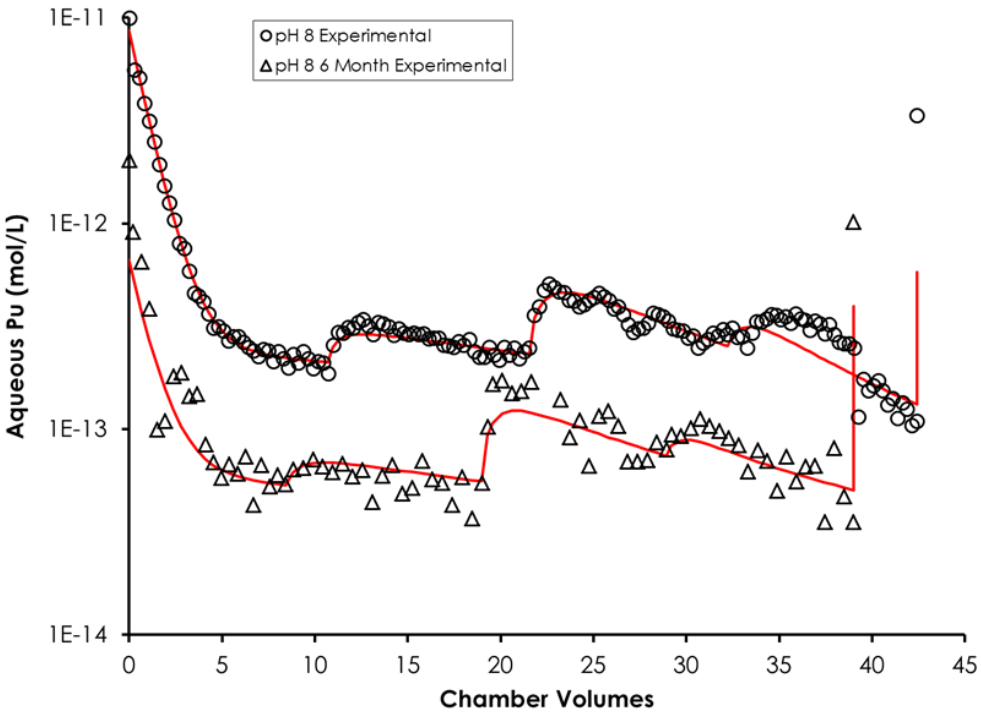

Figure 6-5. Model fits (red lines) to 3-week equilibrated (circles) and 6 month equilibrated (triangles) pH 8 flow cell desorption data. The 3 week and 6 months refers to the adsorption pre-equilibration time prior to the start of the desorption experiment.

Table 6-1. Flow cell data fitting results. 2SD errors reported. See Begg et al. (submitted) for details.

		pH 8 3-week data	pH 8 6-month data	pH 6 3-week data	pH 6 3-week data	pH 4 3-week data
k_1	log(min^{-1})	-1.58 +- 0.41	-1.00 +- 0.36	-1.21 +- 0.19	-1.27 +- 0.51	-1.27
k_{-1}	log(min^{-1})	-0.31 +- 0.53	-0.60 +- 0.28	-0.68 +- 0.28	-0.24 +- 0.62	-0.24
K_1*1000	log(ml/g)	1.7 +- 0.7	2.6 +- 0.5	2.5 +- 0.3	2.0 +- 0.8	
k_2	log(min^{-1})	-2.42 +- 0.30	-2.36 +- 0.45	-3.24 +- 0.12	-2.72 +- 0.37	-2.54[a]
k_{-2}	log(min^{-1})	-4.09 +- 0.15	-3.82 +- 0.31	-4.52 +- 0.27	-4.21 +- 0.15	-4.51[a]
k_3	log(min^{-1})	-1.67 +- 0.31	-1.65 +- 0.32	-1.24 +- 0.21	-1.16 +- 0.19	-1.16
k_{-3}	log(min^{-1})	-3.31 +- 0.16	-3.48 +- 0.23	-3.69 +- 0.19	-3.55 +- 0.10	-3.55
K_3*1000	log(ml/g)	4.6 +- 0.3	4.8 +- 0.4	5.4 +- 0.3	5.4 +- 0.2	
k_4	log(min^{-1})	-4.17 +- 0.04	-4.77 +- 0.10	-4.05 +- 0.11	-3.94 +- 0.06	-3.94
k_{-4}	log(min^{-1})	-5.91 +- 0.23	-6.26 +- 0.17	-5.78 +- 0.23	-5.76 +- 0.12	-6.36 [a]
ψ_{-4}	log(ψ_{-4})	1	1	1	1	1
Residuals		3.3	6	3.6	2.2	
Net K_d[c]	log(ml/g)	5.1 +- 0.3	5.5 +- 0.9	5.5 +- 0.5	5.3 +- 0.5	6.3

[a] Values adjusted by hand to achieve a reasonable fit to the flow cell data. All other value taken direction from the fit to the pH 6 data.

The effective simulation of Pu sorption/desorption behavior using reversible first order reaction constants suggests that an irreversibly sorbed Pu component is not present. Furthermore, isotherm data suggest that the K_d value (as a measure of adsorption affinity) of Pu is also not concentration-dependent. This leads to a relatively simple conceptual and numerical approach for predicting colloid facilitated transport. However, desorption data collected in theseflow cell experiments accessed <12% of the total Pu. As a result, these

data cannot unequivocally prove that an irreversibly sorbed component does not exist on the montmorillonite surface. As discussed in earlier chapters of this report, it leaves open the possibility of some fraction of the sorbed Pu being irreversibly bound to the colloid. This has significant implications to the long term migration of radionuclides associated with colloids as it leaves open the possibility that some fraction of the colloid-bound radionuclide source will be permanently bound to migrating colloids.

7. STABILITY OF INTRINSIC PU COLLOIDS

As stated earlier, colloid-facilitated transport may occur via intrinsic or pseudocolloid transport processes. In the previous sections, the discussion was focused on pseudocolloid transport. Here, we provide some insight into the behavior of intrinsic Pu colloids. From a transport modeling perspective, the numerical approach to simulating the behavior of intrinsic and pseudocolloids is quite similar. The ability of radionuclides to migrate downgradient will still be a function of the colloid filtration rate and the chemical stability of the radionuclide. For pseudocolloids, this chemical stability is governed by the rate of radionuclide desorption. For intrinsic colloids, the chemical stability is principally governed by the rate of intrinsic colloid dissolution.

In the past few years, LLNL has examined the dissolution behavior of three different types of Pu oxide nanoparticles in the presence of montmorillonite at 25 and 80°C under atmospheric conditions. One set of Pu nanoparticle was freshly precipitated in alkaline solutions (the same solutions used in the isotherm and flow cell experiments). The second type of nanoparticle was prepared in acidic solution by heating (60-80ºC) for 30 minutes. The third type was calcined at high temperature (400ºC) to produce highly ordered PuO_2. Note that these experiments were not conducted with the intent of mimicking specific repository conditions, but rather they were intended to evaluate differences in the stability of intrinsic Pu colloids generated under different conditions irrespective of whether they have direct relevance to repository environments. In all cases, dialysis membranes were used to segregate intrinsic Pu nanoparticles from montmorillonite nanoparticles (Fig. 7-1). The goal of these experiments was to test whether intrinsic Pu nanoparticles were unstable relative to the Pu-montmorillonite pseudo-colloids. If true, this would indicate that pseudocolloids were more likely to control colloid facilitated transport of Pu in the environment.

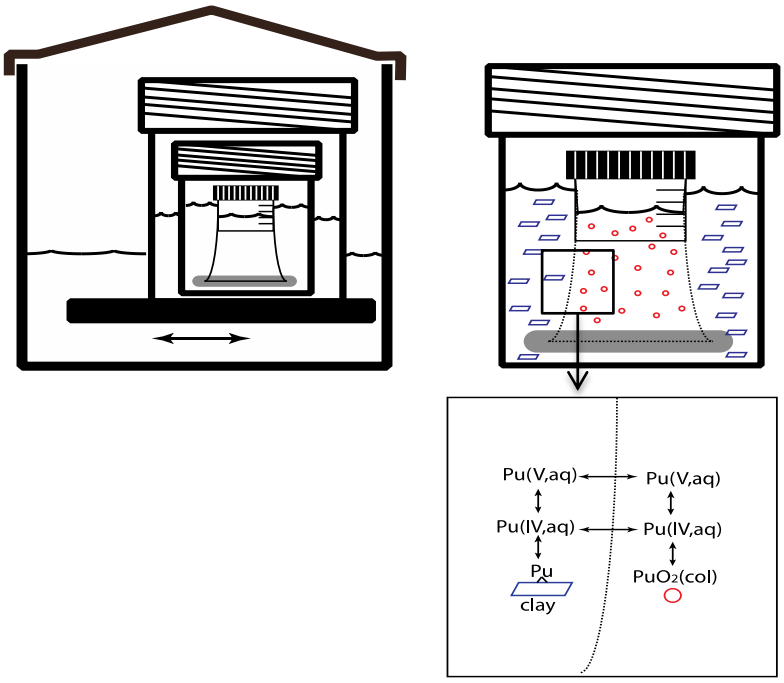

Figure 7-1. Experimental design using a dialysis membrane to separate Pu intrinsic nanoparticles (placed inside dialysis tubing, red circles) from montmorillonite (placed outside the tubing, blue rectangles, 1 g/L in experiments described here). For Pu-montmorillonite sorption to occur, Pu intrinsic nanoparticles must dissolve and diffuse through the membrane and adsorb to the montmorillonite.

The freshly precipitated Pu nanoparticles prepared under alkaline conditions were found to be unstable over a timescale of months at both 25ºC and 80ºC, with elevated temperatures enhancing dissolution rates (Fig. 7-2). In contrast, Pu nanoparticles prepared from an acidic stock remained stable over the 3 months investigated and high fired Pu oxides did not suggest any dissolution over similar timeframes (data not shown). Clearly, conditions of Pu nanoparticle formation will have a significant impact on its stability over time. Pu precipitation under mild temperature and solution conditions will lead to unstable Pu nanoparticle formation while higher heat loads and/or acidic conditions may produce more stable nanoparticles. The results suggest that nuclear repository scenarios that include higher heat loading may result in stabilization of Pu oxide phases, which can lead to greater migration of intrinsic Pu nanoparticles. Complicating our conceptual model further, recent investigations regarding the physical stability of Pu intrinsic colloids suggest that their association with native aluminosilicate colloids (i.e., "adsorption" of the Pu intrinsic colloids to the surfaces of aluminosilicate colloids) may be the most likely mechanism leading to transport of intrinsic Pu colloids (Abdel-Fattah et al., 2013).

The repository temperature history, combined with the predicted timing of canister failure, re-saturation of the repository near field, presence of natural and anthropogenic colloids, and other factors will all play a role in the evolution of any specific repository scenario and the potential for Pu mobilization. While uncertainties associated with each of the mechanisms that affect colloid facilitated transport remain, numerical approaches and the associated constants reported here and in the literature provide a roadmap for incorporation of colloid-facilitated transport processes into nuclear waste repository performance assessment.

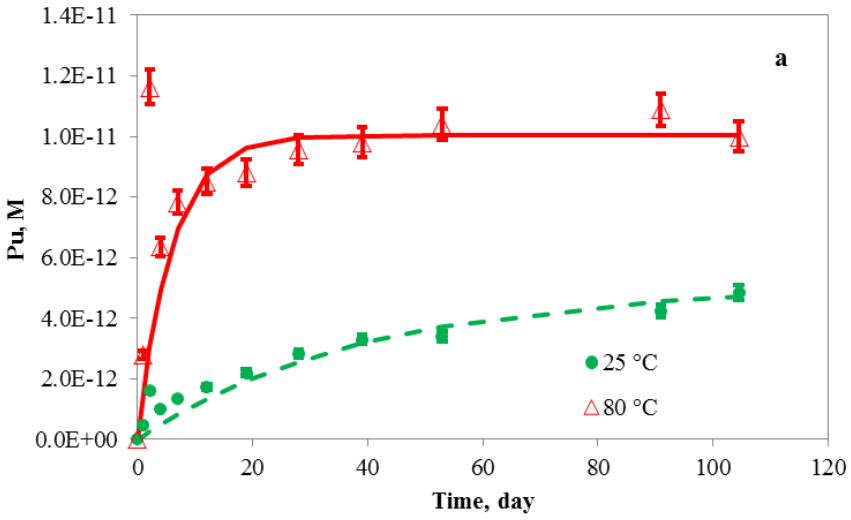

Figure 7-2. Pu concentrations outside the dialysis bag as a function of time for the Pu intrinsic nanoparticles-montmorillonite experiments at 25 and 80 ºC. Curves were fit to the data using a pseudo 1st order reaction. Initial Pu intrinsic colloid concentration inside the dialysis bag was 1.1×10^{-10} mol L^{-1}; the maximum concentration upon complete dissolution was expected to be 1.1×10^{-11} mol L^{-1}.

8. CONCLUSIONS

The most important processes affecting colloid-facilitated radionuclide transport over the long time and distance scales relevant to nuclear waste repository risk assessments are radionuclide desorption (or any other type of dissociation) from colloids and irreversible filtration of colloids. Specifically, the rates of radionuclide desorption or dissociation *and* the rates of irreversible colloid filtration must *both* be slow relative to transport time scales for colloid-facilitated radionuclide transport to contribute significantly to radionuclide fluxes at a compliance boundary. Furthermore, there must be a *joint* occurrence of these two slow processes for significant colloid-facilitated radionuclide transport to occur; if radionuclides remain strongly associated with colloids that do not migrate, or if colloids that transport efficiently do not have a strong association with radionuclides, then colloid-facilitated transport will not be observed. Under these joint conditions, a small fraction of radionuclide mass will effectively transport conservatively (with no retardation) to the compliance boundary.

Colloid-facilitated radionuclide transport under conditions of fast radionuclide adsorption/desorption rates onto both colloids and immobile surfaces (relative to transport time scales) will occur only if the product of the effective radionuclide partition coefficient on colloids and the steady-state colloid concentration (i.e., $K_c C_c$, in the terminology of this report) exceeds 1.0 by more than a few percent. Colloid filtration rates in this case do not matter; it is steady-state colloid concentrations that govern the magnitude of colloid-facilitated transport. This condition is considered to be unlikely, as it generally requires larger concentrations of colloids than are typically observed in nature. However, if it does occur, it will not result in a small fraction of radionuclide mass transporting conservatively, but rather it will result in a relatively large fraction of radionuclide mass being transported with a smaller effective retardation factor than the radionuclide in the absence of colloids.

Relatively mature models exist for describing colloid-facilitated radionuclide transport, including the one presented in Chapter 2 of this report. The principle challenge associated with quantifying the contribution of colloid-facilitated radionuclide transport to nuclear waste repository risk lies in properly parameterizing such models. Transport time scales to a compliance boundary in repository risk assessments typically range from many years to many millennia, and if radionuclide desorption rate constants from colloids or irreversible colloid filtration rate constants approach the inverse of these time scales, then colloid-facilitated transport could potentially contribute to risk. The problem is that such time scales are inaccessible in laboratory or field experiments of reasonable duration, so unless an experiment is conducted in which *all* of the radionuclide mass associated with colloids becomes dissociated from the colloids or *all* of the colloids become irreversibly filtered during the time scale of the experiment, one cannot rule out the possibility that the fraction of radionuclide or colloid mass that was not dissociated or filtered would remain associated or unfiltered over the relevant transport time scale. It then becomes a matter of determining whether the *joint* colloid-facilitated radionuclide mass fraction (i.e., the product of the radionuclide fraction that does not desorb from colloids and the fraction of colloids hosting such non-desorbing radionuclides that do not filter) can be tolerated in repository risk assessments.

If a risk threshold would be exceeded if this entire joint mass fraction were assumed to transport conservatively, then the logical next step would be to experimentally evaluate the time-scale dependence of radionuclide desorption rate constants and colloid filtration rate constants to obtain insights into the potential for rates that are slow enough to matter over repository time scales (as in Chapter 3 of this report). However, when one considers the possibility of multiple types of colloids that may have different filtration characteristics and multiple radionuclide adsorption sites on colloids that have different desorption rates (or radionuclide transformations on surfaces that result in some of the radionuclide mass becoming very strongly associated with colloids, as in Chapter 6), it becomes extremely difficult to make a defensible case that colloid-facilitated radionuclide transport will have no contribution to risk, even if extrapolated time-scale trends suggest this. The possibility of intrinsic radiocolloid formation, or the generation of waste

form degradation or corrosion-product colloids that have radionuclides strongly-associated with them (perhaps incorporated directly into their structure), puts the onus on evaluating the long-term stability and transport behavior of such colloids, as it must almost be assumed that radionuclide associations with such colloids, provided the colloids are not unstable with respect to dissolution, is strong enough to last repository transport time scales. Evaluation of colloid stability and transport behavior over such time scales is extremely challenging – probably more so than evaluating radionuclide associations with colloids.

New or improved experimental methods are needed to address the above challenges. One such method, demonstrated in Chapter 4, is to conduct sequential injections into columns to effectively strip out the effects of radionuclide adsorption sites on colloids that have rapid desorption rates and also colloids that filter rapidly in the early columns so that slower radionuclide desorption rates and slower colloid filtration rates that are of greater importance can be more effectively interrogated in later columns. However, this approach is still subject to the same time-scale limitations as any other experimental approach, so while it may help in refining the radionuclide or colloid mass fractions that can contribute to risk, it cannot completely rule out the possibility of colloid-facilitated transport (unless no radionuclide mass is recovered in the effluent of the final column). Another method is to focus on interrogation of radionuclide desorption rates in a flow-through reactor; such a method is demonstrated in Chapter 6. This method has the advantage that it can interrogate desorption rates over longer time scales than can be typically achieved in a column experiment. However, it does not address colloid filtration rates, and it still ultimately has the time-scale limitations inherent to all experiments. A logical adaptation of this method would be to include representative immobile solid surfaces in the reactor to evaluate radionuclide desorption rates from colloids in the presence of these competing surfaces. Such 'ternary' system experiments have been conducted by others (Huber et al., 2011; Xie et al., 2014), and in principle they should provide more conservative estimates of radionuclide desorption rate constants from colloids (i.e., more rapid desorption rates).

The introduction of either flow or geochemical perturbations (or both) should also be considered in future experiments. Such perturbations could induce colloid detachment from surfaces and/or radionuclide desorption from surfaces that might not otherwise be observed under steadier conditions, and the magnitude of the perturbations could be incrementally increased to evaluate their incremental effects. This approach would represent a shift of experimental paradigm away from trying to determine rate constants under relevant conditions to evaluating what it takes to cause behavior that will make a difference in risk assessments over long time scales. While it can be challenging to make translations from observations under perturbed conditions to steady conditions that are considered more relevant, these types of observations could yield valuable insights into whether colloid filtration or radionuclide adsorption onto colloids is truly irreversible versus just too slow to observe under steady conditions. Furthermore, if a mechanistic basis exists or can be developed to make defensible translations from observations under the perturbed conditions to expected behavior under more relevant conditions, this method could become very useful for extrapolating perturbed observations to longer time scales under steadier conditions.

9. ACKNOWLEDGMENTS

This work was supported by the Used Fuel Disposition Campaign of the Department of Energy's Nuclear Energy Program. The authors thank David Sevougian for conducting a thorough technical review of the report, and Shaoping Chu for helping assemble and format the report. Los Alamos National Laboratory is managed and operated by Los Alamos National Security, LLC for the U.S. Department of Energy's National Nuclear Security Administration under contract DE-AC52-06NA25396. Lawrence Livermore National Laboratory is managed and operated by Lawrence Livermore National Security, LLC for the U.S. Department of Energy's National Nuclear Security Administration under Contract DE-AC52-07NA27344. Sandia National Laboratories is a multi-mission laboratory managed and operated by Sandia Corporation, a wholly owned subsidiary of Lockheed Martin Corporation, for the U.S. Department of Energy's National Nuclear Security Administration under contract DE-AC04-94AL85000.

10. REFERENCES

Abdel-Fattah, A. I., Zhou, D. X., Boukhalfa, H., Tarimala, S., Ware, S. D., and Keller, A. A. 2013. Dispersion stability and electrokinetic properties of intrinsic plutonium colloids: Implications for subsurface transport. *Environ. Sci. Technol.*, 47, 5626-5634.

Andersson, P., Byegard, J., Dershowitz, W., Doe, T., Hermanson, J., Meier, P., Tullborg,E., and Winberg, A. 2002. *TRUE Block Scale project. Final report 1(4). Characterisation and model development.* Technical Report 02-13, Swedish Nuclear Fuel and Waste Management Co., Stockholm.

Bates, J.K., Bradley, J.P., Teetsov, A., Bradley, C.R., and Ten Brink, M., 1992. Colloid formation during waste form corrosion: Implications for nuclear waste disposal. *Science*, 256, 649–651.

Begg, J. D., Zavarin, M., and Kersting, A. B., 2014. Plutonium Desorption from Mineral Surfaces at Environmental Concentrations of Hydrogen Peroxide. *Environ. Sci. Technol.*, 48, 6201-6210.

Begg, J. D., Zavarin, M., and Kersting, A. B. Submitted. Desorption of plutonium from montmorillonite: An experimental and modeling study. *Geochim. et Cosmochim. Acta*.

Begg, J.D., Zavarin, M., Zhao, P., Tumey, S.J., Powell, B., and Kersting, A.B. 2013. Pu(V) and Pu(VI) sorption to montmorillonite, *Environ. Sci. Technol.*, 47(10), 5146-5153.

Begg, J.D., Zavarin, M., Tumey, S.J., and Kersting, A.B. 2015. Plutonium sorption and desorption behavior on bentonite, *J. Environ. Radioactivity*, 141, 106-114.

Benedicto, A., Begg, J. D., Zhao, P., Kersting, A. B., Missana, T., and Zavarin, M. 2014. Effect of major cation water composition on the ion exchange of Np(V) on montmorillonite: NpO_2^+-Na^+-K^+-Ca^{2+}-Mg^{2+} selectivity coefficients. *Appl. Geochem.*, 47, 177-185.

Boukhalfa, H., Reilly, S. D., and Neu, M. P. 2007. Complexation of Pu(IV) with the natural siderophore desferrioxamine B and the redox properties of Pu(IV)(siderophore) complexes. *Inorganic Chemistry* 46, 1018-1026.

Chun, B. and Ladd, A. J. C. 2004. The electroviscous force between charged particles: Beyond the thin-double-layer approximation, *J. Colloid Interface Sci.*, 274, 687-694.

Contardi, J.S., Turner, D.R., and Ahn, T.M. 2001. Modeling colloid transport for performance assessment. *J. Contam. Hydrol.*, 47, 323–333.

Degueldre, C., B. Baeyans, W. Goerlich, et al. 1989. Colloids in water from a subsurface fracture in granitic rock, Grimsel Test Site, Switzerland. *Geochim. Cosmochim. Acta*, 53, 603-610.

Dittrich, T.M., Boukhalfa, H., Ware, S.D., and Reimus, P.W. 2015. Laboratory investigation of the role of desorption kinetics on americium transport associated with bentonite colloids. *J. Environ. Radioactivity*, 148, 170-182.

Gadd, G. M. 1996. Influence of microorganisms on the environmental fate of radionuclides, *Endeavor*, 20(4), 150-156.

Hiemenz, P. C. 1986. *Principles of Colloid and Surface Chemistry*, 2nd ed., Marcel Dekker, New York.

Huber, F., Kunze, P., Geckeis, H., and Schäfer, T. 2011. Sorption reversibility kinetics in the ternary system radiocuclide-bentonite colloids/nanoparticles-granite fracture filling material, *Appl. Geochem.*, 26, 2226-2237.

Ibaraki, M. and Sudicky, E. A. 1995. Colloid-facilitated contaminant transport in discretely fractured porous media: 1. Numerical formulation and sensitivity analysis, *Water Resour. Res.*, 31(12), 2945-2960.

Israelachvili, J. N. 1992. *Intermolecular and Surface Forces*, 2nd ed., Academic Press, London/New York.

Kalmykov, S. and Denecke, M., eds. 2011. *Actinide Nanoparticle Research*, Springer-Verlag, Berlin.

Kalmykov, S.N., Zakharova, E.V., Novikov, A.P., Myasoedov, F.M., and Utsunomiya, S. 2011. Effect of redox conditions on actinide speciation and partitioning with colloidal matter, in *Actinide Nanoparticle Research*, Kalmykov, S., Denecke, M., Eds., Springer-Verlag, Berlin, pp. 361–375.

Kersting, A. B. 2012. Impact of colloidal transport on radionuclide migration in the natural environment, Ch. 10 (pp. 384-410) in *Radionuclide behaviour in the natural environment: Science, implications and lessons for the nuclear industry*. Elsevier/Woodhead Publishing Series, ISBN: 978-0-85709-132-1.

Kersting, A. B. and Zavarin, M. 2011. Colloid-facilitated transport of plutonium at the Nevada Test Site, NV, USA, in *Actinide Nanoparticle Research*, Kalmykov, S. and Denecke, M., eds., Springer-Verlag, Berlin, pp. 399-412.

Kim, J.I., Zeh, P., and Delakowitz, B. 1992. Chemical interactions of actinide ions with groundwater coloids in Gorleben aquifer systems, *Radiochim. Acta*, 58-59(1), 147-154.

Kosakowski G. and Smith, P. 2004. *Modelling the Transport of Solutes and Colloids in a Water-Conducting Shear Zone the Grimsel Test Site*, Nagra Techncial Report 04-01, Nagra, Wettingen, Switzerland.

Lin, J., Dang, H., Xie, J., Li, M., Zhou, G., Zhang, J., Zhang, H., and Yi, X. 2014. Goethite colloid-enhanced Pu transport through a single saturated fracture in granite, *J. Cont. Hydrol.*, 164, 251-258.

Lührmann, L., Noseck, U., and Tix, C. 1998. Model of contaminant transport in porous media in the presence of colloids applied to actinide migration in column experiments. *Water Resour. Res.*, 34, 421–426.

McCarthy, J. F. 1998. Colloid-facilitated transport of contaminants in groundwater: Mobilization of transuranic radionuclides from disposal trenches by natural organic matter, *Phys. Chem. Earth*, 23(2), 171-178.

Meier, H., Zimmerhackl, E., and Zeitler, G. 2003. Modeling of colloid-associated radionuclide transport in porous groundwater aquifers at the Gorleben site, Germany. *Geophys. J. R. Astron. Soc.* 37, 325–350.

Missana, T., Garcia-Gutierrez, M. and Alonso, U. 2004. Kinetics and irreversibility of cesium and uranium sorption onto bentonite colloids in a deep granitic environment, *Appl. Clay Sci.*, 26, 137-150.

Molnar, I. L., Johnson, W. P., Gerhard, J. I., Willson, C. S., and O'Carroll, D. M. 2015. Predicting colloid transport through saturated porous media: A critical review, *Water Resour. Res.*, 51(9), 6804-6845.

Möri, A., ed. 2004. *The CRR final project report series I: Description of the Field Phase – Methodologies and Raw Data*. Nagra Technical Report NTB 03-01. Nagra, Wettingen, Switzerland.

Neck, V., Altmaier, M., Seibert, A., Yun, J. I., Marquardt, C. M., and Fanghanel, T. 2007. Solubility and redox reactions of Pu(IV) hydrous oxide: Evidence for the formation of PuO2+x(s, hyd). *Radiochimica Acta*, 95, 193-207.

Noseck, U., Flügge, J., Reimus, P., Lanyon, B., Schäfer, T., Cvetkovic, V., and Blechschmidt, I. 2016. *GTS Phase VI – CFM Phase 2: Modelling of Tracer, Colloid, and Radionuclide/Homologue Transport for Dipole 06.002 – Pinkel surface packer*. NTB 16-06, NAGRA Technical Report, Switzerland.

Poinssot, C. and Geckeis, H. 2012. *Radionuclide behaviour in the natural environment: Science, implications and lessons for the nuclear industry*. Elsevier/Woodhead Publishing Series, ISBN: 978-0-85709-132-1.

Powell, B. A., Fjeld, R. A., Kaplan, D. I., Coates, J. T., and Serkiz, S. M. 2004. $Pu(V)O_2^+$ adsorption and reduction by synthetic magnetite (Fe_3O_4). *Environ. Sci. Technol.*, 38, 6016-6024.

Powell, B. A., Fjeld, R. A., Kaplan, D. I., Coates, J. T., and Serkiz, S. M. 2005. PuO_2^+ adsorption and reduction by synthetic hematite and goethite. *Environ. Sci. Technol.*, 39, 2107-2114.

Reiller, P. E. and Buckau, G. 2012. Impacts of humic substance on the geochemical behaviour of radionuclides, Ch. 5 (pp. 103-160) in *Radionuclide behaviour in the natural environment: Science, implications and lessons for the nuclear industry*. Elsevier/Woodhead Publishing Series, ISBN: 978-0-85709-132-1.

Reimus, P. W. and Boukhalfa, H. 2014. *Chancellor Water Colloids: Characterization and Radionuclide Associated Transport, Final Report for NNSS Underground Test Area Program*, LA-UR-14-27538, Los Alamos National Laboratory, Los Alamos, NM.

Ruckenstein E. and Prieve, D. C. 1976. Adsorption and desorption of particles and their chromatographic separation, *AIChE J.*, 22(2), 276-283.

Ruggiero, C. E., Matonic, J. H., Reilly, S. D., and Neu, M. P. 2002. Dissolution of plutonium(IV) hydroxide by desferrioxamine siderophores and simple organic chelators. I*norganic Chemistry*, 41, 3593-3595.

Ryan J. N. and Gschwend P. M. 1994. Effects of ionic strength and flow rate on colloid release: Relating kinetics to intersurface potential energy. *J. Colloid Interface Sci.*, 164, 21-34.

Sanchez, A. L., Murray, J. W., and Sibley, T. H. 1985. The adsorption of plutonium IV and plutonium V on goethite. *Geochim. Cosmochim. Acta*, 49, 2297-2307.

Schäfer, T., Huber, F., Seher, H., Missana, T., Alonso, U., Kumke, M., Eidner, S., Claret, F., and Enzmann, F. 2012. Nanoparticles and their influence on radionuclide mobility in deep geological formations. *Appl. Geochem.*, 27, 390–403.

Smith, P. A. and Degueldre, C. 1993. Colloid-facilitated transport of radionuclides through fractured media. *J. Contam. Hydrol.*, 13, 143–166.

Soderholm, L., Almond, P.M., Skanthakumar, S., Wilson, R.E., and Burns, P.C. 2008. The structure of the plutonium oxide nanocluster $[Pu_{38}O_{56}Cl_{54}(H_2O)^8]^{14-}$, *Angew. Chem. Int. Ed*. 47, 298–302.

Stumm W. 1992. *Chemistry of the solid-water interface: processes at the mineral-water and particle-water interface in natural systems*. Wiley Press, Chicago, IL.

Vilks, P. and Bachinski, D. B. 1996. Characterization of organics in Whiteshell Research Area groundwater and the implications for radionuclide transport, *Applied Geochem.*, 11, 387-402.

Vilks, P. and Baik, M. 2001. Laboratory migration experiments with radionuclides and natural colloids in a granite fracture. *J. Contam. Hydrol.* 47, 197-210.

Viswanathan, H., et al., 2016. *Crystalline and Crystalline International Disposal Activities, Used Fuel Disposition Campaign Milestone Report - Chapter 2, Interpretation of Colloid-Facilitated Radionuclide Transport Experiments in a Crystalline Granodiorite at the Grimsel Test Site, Switzerland*. FCRD-UFD-2016-000626, LA-UR-16-26212.

Walther, C., Rothe, J., Brendebach, B., Fuss, M., Altmaier, M., Marquardt, C.M., Büchner, S., Cho, H.-R., Yun, J.-I., and Seibert, A. 2009. New insights in the formation processes of Pu(IV) colloids. *Radiochim. Acta*, 97, 199–207.

Wang, Y. 2014. Nanogeochemistry: Nanostructures, emergent properties and their control on geochemical reactions and mass transfers, *Chemical Geology*, 378-379, 1-23.

Wang, Y., et al. 2013. *Natural System Evaluation and Tool Development – International Collaborations: FY13 Progress Report, Used Fuel Disposition Campaign Milestone Report - Chapter 2, Interpretations of Colloid-Facilitated Transport Experiments at the Grimsel Test Site from 2008 through 2012*. FCRD-UFD-2013-000628.

Wang, Y., et al. 2014a. *Used Fuel Disposal in Crystalline Rocks: Status and FY14 Progress, Used Fuel Disposition Campaign Milestone Report - Chapter 6, Laboratory Investigation of Colloid Facilitated Transport of Americium by Bentonite Colloids in a Granodiorite System*. FCRD-UFD-2014-000060.

Wang, Y., et al. 2014b. *Used Fuel Disposal in Crystalline Rocks: Status and FY14 Progress, Used Fuel Disposition Campaign Milestone Report - Chapter 7, Evaluation of Alternative Descriptions of Desorption of Tri- and Tetravalent Solutes from Bentonite Colloid in Tracer Tests at the Grimsel Test Site.* FCRD-UFD-2014-000060.

Wang, Y., et al. 2015. *Used Fuel Disposal in Crystalline Rocks: FY15 Progress Report, Used Fuel Disposition Campaign Milestone Report - Chapter 8, Laboratory Investigation of Colloid Facilitated Transport of Cesium by Bentonite Colloids in a Crystalline Rock System*. FCRD-UFD-2015-000125.

Xie, J., Lin, J., Zhou, X., Li, M., and Zhou, G. 2014. Plutonium partitioning in three-phase systems with water, colloidal particles, and granites: New insights into distribution coefficients, *Chemosphere*, 99, 125-133.

Xie, J., Lu, J., Lin, J., Zhou, X., Zhou, G., and Zhang, J. 2013a. The dynamic role of natural colloids in enhancing plutonium transport through porous media, *Chem. Geology*, 360-361, 134-141.

Xie, J., Wang, X., Lu, J., Zhou, X., Lin, J., Li, M., Xu, Q, Du, L., Liu, Y., and Zhou, G. 2013b. Colloid-associated plutonium transport in the vadose zone sediments at Lop Nor, *J. Environ. Radioactivity*,. 116, 76-83.

Yamaguchi, T., Nakayama, S. Vandergraaf, T.T., Drew, D.J., and Vilks, P. 2008. Radionuclide and colloid migration in a quarried block of granite under in-situ conditions at a depth of 240 m, *J. Power Energy Sys.*, 2(1), 186-197.

Yao, K-M., Habibian, M. T., and O'Melia, C. R. 1971. Water and waste water filtration: Concepts and applications, *Environ. Sci. Technol.*,5(11), 1105-1112.

Zänker, H. and Hennig, C. 2014. Colloid-borne forms of tetravalent actinides: A brief review, *J. Contaminant Hydrol.*, 157, 87-105.

Zavarin, M., Bourbin, M., Kersting, A. B., Powell, B. A., and Zhao, P. 2008. Examination of the Effects of Ionic Strength and pH on Np(V) and Pu(V) Sorption to Montmorillonite, A*merican Chemical Society - Geochemistry Division/Clay Minerals Society Symposium*, New Orleans, LA.

Zavarin, M., Powell, B.A., Bourbin, M., Zhao, P.H., and Kersting, A.B., 2012. Np(V) and Pu(V) ion exchange and surface-mediated reduction mechanisms on montmorillonite. *Environ. Sci. Technol.*, 46, 2692–2698.

Zhao, P., Begg, J. D., Zavarin, M., Tumey, S. J., Williams, R., Dai, Z. R., Kips, R., and Kersting, A. B. 2016. Plutonium(IV) and (V) Sorption to Goethite at Sub-Femtomolar to Micromolar Concentrations: Redox Transformations and Surface Precipitation. *Environ. Sci. Technol.*, 50, 6948-6956.

Appendix A

Nanogeochemistry of Colloidal Particles

APPENDIX A—NANOGEOCHEMISTRY OF COLLOIDAL PARTICLES

Colloid particles are ubiquitous in natural systems, with their sizes ranging from ~ 1 to 1000 nm (e.g., Honeyman and Ranville, 2002). Fine colloidal particles are called nanoparticles (~1 to 100 nm). Recently emerging nanogeochemical studies on nanoparticles provide a new perspective for understanding the surface chemistry and stability of colloid particles in natural systems (Wang, 2014). A comprehensive review on this topic is provided by Wang (2014). The following is an excerpt from that review article.

Size-dependent surface chemistry

Surface charge is a key factor determining the stability of nanoparticle suspensions and the ion sorption capability of the particles. The effect of particle size on surface charge has not been fully understood, partly due to the fact that most of the measurements reported are not normalized to specific surface areas. Traditional surface complexation models may not be applicable to particles with diameters smaller than 10 nm because the planar surface assumption would be seriously violated due to the high curvature of the electric double layer (e.g., Abbas et al. 2008). Sonnefeld (1993) have developed a model for a spherical particle using an approximate solution of the Poisson-Boltzmann equation. The model predicts an increase in surface charge density with decreasing particle size. The charge increase becomes pronounced for a particle with a diameter <10 nm. This effect is attributed to the enhanced counterion screening efficiency of the electrolyte solution around nanoparticles as compared with large particles. The result has been confirmed by Monte-Carlo simulations (Abbas et al, 2008, Fig. 4). The model prediction seems supported by limited experimental observations. Madden et al. (2006) measured zeta potentials on 7 nm and 25 nm hematite particles over a pH range of 4 to 11. The measurements show that the finer particles systematically exhibit higher surface potentials than the coarser particles, with the point of zero charge (PZC) remaining more or less the same.

However, contradictory results have also been reported. Diedrich et al. (2012) measured zeta potentials for amorphous silica nanoparticles with particle sizes ranging from 25 to 177 nm over a wide range of pH vales. The zeta potential on the smallest (25 nm) particles shows less negative than those for larger particles. This discrepancy may be caused by particle agglomeration, which tends to mask the surface chemistry of individual particles. In addition, the particles used in this measurement seem larger than the typical size range (<10 nm) for the effect of nano-confinement (Fig. A-1). Nevertheless, this discrepancy points out the necessity for additional work, especially on the effect of particle size on the PZC.

Associated with the surface charge density changes, the surface sorption on nanoparticles may also vary with the particle size. Zeng et al. (2009) studied U(VI) sorption on aerosol-synthesized hematite particles ranging from 12 to 125 nm in size. The adsorption affinity was found to increase as the particle size decreases. Similarly, Cu^{2+} sorption edges were measured on hematite nanoparticles with average diameters of 7 nm, 25 nm, and 88 nm (Madden et al., 2006). The sorption edge for 7 nm hematite is shifted approximately 0.6 pH units lower than that for the 25 nm and 88 nm samples, indicating an adsorption affinity sequence of 7 nm > 25 nm = 88 nm. The actual mechanism for such dependence is not thoroughly understood. Madden et al. (2006) attribute the high adsorption affinity of Cu^{2+} for the smallest particles to the changes in surface structure, arguing that Cu^{2+} preferentially binds to sites that accommodate the Jahn–Teller distortion of its coordination to oxygen, while Zeng et al. (2009) show that the difference in U(VI) sorption is probably not the result of lattice distortion because no significant lattice distortion has been detected from XAFS spectroscopic measurements. Similar sorption edge shifts were observed for Pb(II) sorption onto hematite in the presence or absence of microbial siderophore (Barton et al., 2011). The Pb sorption edge is shifted to lower pH values by about 0.5 pH units for < 10 nm hematite particles as compared to that for the bulk phase, whereas maximum sorption density (at pH $\geq$ 6) is unaffected by particle size. Interestingly, the presence of microbial siderophore has little or no effect on Pb(II) sorption on particle smaller than 10 nm, while it reduces the sorption on the 40 nm particles by ~20% at pH $\geq$ 6, which probably indicates that large organic molecules such as siderophore may be hard to attach to a highly curved particle surface because additional energy may be required for molecular conformation on the surface.

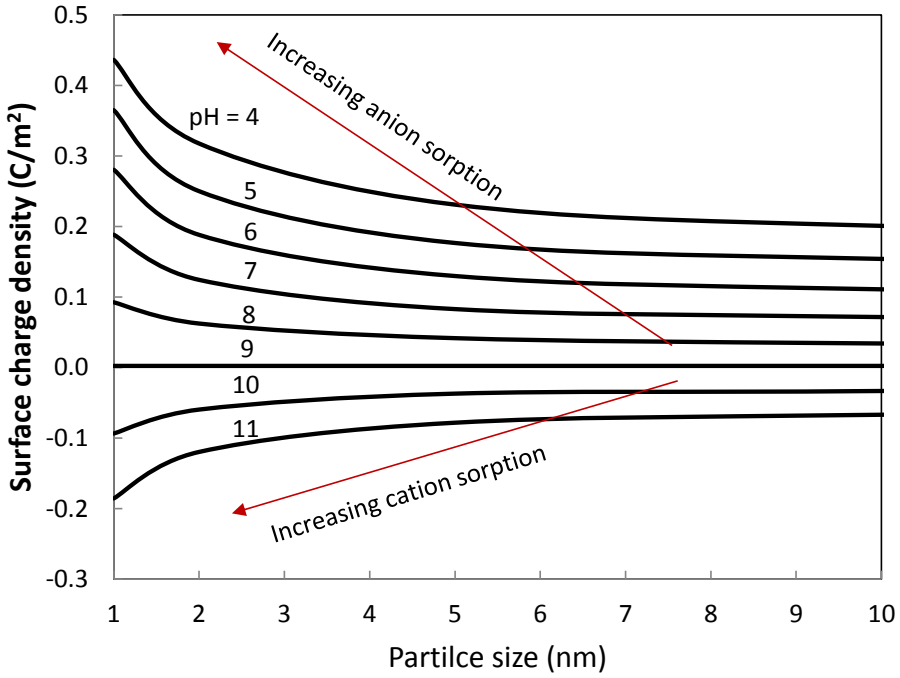

Figure A-1. Surface charge density predicted by Monte Carlo simulations for goethite nanoparticles as a function of particle size. Data are from Abbas et al. (2008). Associated with the surface charge changes, both cation and anion sorption capabilities are enhanced by size reduction.

However, in some other cases, the dependence of surface sorption on particle size is not that clear. For instance, Jegadeesan et al. (2010) investigated aqueous As (III) and As (V) sorption on nanosized amorphous and crystalline TiO_2. They have found that sorption capacities per mass of different TiO_2 polymorphs are dependent on sorption site density, particle size and crystalline structure. When normalized to the surface areas, As (III) surface coverage on the TiO_2 surface remains more or less constant for particles between 5 and 20 nm, while As (V) surface coverage seems to increase with the degree of crystallinity.

The emergent functional relationship between surface sorption and particle size suggests the necessity for revisiting some basic assumptions in the existing colloid-facilitated transport models. The existing models generally treat colloidal particles, regardless of their sizes, in the same way as the corresponding bulk phase in terms of their surface properties and phase stabilities. The data obtained so far from nanogeochemical studies, however, indicate that nanoparticles, especially with sizes <10 nm, may have significantly higher sorption affinity than larger colloidal particles and therefore are expected to play a more significant role in chemical transport in natural systems than previously thought (Banfield and Zhang, 2001; Waychunas et al., 2005; Hochella et al., 2008).

Furthermore, surface chemistry also determines the stability of a nanoparticle suspension, which in turn affects the mobility of the particles and their ability for chemical transport. It has been found that the stability of a nanoparticle suspension is also size-dependent. He et al. (2008) studied the aggregation behavior of 12, 32, and 65 nm (hydrated radius) hematite particles under environmentally relevant pH (5-9) and ionic strength conditions (1-200 mM NaCl). The isoelectric point pH_{iep} (pH of zero zeta potential) of the hematite has been found to be around pH 7.8, 8.2, and 8.8, for the 12, 32, and 65 nm particles, respectively. At the same ionic strength and pH conditions, different particle sizes display different tendency for aggregation. At the same ionic strength, aggregation rates are higher for smaller particles. The critical coagulation concentration decreases as the particle size decreases. For a given ionic strength,

aggregation rates are slow at low pH and then drastically increase at pH close to the isoelectric points. The fast aggregation region shifts to lower pH as the particle size decreases. Such size-dependent behaviors may be related to the change of pH_{iep} with particle size or the increasing particle concentration for finer particle suspensions.

Size-dependent reaction kinetics

Nanoparticles can exhibit different dissolution behaviors than their bulk phase counterparts. The surface-normalized non-oxidative dissolution rate of galena nanocrystals (~14 nm) in acidic solutions, normalized to surface area, has been found to be 10-100 times higher than that of the bulk phase under similar conditions (Liu et al., 2008, 2009). A transmission electron microscopy (TEM) and X-ray photoelectron spectroscopy (XPS) study has revealed that the enhanced dissolution rate is probably due to the higher percentage of reactive sites on nanocrystal surfaces. In addition, {111} and {110} faces generally dissolve faster on nanocrystals, which may reflect the fewer coordination number of Pb on those faces. Interestingly, the dissolution has been found to be greatly inhibited if nanocrystals are closely adjacent to each other (1-2 nm or less). Lanzl et al. (2012) have examined the dissolution of hematite nanoparticles (8 and 40 nm α-Fe_2O_3) over a wide range of pH and across a spectrum of dissolution mechanisms including proton-promoted, ligand-promoted, and photochemical dissolution. The dissolution rate normalized to mass for 8 nm particles has been found to be 3.3 to 10-fold higher than that for 40 nm particles. The difference in reactivity cannot be fully explained by the difference in specific surface area and is probably due to the difference in the fraction of accessible reactive surface area in the aggregates. Particle aggregation can be an important factor complicating data interpretation for nanoparticle dissolution experiments. In addition, for comparably sized hematite aggregates, the reactivity can also vary greatly with the way the nanoparticles are synthesized (Lanzl et al., 2012).

However, an opposite trend has been reported for size-dependent mineral dissolution. Diedrich et al. (2012) have determined the dissolution rate of amorphous silica nanoparticles as a function of particle size over a size range of 25 to 177 nm under far-from-equilibrium conditions. The rate normalized to BET surface area has been found to decrease with decreasing particle size. The actual mechanism for this decrease yet to be clarified.

Note that most of the existing dissolution experiments have been conducted under far-from-equilibrium conditions. For a system close to equilibrium, another dissolution mechanism may come into play (Tang et al., 2004). It is known that the dissolution rate of a bulk phase is determined by the movement of step waves around etch pits developed on crystal surfaces. The spreading of step trains does not occur spontaneously until the pit size reaches a critical value. The critical pit size increases with decreasing degree of undersaturation of solution with respect to the bulk mineral phase. As the particles become smaller due to dissolution, the dissolution rate decreases and eventually diminishes as the particle size approaches the critical pit size (Fig. A-2). Step spreading can be inhibited when the particle size becomes equal or smaller than the critical pit size. This self-inhibiting mechanism tends to occur for a sparingly soluble mineral phase, and it has been experimentally demonstrated by Tang et al. (2004) for the dissolution of apatite particles. For a given degree of undersaturation, the apatite crystallites remaining at the end of each dissolution experiment practically have the same size distribution regardless of their initial sizes. This self-inhibiting effect has two important geochemical implications. First, biological materials such as bones and shells are generally nanocomposite with nanoparticles as building blocks (Alvisatos 2000). There is a good reason for organisms to select nanosized particles, because of their resistance to demineralization and also because of their high flexibility for structural construction. Secondly, it is generally assumed that colloidal particles in a solution that are unsaturated with respect to their bulk phase will not be stable and therefore dissolve rapidly. This assumption may no longer be valid. Nanosized particles could be resistant to dissolution when their sizes approach a critical pit size.

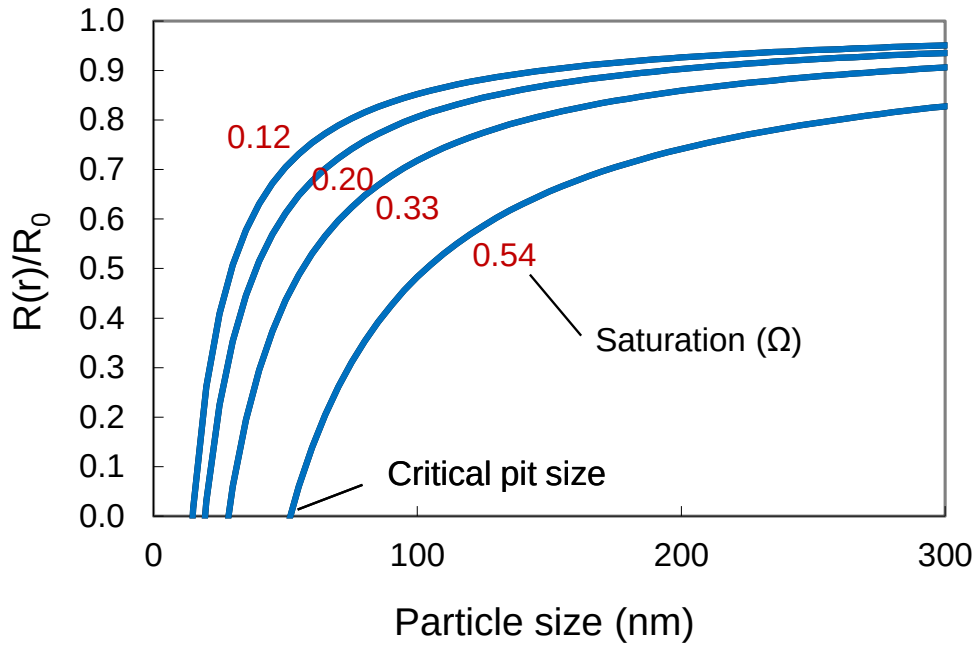

Figure A-2. Dissolution rate of apatite nanoparticles as a function of particle size and unsaturation degree. Re-plotted from Wang (2014) with corrections.

Therefore, small colloidal particles, once formed, may persist for a long time period in geologic media even if the pore water is undersaturated with the corresponding bulk mineral phase. This postulation seems consistent with a possible long-distance migration of plutonium colloids observed at the Nevada Test Site (Kersting et al., 1999).

Appendix A References

Abbas, Z., Labbez, C., Nordholm, S., and Ahlberg, E., 2008, Size-dependent surface charging of nanoparticles. *Journal of Physical Chemistry*, C 112, 5715-5723.

Alivisatos, A. P., 2000, Enhanced: Naturally aligned nanocrystals. *Science*, 289, 736-737.

Banfield, J. F. and Zhang, H. Z., 2001, Nanoparticles in the environment. *Reviews in Mineralogy & Geochemistry*, 44, 1-58.

Barton, L. E., Grant, K. E., Kosel, T., Quicksall, A. N., and Maurice, P. A., 2011, Size-dependent P_b sorption to nanohematite in the presence and absence of a microbial siderophore. *Environ. Sci. Technol*., 45, 3231-3237.

Diedrich, T., Dybowska, A., Schoot, J., and Valsami-Jones, E., 2012, The dissolution rates of SiO_2 nanoparticle size. *Environ. Sci. Technol*., 46, 4909-4915.

He, Y. T., Wan, J., and Tokunaga, T., 2008, Kinetic stability of hematite nanoparticles: the effect of particle sizes. *J. Nanopart. Res*., 10, 321-332.

Hochella, M. F., Jr., Lower, S. K., Maurice, P. A., Penn, R. L., Sahai, N., Sparks, D. L., and Twining, B. S., 2008, Nanominerals, mineral nanoparticles and Earth systems. *Science*, 319, 1631-1635.

Honeyman, B. B. and Ranville, J. F., 2002, Colloid properties and their effects on radionuclide transport through soils and groundwaters. In: *Zhang, P.-C. & Brady, P. V. (eds.) Geochemistry of Soil Radionuclides. Madison, Wisconsin, Soil Science Society of America*, no.59, pp.131-163.

Jegadeesan, G., Al-Abed, S. R., Sundaram, V., Choi, H., Scheckel, K. G., and Dionysiou, D. D., 2010, Arsenic sorption on TiO2 nanoparticles: Size and crystallinity effects. *Water Research*, 44, 965-973.

Kersting, A. B., Efurd, D. W., Finnegan, D. L., Rokop, D. J., Smith, D. K., and Thompson, J. L., 1999, Migration of plutonium in ground water at the Nevada Test Site. *Nature*, 397, 56-59.

Lanzl, C. A., Baltrusaitis, J., Cwiertny, D. M., 2012, Dissolution of hematite nanoparticle aggregates: Influence of primary particle size, dissolution mechanism, and solution pH. *Langmuir*, 28, 15797-15808.

Liu, J., Aruguete, M., Jinschek, J. R., Rimstidt, J. D., and Hochella Jr, M. F., 2008, The non-oxidative dissolution of gelna nanocrystals: Insights into mineral dissolution rates as function of grain size, shape, and aggregation state. *Geochim. Cosmochim. Acta*, 72, 5984-5996.

Liu, J., Aruguete, M., Murayama, M., and Hochella Jr., M. F., 2009, Influence of size and aggregation on reactivity of an environmentally and industrially relevant nanomaterial (PbS). *Environ. Sci. Technol*., 43, 8178-8183.

Madden, A. S., Hochella Jr., M. F., and Luxton, T. P., 2006, Insights for size-dependent reactivity of hematite nanomineral surface through Cu^{2+} sorption. *Geochim. Cosmochim. Acta*, 70, 4095-4104.

Sonnefeld J., 1993, An analytic expression for the particle size dependence of surface acidity of colloidal silica. *J. Colloid Interfacial Sci*., 155, 191-199.

Tang, R. K., Wang, L. J., and Nancollas, G. H., 2004, Size-effects in the dissolution of hydroxyapatite: an understanding of biological demineralization. *J. Mater. Chem*., 14, 2341-2346.

Wang, Y., 2014, Nanogeochemistry: Nanostructures, emergent properties and their control on geochemical reactions and mass transfers, *Chemical Geology*, 378-379, 1-23.

Waychunas, G. A., Kim, C. S., Banfield, J. F., 2005, Nanoparticulate iron oxide minerals in soils and sediments: unique properties and contaminant scavenging mechanisms. *J. Nanoparticle Research*, 7, 409-433.

Zeng, H., Singh, A., Basak, S., Ulrich, K.-U., Sahu, M., Biswas, P., Catalano, J. G., and Giammar, D. E., 2009, Nanoscale size effects on uranium(VI) adsorption to hematite. *Environ. Sci. Technol*., 43, 1373-1378.